

Minufiya Journal of Electronic Engineering Research

Faculty of Electronic Engineering - Minufiya University

- **Performance Evaluation of Coded Cooperative Relay Based OFDM
Wireless Communication System** 01
Ahmed S. Mohamed, Mohammed Abd-Elnaby and Sami A. El-Dolil
- **Performance Study of Different Approaches Used in the Design of
Hierarchical Routing Protocols for Wireless Sensor Network** 25
Amr M. Kishk, Nagy W. Messiha, Nawal A. El-Fishawy, Abd-Elrahman A. Alkafs, and
Ahmed H. Madian
- **Two Efficient Unit Cell Designs for Polarization Independent 5-G
Reflectarrays** 53
Rania Elsharkawy, A.R. Sebak, Moataza Hindy, Osama M. Haraz, Adel A. Saleeb, and
El-Sayed M. El-Rabaie Darwish
- **A Survey of Different Steganography Techniques** 66
E. A. Elshazly, Safey A. S. Abdelwahab, R. M. Fikry, O. Zahran, S. M. Elaraby and M.
El-Kordy
- **Maximum Power Techniques of Wind Energy System** 103
Walaa Mohammed and Galal.Atlam
- **Maximum Power Point Tracker of PV using Fuzzy Controller** 119
Walaa Mohammed and Galal.Atlam

25 – 1



كلية الهندسة الإلكترونية – جامعة المنوفية
Faculty of Electronic Engineering-Minufiya University

Vol. 25 - No. 1

January 2016

ISSN 1687-1189

رقم الإيداع: 52/2/2002

Minufiya Journal of Electronic Engineering Research (MJEER)

**Faculty of Electronic Engineering,
Minufiya University, Menouf, 32952, Egypt.**

Editorial Board:

Editor-in-Chief:

Prof. Dr. Mohamed A. El-Bardiny

Co-Editor:

Prof. Dr. Mohamed F. El-Kordy

Managing Editor:

Prof. Dr. El-Sayed M. El-Rabiee

Executive Editor:

Assoc. Prof. Gamal Mahrous ATTIYA

Scientific Advisory Committee:

Prof. Dr. Kamal H. Awad-Allah

Prof. Dr. Taha El-Sayed Taha

Prof. Dr. Magdy M. Kamel

Ass. Prof. Ayman El-Sayed

Ass. Prof. Ahmed E. Bahnasy

Ass. Prof. Mohamed El-Barawany

Ass. Prof. Fathy E. Abd Elsamea

Ass. Prof. Mohamed Hamdy

Administrative Secretary:

Mr. Yasser M. Hegazy

Mrs. Heba A. Mohammed

Mrs. Sabah M. Anbar

Performance Evaluation of Coded Cooperative Relay Based OFDM Wireless Communication System

Ahmed S. Mohamed, Mohammed Abd-Elnaby and Sami A. El-Dolil

Faculty of Electronic Engineering, Menoufia University, Menouf, Egypt.

(Received: 13-October-2015 – Accepted: 29-November-2015)

Abstract

This paper investigates the performance of a coded cooperative relay based Orthogonal Frequency Division Multiplexing (OFDM) wireless communication system using native rate 1/2 convolutional code and rate 1/3 turbo code. These investigations are focused on evaluating the performance of the proposed coded cooperative wireless communication system over both Additive white Gaussian Noise (AWGN) channel and different Stanford University Interim (SUI) channel models. The performance of the proposed coded cooperative relay based system is evaluated using MATLAB computer simulations and compared with direct transmission and other cooperative protocols i.e., Amplify-and-Forward (AAF) and Decode-and-Forward (DAF). The performance indicators used for comparison are Bit-Error Rate (BER) and spectral efficiency. The results show that the proposed coded cooperative system achieves lower Signal-to-Noise Ratio (SNR) values for the desired BER and achieves high spectral efficiency as compared to direct transmission, AAF and DAF based cooperative protocols. Finally, the results of computer simulations are included to demonstrate the efficiency of the proposed scheme.

1. Introduction

Transmission over wireless channels endures from random fluctuations in signal level known as fading and from co-channel interference [1]. Diversity is a powerful technique to mitigate fading and improve robustness to interference. In classical diversity techniques, the data signal

is conveyed to the receiver over multiple (ideally) independently fading signal paths (in time/frequency/space) [2]. Appropriate combining at the receiver realizes diversity gain, thereby improving link reliability. There are several approaches to implement diversity in a wireless transmission. Multiple antennas can be used to achieve diversity but multiple antennas are not always available or the destination is just too far away to get good signal quality. To achieve diversity in wireless communication networks, an interesting approach might be to build a cooperative relay network [3-6]. Meanwhile, cooperative relay technology is regarded widely as a key technology for increasing diversity gain in various types of wireless communication systems, including next-generation mobile communication systems [7-9], such as 3rd Generation Partnership Project (3GPP) Long Term Evolution-Advanced (LTE-A).

One of the main challenges faced by the 3GPP LTE-A standard is providing high throughput to cell edge users. Cell edge performance is becoming more important as cellular systems employ higher bandwidths with the same amount of transmit power and use higher carrier frequencies with infrastructure designed for lower carrier frequencies. One solution to improve coverage is to use the fixed relays to transmit data between the Base Stations (BSs) and Mobile Stations (MSs) through multi-hop communication. For this reason, relay technologies have been actively studied and considered in the standardization process of next-generation mobile broadband communication systems. As a next-generation 3GPP standard, LTE-A exclusively takes the relay technology into account [10].

The relaying protocols for cooperative wireless communication systems can be generally categorized into fixed relaying schemes and adaptive relaying schemes. Fixed relaying has the advantage of easy implementation, but the disadvantage of low bandwidth efficiency. This is because half of the channel resources are allocated to the relay for transmission, which reduces the overall rate. This is true especially when the source–destination channel is not very bad, because in such a scenario a high percentage of the packets transmitted by the source to the destination could be received correctly by the destination and this result in waste of channel resources allocated to source-relay channel. The inefficient utilization of the channel resources in cooperative diversity networks using fixed relaying can be enhanced by using adaptive relaying protocols, comprising selective and incremental relaying. In fixed relaying, the channel resources are divided between the source and the relay in a fixed (deterministic) manner. The processing at the relay differs

according to the employed protocol, such as AAF, DAF, Selective Relaying (SR) [11-17], coded cooperative [18] and Compress-And-Forward (CAF). As common in these schemes, the cooperative transmissions are initiated by first having the source node broadcasts the data signal to both the relay node and the destination node. If the AAF scheme is employed, the relay node simply amplifies the received signal and forwards it directly to the destination node without explicitly decoding the message. If the DAF scheme is employed, the relay will decode and regenerate a new message which will be transmitted to the destination in the subsequent time slot. At the destination, signals from both the source and the relay are combined to provide better detection performance. As an extension to the DAF scheme, the message generated by the relay can be re-encoded to provide additional error protection, this type of relaying protocols can be referred to as coded cooperative relaying.

This paper proposes a coded cooperative relay based OFDM wireless communication system. Investigations are focused on evaluating the performance of the proposed system over AWGN and different SUI channel models using different Forward Error Correction (FEC) codes i.e., native rate 1/2 convolution code and rate 1/3 turbo code. The performance of the proposed coded cooperative system is evaluated using MATLAB simulations and compared with direct transmission and other cooperative protocols i.e., AAF and DAF.

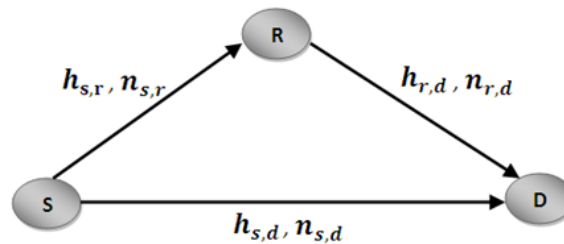


Figure1: A Single Relay Cooperative Model [11]

The rest of the paper is organized as follows. In section II, we introduce a system model of the proposed system include single relay cooperative model with OFDM transceiver structure. Description of FEC code schemes including convolutional code and turbo code is presented in Section III. The simulation model of the proposed coded cooperative communication system is presented in Section IV. Section V shows the MATLAB simulation results, followed by conclusions in Section VI.

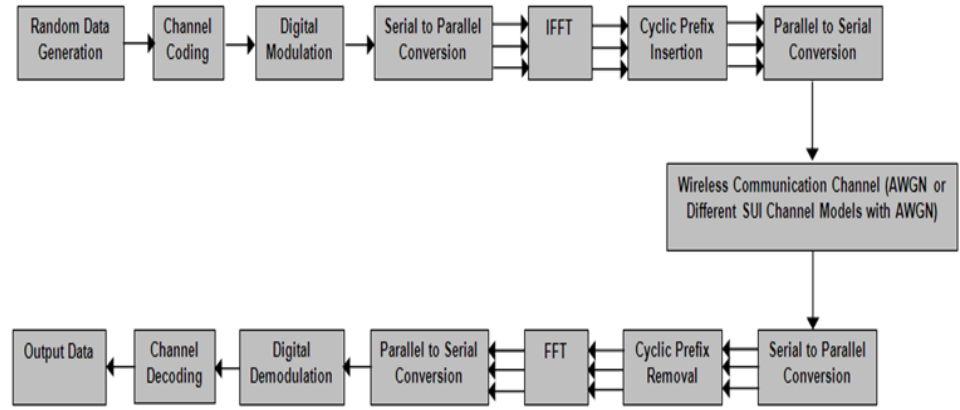


Figure 2: OFDM Transceiver Structure [23]

2. SYSTEM MODEL

Consider a wireless communication system as shown in Fig.1 with one source node S which communicates with a destination node D through relay node R . The source node broadcasts the information symbols to both the destination and the relay. The received signals $y_{s,d}$ and $y_{s,r}$ at the destination node and the relay node, respectively, can be written as [11].

$$y_{s,d} = \sqrt{p} h_{s,d} x + n_{s,d} \quad (1)$$

$$y_{s,r} = \sqrt{p} h_{s,r} x + n_{s,r} \quad (2)$$

Where, p is the transmitted power at the source, x is the transmitted information symbol, $n_{s,d}$ and $n_{s,r}$ are additive noise, $h_{s,d}$ and $h_{s,r}$ are the channel coefficients from the source to the destination and from the source to the relay, respectively. The channel coefficients $h_{s,d}$, $h_{s,r}$ are modeled as zero-mean complex Gaussian random variables with variances $\delta_{s,d}^2$, $\delta_{s,r}^2$ respectively. The noise terms $n_{s,d}$ and $n_{s,r}$ are modeled as zero-mean complex Gaussian random variables with variance N_0 . The relay node forwards a processed version of the information symbols received from the source node to the destination and this can be modeled as [11]:

$$y_{r,d} = Q(y_{s,r}) h_{r,d} + n_{r,d} \quad (3)$$

Where, the function $Q(\cdot)$ depends on the cooperative protocol implemented at the relay node, $h_{r,d}$ is the channel coefficient from relay to destination and $n_{r,d}$ is an additive noise [11].

In order to evaluate the performance of the proposed coded cooperative OFDM based wireless communication system we considered transmission over both AWGN channel and different SUI channel models with AWGN. SUI channel models are an extension of the earlier work by AT&T wireless and Erceg et. al [19]. In this model a set of six channels was selected to address three different terrain types that are typical of the continental US [20]. This model can be used for simulations, design and development and testing of technologies suitable for fixed broadband wireless applications. More details of the channel parameters for different SUI channel models are given in [21].

The proposed coded cooperative system is based on OFDM. In last decades, OFDM based communication systems have been identified as one of the key transmission techniques for next generation wireless communication systems [22]. The main attractions of OFDM are spectrum efficiency, handling the multi-path interference and mitigate Inter-Symbol Interference (ISI) which causing higher BER in frequency selective fading environments [23].

The spectrum efficiency of OFDM based wireless communication systems can be achieved by using orthogonal subcarriers and the ISI can be eliminated by adding a guard interval. Figure 2 shows the block diagram of OFDM transceiver structure that is implemented at each node of the proposed single relay cooperative model. Channel coding becomes an indivisible part in most OFDM based wireless communication systems and a significant amount of research work has focused on optimum encoder, decoder and interleaver design for information transmission over multipath fading channels. The channel coding is used in wireless communication systems to provide high data rates over severe multipath fading channels. In OFDM based wireless communications systems, several error-correction codes have been applied such as convolutional codes, Reed-Solomon (RS) codes and turbo codes.

3. FORWARD ERROR CORRECTION (FEC) CODES

In wireless communication systems, errors in data transmission come from many different sources i.e., random noise, interference, channel fading and physical defects. These channel errors must be reduced to an acceptable level to ensure reliable data transmission. To combat errors, two main strategies can be used either stand-alone or combined. The first one is the Automatic Repeat Request (ARQ). An ARQ system attempts to detect the presence of errors in the received data. If any errors are found, the receiver notifies the transmitter of the existence of errors. The transmitter then resends the data until they are correctly received. The second strategy, known as the Forward Error Correction (FEC), the FEC not only detects the errors but also corrects them, so that errors in data retransmission can be avoided. In many practical applications retransmission may be difficult or not even feasible at all. For example, it is impossible for any receiver in a real-time broadcasting system to request data to be resent. In this case, FEC is the only viable solution [24]. There are several FEC codes available. However, popular used FEC codes are Cyclic Redundancy Check (CRC) code, convolutional code and turbo code. In this section the convolutional and turbo codes are discussed in more details.

A. CONVOLUTIONAL CODE

Before the introduction of turbo codes, power efficient communications was achieved by either using strong convolutional code or using a serial concatenation of a convolutional code and block code. Convolutional codes were first introduced by Elias in 1955 [25]. Since then they have gained vast popularity in practical applications. The convolutional codes are not only equal or sometimes even superior to block codes in performance but also provide relatively simpler decoding process. A convolutional code adds redundancy to a continuous stream of input data by using a linear shift register. A convolutional code is specified by three parameters: the codeword length n , the message length k , and the constraint length v which is the total number of bits that each output depends on. The constraint length of a convolutional code depends on the memory depth of the code m [26].

$$v=m+1 \quad (4)$$

For a rate k/n convolutional encoder, each set of n output symbols is a linear combination of the current set of k input bits and m bits stored in the shift register. The convolutional encoder used in this paper has native rate of $1/2$, a constraint length of 7 and two generator polynomials as given in Equations (5) and (6). The outputs of the convolutional encoder are the two codeword bits X and Y as shown in Fig.3 [26].

$$G_1 = 171_{OCT} \quad \text{For X} \quad (5)$$

$$G_2 = 133_{OCT} \quad \text{For Y} \quad (6)$$

The encoded data output from the convolutional encoder are interleaved by a block interleaver. The size of the block is depended on the numbers of bit encoded per subchannel in one OFDM symbol. In IEEE 802.16, the interleaver is defined by two step permutation. The first permutation ensures that adjacent coded bits are mapped onto nonadjacent subcarriers. The second permutation ensures that adjacent coded bits are mapped alternately onto less or more significant bits of the constellation, thus avoiding long runs of unreliable bits [26].

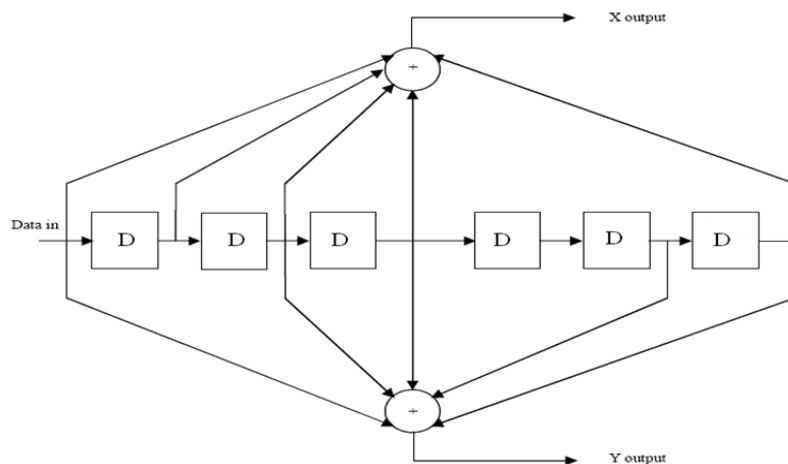


Figure 3: Structure of Rate 1/2 Convolutional Encoder [26]

B. TURBO CODE

Turbo code is a form of FEC codes that is used to improve the channel capacity. The turbo encoder scheme used in this paper is a Parallel Concatenated Convolutional Code (PCCC) with two identical 8-state

Recursive Systematic Convolutional (RSC) encoders and a contention-free Quadratic Permutation Polynomial (QPP) internal interleaver as shown in Fig.4. The RSC encoder has a rate equals 1/2 and is termed a constituent encoder. The input to the first constituent encoder is the input bit stream to the turbo encoder and the input to the second constituent encoder is the output of the QPP interleaver which is a permuted version of the input bit stream.

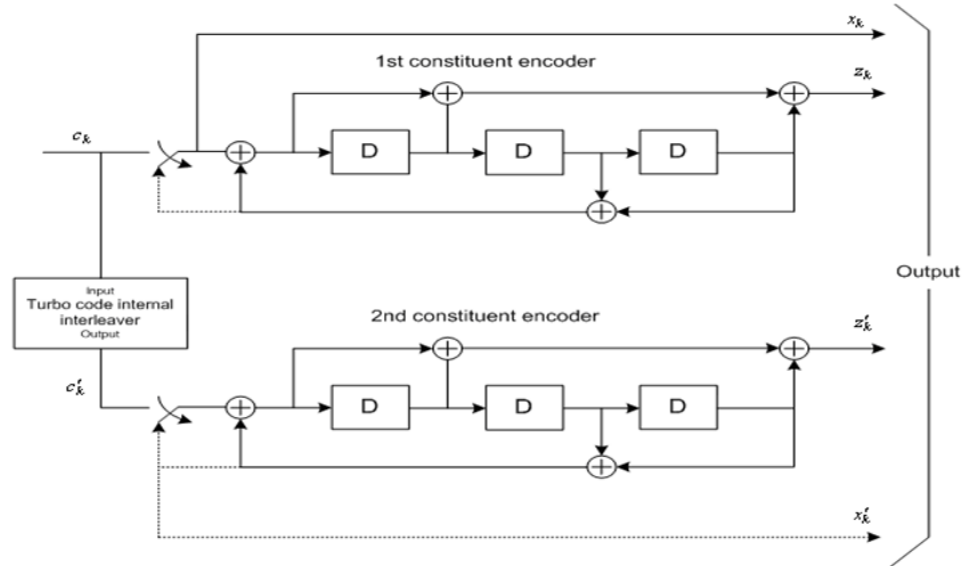


Figure 4: Structure of Rate 1/3 Turbo Encoder (dotted lines apply for trellis termination only) [27]

The coding rate of turbo encoder is 1/3 and the transfer function of the 8-state constituent encoder is given by [27]:

$$G(D) = \begin{bmatrix} 1 & g_1(D) \\ & g_0(D) \end{bmatrix} \quad (7)$$

Where,

$$g_0(D) = 1 + D^2 + D^3 \quad (8)$$

$$g_1(D) = 1 + D + D^3 \quad (9)$$

The input bits to the turbo encoder are denoted by $c_0, c_1, c_2, c_3, \dots, c_{K-1}$, and the bits output from the first and second 8-state constituent encoders are

denoted by $z_0, z_1, z_2, z_3, \dots, z_{K-1}$ and $z'_0, z'_1, z'_2, z'_3, \dots, z'_{K-1}$, respectively. The bits output from the turbo code internal interleaver are denoted by $c'_0, c'_1, \dots, c'_{K-1}$, and these bits are the input bit stream to the second 8-state constituent encoder, where K is the number of input bits. The output of the QPP interleaver is a permuted version of the input data, the relationship between the QPP interleaver input and output bits is given as follows[27]:

$$c'_i = c_{\Pi(i)}, i=0, 1, 2 \dots (K-1) \quad (10)$$

Where, the relationship between the output index i and the input index $\Pi(i)$ satisfies the following quadratic form [27]:

$$\Pi(i) = \left(f_1 \cdot i + f_2 \cdot i^2 \right) \bmod K \quad (11)$$

The parameters f_1 and f_2 depend on the block size K [27]. In a normal convolutional encoder, the encoder is driven to an all zero state upon termination by appending zeros onto the end of the input data stream. As the decoder knows the start and end state of the encoder it can decode the data. Driving a RSC encoder to an all zeros state using this method is not possible. To overcome this problem trellis termination is used. Upon termination the tail bits are fed back to the input of each encoder using a switch. The first three tail bits are used to terminate each encoder.

4. SIMULATION MODEL

This section presents the simulation model and discusses the simulation results. As we have stated before, our research goal is to evaluate the performance of coded cooperative relay based OFDM wireless communication system. The system model and block diagram of transceiver structure at each node are shown in Figures 1&2. We have employed MATLAB to write a computer program designed for simulation of the proposed system to allow various parameters of the system to be varied and tested. The possible considered parameters and their corresponding values are given in Table 1.

Table 1: Simulation Parameters [23]

Parameters	Values
System Bandwidth	5 MHz
Sampling Rate	5 Mega-Samples per Second
Digital Modulation	QPSK
IFFT Size	512
Cyclic Prefix Length	20 Samples (4 μ s)
Subcarrier Spacing	9.765625 kHz
Considered Channels	AWGN, Different SUI Channel
FEC Codes	Convolutional ,Turbo
Convolutional Code Rate	1/2
Convolutional Code Decoding	Viterbi Decoding
Turbo Code Rate	1/3
Turbo Decoding	Log-MAP
Maximum Turbo Decoder	10
Channel Equalization	Minimum Mean Square Error

In order to evaluate the performance of the proposed coded cooperative system we considered transmission over AWGN and for multipath channel, we consider different SUI channel models with AWGN. The SUI models are divided into three types of terrains, namely A, B and C. Type A is associated with maximum path loss and is appropriate for hilly terrain with moderate to heavy foliage densities. Type C is associated with minimum path loss and applies to flat terrain with light tree densities. Type B is characterized with either mostly flat terrains with moderate to heavy tree densities or hilly terrains with light tree densities. The SUI-1, SUI-2 and SUI-3 models are applicable for Line-of-Sight (LOS) conditions, and SUI-4, SUI-5 and SUI-6 models are applicable for Non-Line-of-Sight (NLOS) conditions. The SUI-1 and SUI-2 models classified as Terrain Type C , The SUI-3 and SUI-4 models classified as Terrain Type B, and The SUI-5 and SUI-6 models classified as Terrain Type A. Our simulation model based only on three SUI channel models SUI-1, SUI-2 and SUI-3 which cover terrains B and C. In the simulation model the length of the Cyclic Prefix (CP) is 20 samples (4 μ s) considering maximum channel delay of the SUI-2 channel model, which is 1.1 μ s.

The channel delay profiles of the different SUI channel models are given in Table 2.

Table 2: SUI Channel Models' Parameters [21]

Channel Model		Tap 1	Tap 2	Tap 3
SUI-1	Delay (μ S)	0	0.4	0.9
	Power (dB)	0	-15	-20
SUI-2	Delay (μ S)	0	0.4	1.1
	Power (dB)	0	-12	-15
SUI-3	Delay (μ S)	0	0.4	0.9
	Power (dB)	0	-5	-10
SUI-4	Delay (μ S)	0	1.5	4
	Power (dB)	0	-4	-8
SUI-5	Delay (μ S)	0	4	10
	Power (dB)	0	-5	-10
SUI-6	Delay (μ S)	0	14	20
	Power (dB)	0	-10	-14

5. SIMULATION RESULTS AND DISCUSSION

In this section the simulation results are shown and discussed. MATLAB have been employed to write a computer program designed for simulation of the proposed system to allow various parameters of the system to be varied and tested. The parameters that can be set at the time of initialization are the number of simulated OFDM symbols, CP length, modulation, coding rate, range of SNR values and SUI channel models. Considered that the input data stream to the proposed system is randomly generated. For performance evaluation of the proposed coded cooperative system, the BER and spectral efficiency are commonly used as performance metrics. Considered three scenarios for simulations:

- 1) Direct transmission (without relay), this scenario has only a direct link from source node to destination node.
- 2) Non-Cooperative, this scenario has two hops from source to destination, one from source to relay and the other one form relay to destination.
- 3) Cooperative transmission, in this scenario the source node first broadcasts the data symbols to both relay node and destination node. Based on the protocol implemented at the relay node, the relay node process and retransmits the signal received from source to destination.

In this case the destination node receives two resultant signals that can be combined using appropriate combining technique.

The BER performance of the proposed OFDM based coded cooperative system using either native rate 1/2 for convolutional code and rate 1/3 for turbo code is compared with other cooperation protocols and with direct transmission considering transmission over both AWGN and different SUI channel models. Figures 5, 6 show the performance comparisons between coded and uncoded OFDM based system considering direct transmission over both AWGN and SUI-3 channel mode in terms of BER. The results show that, the BER of AWGN channel gives better performance as compared to SUI-3 channel model. The results also show that, the BER of rate 1/3 turbo code and rate 1/2 convolutional code give better performance compared with uncoded transmission (i.e., in case of SUI-3 channel model for $BER=10^{-2}$ the rate 1/3 turbo code required SNR=15.1 dB compared to SNR=21 dB for convolutional code and SNR=23.2 for uncoded scenario, direct transmission using rate 1/3 turbo code achieved 5.9 dB SNR gain compared to convolutional code and 8.1 dB SNR gain compared to uncoded scenario).

Figures 7, 8 show the performance comparisons between different non-cooperative protocols of OFDM based system considering transmission over both AWGN and SUI-3 channel model in terms of BER. The results show that, using relay node in the non-cooperative protocols improve performance of the system compared to direct transmission scenario for both AWGN and SUI-3 channel model. The results also show that, the non-cooperative scenario using rate 1/3 turbo code and rate 1/2 convolutional code give better performance compared with AAF and DAF non-cooperative scenarios (i.e., in case of SUI-3 channel model for $BER=10^{-2}$ the rate 1/3 turbo code non-cooperative transmission required SNR=10.9 dB compared to SNR=17 dB for convolutional code, SNR=19.9 for DAF and SNR=31 for AAF non-cooperative protocols) non-cooperative transmission using rate 1/3 turbo code achieved 6.1 dB SNR gain compared to non-cooperative rate transmission using 1/2 convolutional code and 9dB SNR gain compared non-cooperative DAF and 20.1 dB SNR gain compared to non-cooperative AAF scenario). Comparing the performance of direct transmission and non-cooperative transmission scenarios over SUI-3 channel model using rate 1/3 turbo code, the results show that non-cooperative scenario achieved 4.2 dB SNR gain compared to direct transmission scenario.

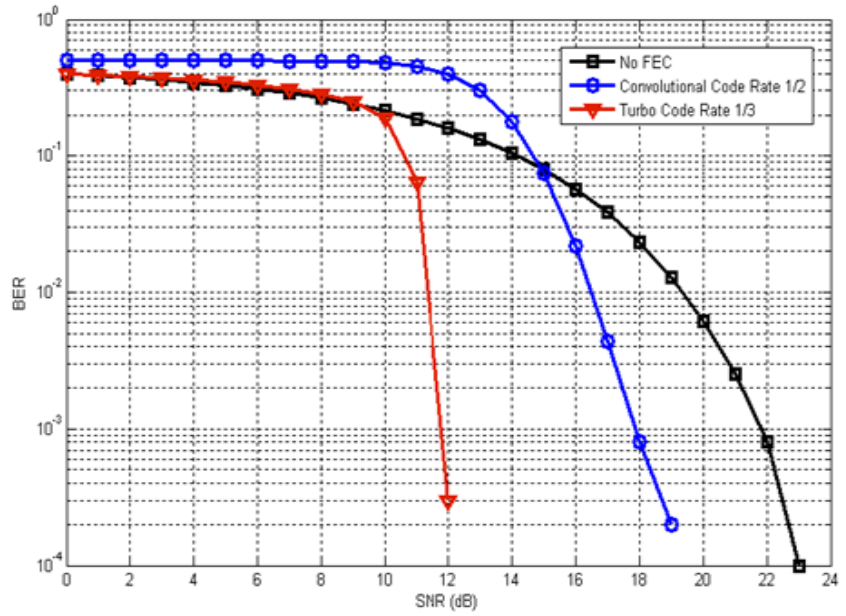


Figure 5: Performance Comparison between Coded and Uncoded OFDM based Direct Transmission over AWGN

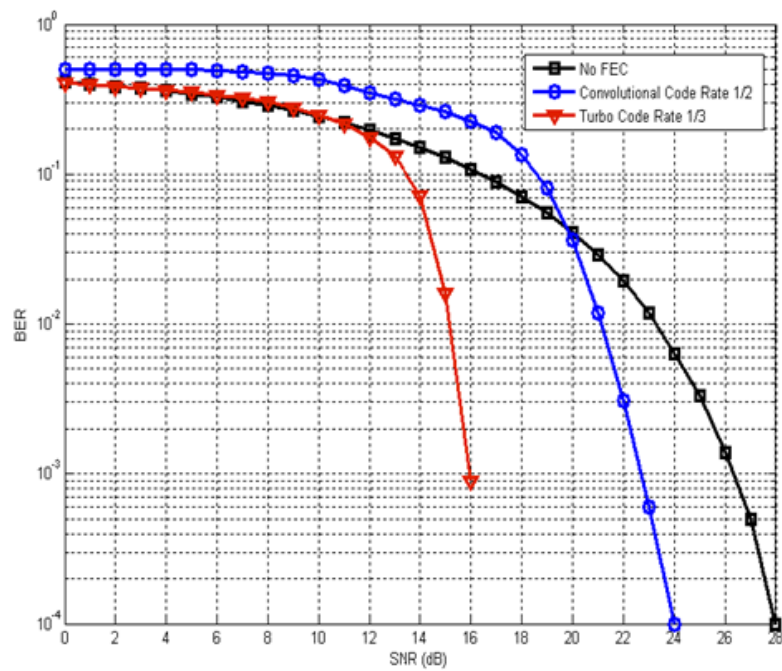


Figure 6: Performance Comparison between Coded and Uncoded OFDM based Direct Transmission System over SUI-3 Channel Model

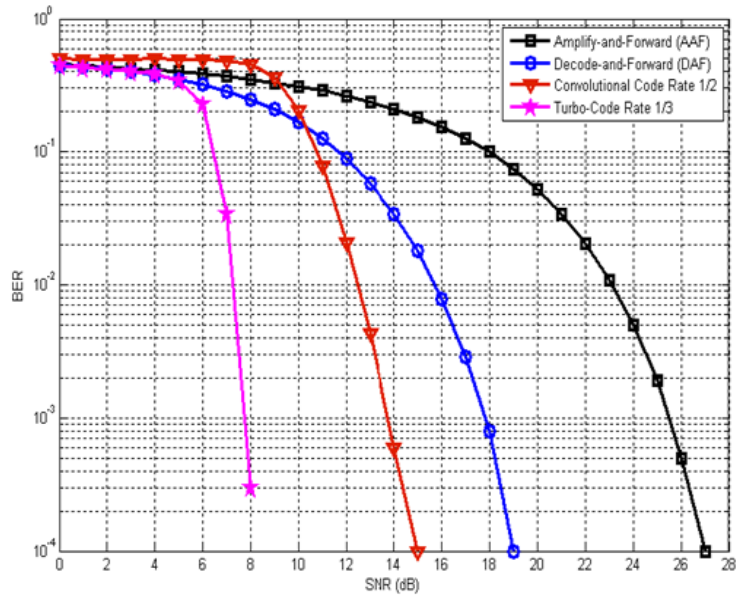


Figure 7: Performance Comparison between Different Non-Cooperative Protocols of OFDM Based System Considering Transmission over AWGN

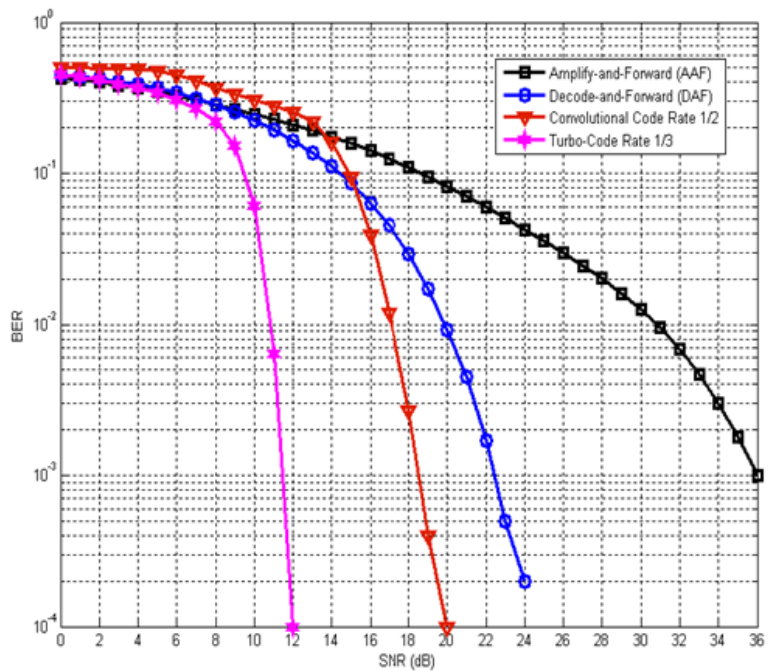


Figure 8: Performance Comparison between Different Non-Cooperative Protocols of OFDM Based System Considering Transmission over SUI-3 Channel Model

Figures 9 and 10 show the performance comparisons between different OFDM based cooperative protocols considering transmission over both AWGN and SUI-3 channel model in terms of BER. These figures conclude that, the BER of cooperative protocols gives better performance compared to direct transmission and non-cooperative protocols considering transmission over both AWGN channel and SUI-3 channel model. Also, we can observe that the proposed coded cooperative system using rate 1/2 convolutional code and rate 1/3 turbo code give better performance compared to other cooperative protocols i.e., AAF and DAF and the performance of coded cooperative system using rate 1/3 turbo code is better compared to coded cooperative system using rate 1/2 convolutional code.

Comparing the performance of direct transmission, non-cooperative transmission and cooperative transmission scenarios over SUI-3 channel model using rate 1/3 turbo code, the results show that cooperative scenario achieved 1.9 dB SNR gain compared to non-cooperative transmission scenario and 6.1 dB SNR gain compared to direct transmission scenario. The SNR levels required to attain BER of 10^{-2} for different cooperative protocols are summarized in Table 3, considering transmission over AWGN and SUI-3 channel model.

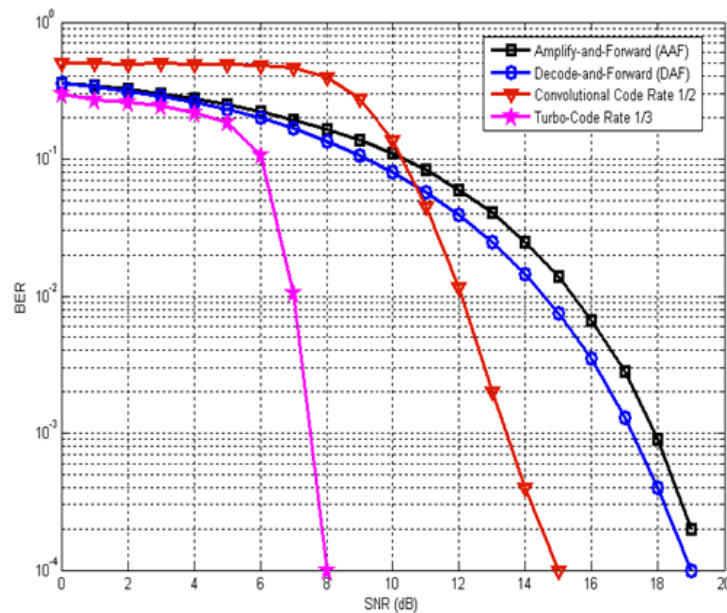


Figure 9: Performance Comparison Between Different Cooperative Protocols of OFDM Based System Considering Transmission over AWGN

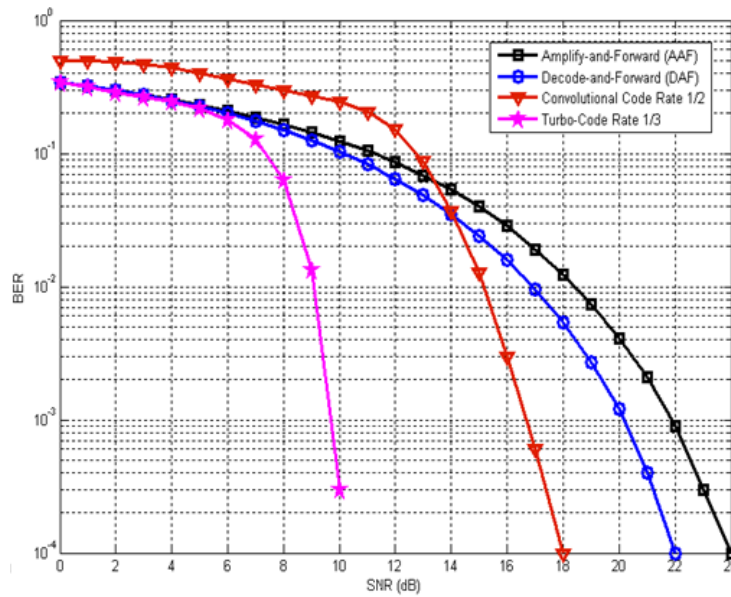


Figure 10: Performance Comparison between Different Cooperative Protocols of OFDM Based System Considering Transmission over SUI-3 Channel Model

Table.3: SNR Required at BER Level 10^{-2} for Direct, Non-Cooperative and Cooperative Scenarios

Transmission Type	Channel Type	Coding Type	SNR (dB) at BER Level 10^{-2}
Direct	AWGN	No-FEC	19.3
		Convolutional code Rate 1/2	16.5
		Turbo Code rate 1/3	11.3
	SUI-3	No-FEC	23.2
		Convolutional code Rate 1/2	21
		Turbo Code rate 1/3	15.1
Non-Cooperative	AWGN	Amplify and Forward (AAF)	23
		Decode and Forward (DAF)	15.8
		Convolutional code Rate 1/2	12.5
		Turbo Code rate 1/3	7.3
	SUI-3	Amplify and Forward (AAF)	31
		Decode and Forward (DAF)	19.9
		Convolutional code Rate 1/2	17
		Turbo Code rate 1/3	10.9
Cooperative	AWGN	Amplify and Forward (AAF)	15.5
		Decode and Forward (DAF)	14.6
		Convolutional code Rate 1/2	12
		Turbo Code rate 1/3	7
	SUI-3	Amplify and Forward (AAF)	18.5
		Decode and Forward (DAF)	17
		Convolutional code Rate 1/2	15.1
		Turbo Code rate 1/3	9

Figures 11, 12, 13, 14 show the performance of different cooperative protocols over different SUI channel models. The results show that the cooperative transmission using rate 1/3 turbo code required lower SNR levels compared to AAF, DAF and coded cooperative transmission using rate 1/2 convolutional code. From these figures it is also clear that the BER performance is better in the case of SUI-1 and SUI-2 channel models when compared to SUI-3 channel model this is because the SUI-3 channel model is a type B terrain with either mostly flat terrains with moderate to heavy tree densities or hilly terrains with light tree densities compared to SUI-1 and SUI-2 channel models which are type C flat terrain with light tree densities (SUI-3 channel model has highest tap power when compared to SUI-1 and SUI-2 channel models as given in Table.2). the results also show that, for rate 1/3 cooperative transmission the SUI-1 channel model achieved .3 dB SNR gain compared to SUI-2 channel model and .6 dB SNR gain compared to SUI-3 channel model. The SNR levels required to attain BER of 10^{-3} for different cooperative protocols are summarized in Table.4, considering transmission over different SUI channel models.

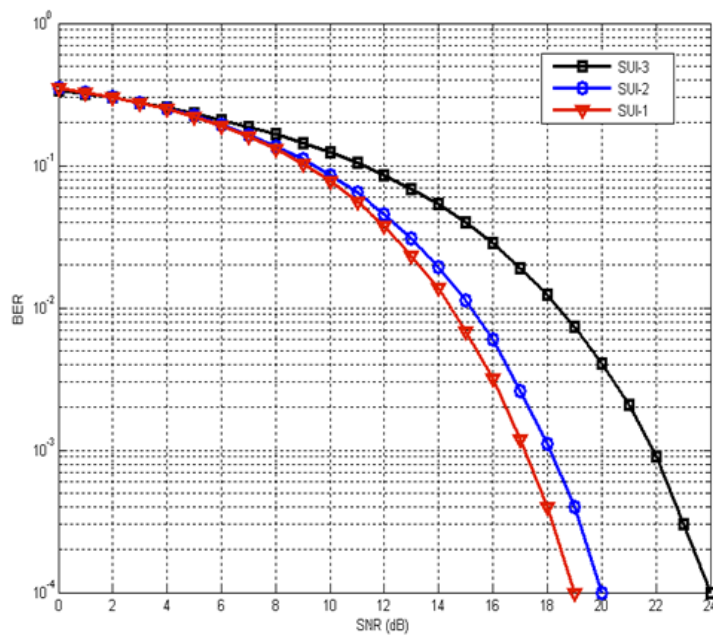


Figure 11: Performance of AAF Cooperative Protocol on Different SUI Channel Models

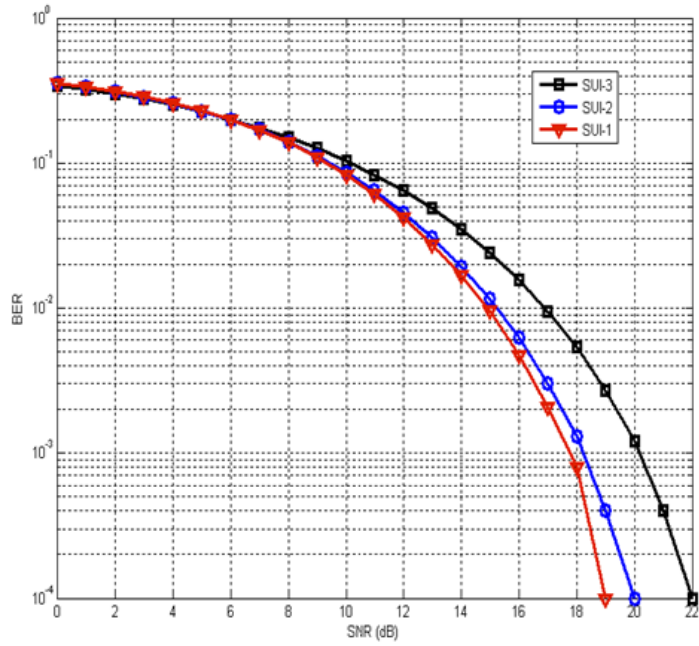


Figure12: Performance of DAF Cooperative Protocol on Different SUI Channel Models

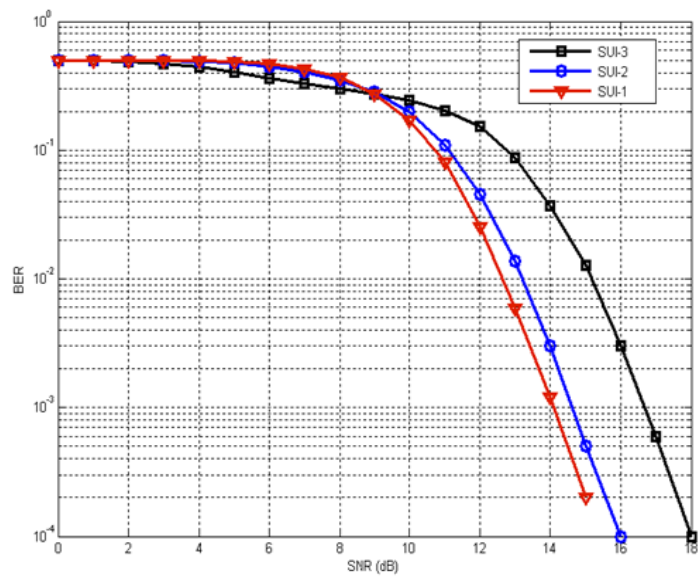


Figure13: Performance of Coded Cooperative Protocol Using Rate 1/2 Convolutional Code on different SUI Channel Models

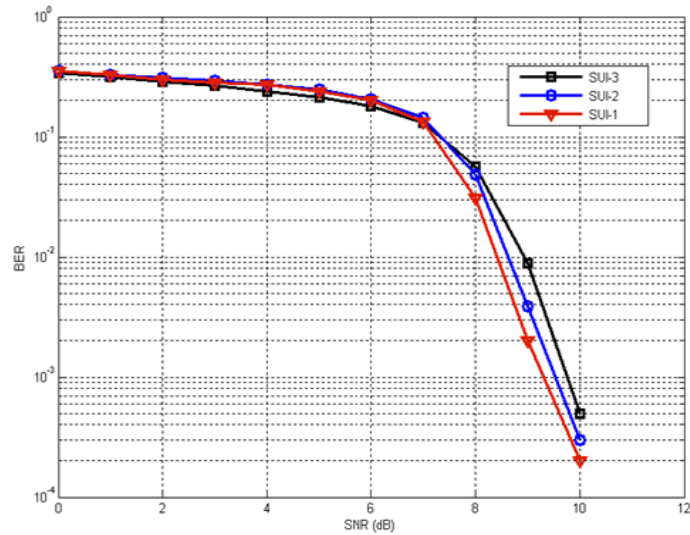


Figure 14: Performance of Coded Cooperative Protocol Using Rate 1/3 Turbo Code on different SUI Channel Models

Table .4: SNR Level Required to Attain BER Level 10^{-3} for Different Cooperative Protocols Considering Transmission over Different SUI Channel models

Cooperative Protocol	SUI-3	SUI-2	SUI-1
Amplify and Forward (AAF)	21.9	18	17.2
Decode and Forward (DAF)	20.1	18.1	17.8
Convolutional code Rate 1/2	16.8	14.7	14
Turbo Code rate 1/3	9.8	9.6	9.4

Figures 15, 16 , 17 show the spectral efficiency in bps/Hz (which is defined as the information rate that can be transmitted over a given bandwidth in a specific communication system [28]) of different transmission scenarios considering transmission over SUI-3 channel model.. From these figures it is clear that, the coded cooperative transmission improved spectral efficient compared to direct transmission and non-cooperative transmission. The results also show that the cooperative transmission using rate 1/3 turbo code required SNR level lower than that required for DAF cooperative transmission and coded cooperative transmission using rate 1/2 convolutional code. The SNR level required to attain. 5 b/s/Hz spectral efficiency level for different

transmission scenarios are tabulated in Table.5 considering transmission over SUI-3 channel model.

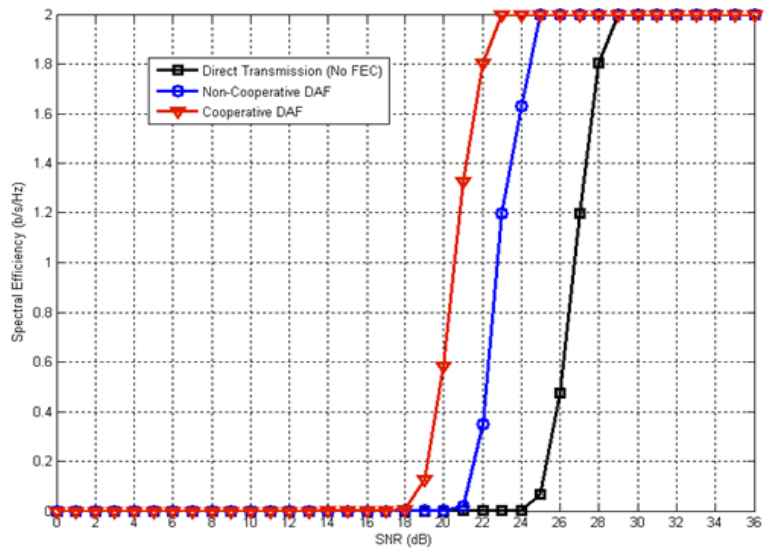


Figure15: Spectral Efficiency of Different Transmission Scenarios Considering No FEC and Transmission over SUI-3 Channel Model

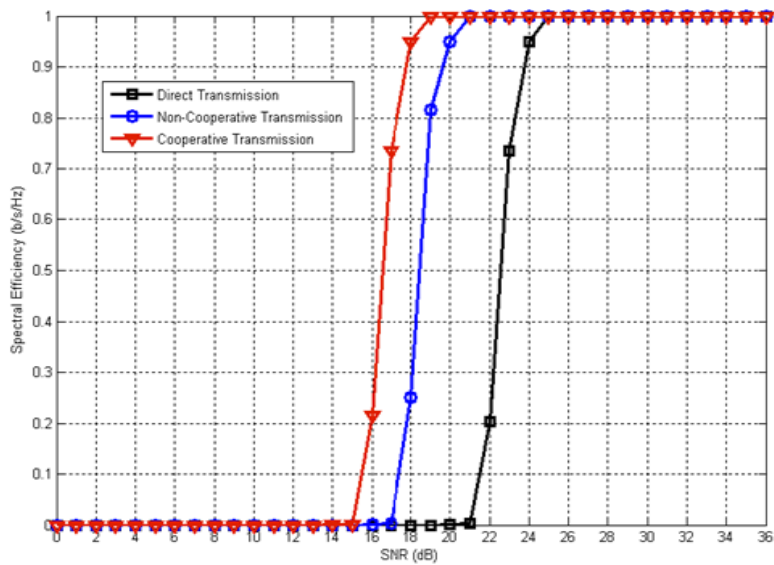


Figure16: Spectral Efficiency of Different Transmission Scenarios Considering Convolutional Code and Transmission over SUI-3 Channel Model

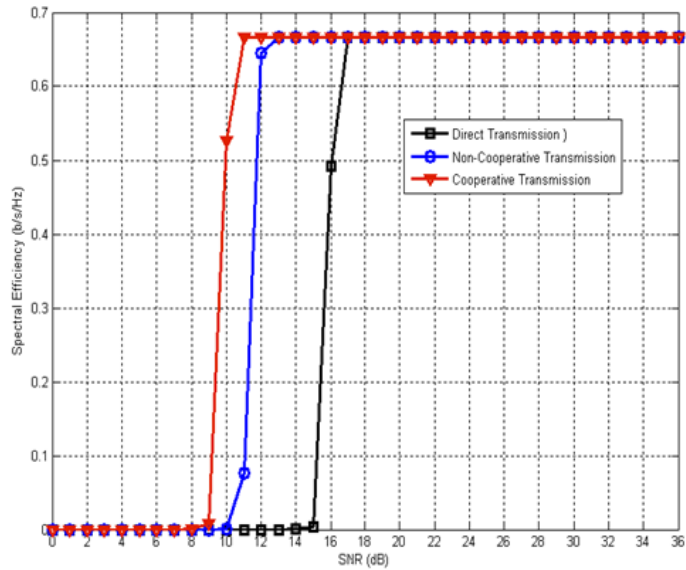


Figure 17: Spectral Efficiency of Different Transmission Scenarios Considering Turbo Code and Transmission over SUI-3 Channel Model

Table 5: SNR Level Required to Attain Spectral Efficiency Level 5 b/s/Hz for Different Transmission Scenarios Considering Transmission over SUI-3Channel Model

Transmission Type	No-FEC	Rate 1/2 Convolutional Code	Rate 1/3 Turbo Code
Direct Transmission	26	22.5	16
Non-Cooperative	22	18.5	11.9
Cooperative	20	16.6	10

6. CONCLUSION

In this paper, the performance of coded cooperative relay based OFDM wireless communication system based on native rate 1/2 convolutional code and rate 1/3 turbo code has been investigated. The BER performance of the proposed coded cooperative system using native rate 1/2 convolutional code and rate 1/3 turbo code is compared with direct transmission and other cooperation protocols i.e., AAF and DAF

considering transmission over both AWGN and different SUI channel models. The results show that the proposed coded cooperative system achieves lower SNR values for desired BER and achieves high spectral efficiency as compared to direct transmission, AAF and DAF based cooperative protocols. The results also show that the cooperative transmission using rate 1/3 turbo code outperforms the performance of cooperative transmission using rate 1/2 convolutional code in terms of both BER and spectral efficiency

References

- [1] M. K. Simon and M.-S. Alouini, "Digital Communication over Fading Channels," 2nd edition. New York: Wiley, 2005.
- [2] Rohit U. Nabar, Helmut Bölcskei, and Felix W. Kneubühler, "Fading Relay Channels: Performance Limits and Space-Time Signal Design," *IEEE JSAC*, vol. 22, no. 6, Aug 2004.
- [3] A. Nosratinia, T. E. Hunter, and A. Hedayat, "Cooperative communication in wireless networks," *IEEE Communications Magazine*, vol. 256, pp. 74-80, Oct. 2004.
- [4] Q Zhang, J Jia, and J Zhang, "Cooperative Relay to Improve Diversity in Cognitive Radio Networks," *IEEE Communications Magazine*, pp. 111-117, Feb. 2009.
- [5] T. E. Hunter, and A. Nosratinia, "Diversity through coded cooperation," *Proc. of IEEE International Symposium on Information Theory*, vol. 220, 2002.
- [6] M. Janani, A. Hedayat, T. E. Hunter and A. Nosratinia, "Coded cooperation in wireless communications: Spacetime transmission and iterative decoding," *IEEE Trans. Signal Process.*, vol. 52, pp. 362-372, Feb. 2004.
- [7] T Beniero, S Redana, J Hämäläinen, B Raaf, "Effect of Relaying on Coverage in 3GPP LTE-Advanced," *IEEE 69th Vehicular Technology Conference, VTC Spring 2009, Barcelona*.
- [8] S. W. Peters and R. W. Heath Jr, "The future of WiMAX: Multi-hop relaying with IEEE 802.16j," *IEEE Communications Magazine*, vol. 1, no. 47, 2009.
- [9] D. Soldani and S. Dixit, "Wireless relays for broadband access," *Communications Magazine, IEEE*, vol. 46, no. 3, pp. 58-66, 2008.
- [10] A Lo, and I Niemegeers, "Multi-hop Relay Architectures for 3GPP LTE-Advanced," *Proceedings of the 2009 IEEE 9th Malaysia International Conference on Communications*, pp 15 -17, Dec. 2009., Kuala Lumpur, Malaysia.

- [11] K. J. Ray Liu, Ahmed K. Sadek, Weifeng SU and Andres. Kwasinski, "Cooperative Communications and Networking," Cambridge University, 2009.
- [12] Y.-W. Peter Hong, Wan-Jen Huang, and C.-C. Jay Kuo, "Cooperative Communications and Networking Technologies and System Design," Springer, 2010.
- [13] J. N. Laneman, D. N. C. Tse, and G. W. Wornell, "Cooperative diversity in wireless networks: low-complexity protocol and outage behavior," IEEE Transactions on Information Theory, vol. 50, no. 12, pp. 3062-3080, Dec. 2004.
- [14] S. Viqar, S. Ahmed, Z. ul Mustafap and W. Ejaz, "Performance Analysis of Cooperative Communication System with a SISO system in Flat Fading Rayleigh channel," IACSIT, Vol.42, no.4, pp.228-233,2012.
- [15] S.Y. Ameen, M. K. Yousif , "Decode and Forward Cooperative Protocol Enhancement Using Interference Cancellation," World Academy of Science, Engineering and Technology International Journal of Electrical, Computer, Energetic, Electronic and Communication Engineering, Vol:8, No:2, 2014.
- [16] R. Titus, Unnikrishnan M, Premkumar C.V, "A Survey on Incremental Relaying Protocols in Cooperative Communication," International Journal of Research in Engineering and Technology (IJRET), Vol. 03, No. 15, Dec-2014.
- [17] K. Narayanan , B. Shafeek International , "Performance Analysis of Cooperative OFDM Systems," International Journal of Advanced Research in Electrical, Electronics and Instrumentation (IJAREEIE), Vol. 3, No. 3, April 2014.
- [18] J. N. Laneman and G. W. Wornell, "Distributed space-time coded protocols for exploiting cooperative diversity in wireless networks," IEEE Transactions on Information Theory, vol. 49, pp. 2415–2525, Oct.2003.
- [19] Bernard Sklar, "Digital Communications: Fundamentals and Applications, "2nd Edition," January 11, 2001.
- [20] V. Erceg, "An empirically based path loss model for wireless channels in suburban environments," IEEE JSAC, vol. 17, no. 7, July 1999, pp. 1205-1211.
- [21] V. Erceg, K.V.S. Hari, M.S. Smith, D.S. Baum et al, "Channel Models for Fixed Wireless Applications", IEEE 802.16.3 Task Group Contributions , Feb. 2001.
- [22] S. Hara and R. Prasad, "Multicarrier Techniques for 4G Mobile Communications," Artech House, first edition, 2003.
- [23] M. Engels, "Wireless OFDM Systems: How To Make Them Work," Kluwer Academic Publishers, 2002.
- [24] Y. Jiang, "A Practical Guide to Error-Control Coding Using MATLAB," Artech House, 2010.

- [25] Elias , “Coding for Noisy Channels,” IRE Conv. Rec., Part 4, 1955, pp. 37–47.
- [26] IEEE 802.16-2004, “ IEEE Standard for Local and Metropolitan Area Networks Part 16: Air Interface for Fixed Broadband Wireless Access Systems,” 1 October, 2004.
- [27] 3GPP TS 36.212 V9.1.0 (2010-03), pp.12-14.
- [28] Keenan, T, Villing, R , “Maximising spectral efficiency in LTE cells,” Signals and Systems Conference (ISSC 2012), IET Irish, pp. 28-29, June 2012.

ملخص البحث

تم في هذا البحث دراسة اداء نظام الاتصال اللاسلكى المعتمد على تكنولوجيا التتابع والتعاون باستخدام العديد من طرق التشفير منها (rate 1/3 turbo code and rate 1/2 convolutional code) مع الاخذ فى الاعتبار العديد من نماذج قنوات الاتصال منها (AWGN & SUI-channel models) . ولتقييم اداء النظام المفترض تم عمل محاكاة للنظام باستخدام برامج الكمبيوتر باستخدام لغة البرمجة (Matlab). تم مقارنة اداء نظام التتابع والتعاون المفترض مع العديد من الانظمة منها نظام التكبير والبث ونظام تفكيك التشفير والبث وذلك مع الاخذ فى الاعتبار العديد من نظم الاتصال منها نظام الاتصال المباشر من المرسل الى المستقبل ونظام الاتصال غير المباشر عن طرق استخدام احد نقاط التتابع وتمت المقارنة باستخدام طرق التشفير المقترحة وبدون استخدامها. ولقد اظهرت النتائج أن نظام التتابع والتعاون باستخدام طرق التشفير المقترحة يحقق اقل معدل اخطاء فى نقل البيانات بالاضافة الى تحقيق أعلى كفاءة طيفية مقارنة بالأنظمة الاخرى.

Performance Study of Different Approaches Used in the Design of Hierarchical Routing Protocols for Wireless Sensor Network

**Amr M. Kishk¹, Nagy W. Messiha², Nawal A. El-Fishawy³, Abd-Elrahman
A. Alkafs¹, and Ahmed H. Madian¹**

¹ Reactor Department, Egyptian Atomic Energy Authority (EAEA), Cairo, Egypt

² Electronics and Communication Engineering, Faculty of Electronic Engineering,
Menouf, Egypt

³ Computer Science and Eng., Faculty of Electronic Engineering, Menouf, Egypt

(Received: 06-October-2015 – Accepted: 07-December-2015)

Abstract

Routing protocols are used to route the sensed data of the sensor nodes in Wireless Sensor Network (WSN) to the network administrator. The choice of the routing protocol effects on the sensor nodes lifetime. This paper discusses different approaches used in the design of the routing protocols and their effectiveness on WSN performance. The routing protocols are classified according to the network structure or the operation of the routing protocol. One of the routing protocols according to the network structure is hierarchical routing protocol. The main aim of hierarchical routing protocols is to optimize energy consumption of sensor nodes by arranging the nodes into clusters. The energy is consumed in the process of sending and receiving data between the sensor nodes in WSN and also in the process of network clustering periodically. Different approaches are introduced through many hierarchical routing protocols. Their performance are compared with each other using popular metrics such as WSN lifetime and throughput. The results show that the dependence on Cluster Heads (CHs) lifetime to elect new CHs enhances the WSN lifetime in comparison with the periodic CH elections.

1. Introduction

Wireless Sensor Network (WSN) comprises a large number of sensor nodes that are densely deployed [1]. It aims to transfer the sensed data from the sensor nodes to the network administrator. Every sensor node mainly consists of four basic components: a sensing unit, a processing unit, a communication unit, and a power unit [2]. The sensor node depends on the battery as an energy source in WSN. The most of the energy consumption in WSN comes from data reception and transmission. So, the data transmission in WSN is organized by a routing protocol [2]. In order to prolong the lifetime of the WSN, designing efficient routing protocol is critical.

The routing protocols can be classified according to network structure or routing protocol operation [3]. In the case of network structure, the routing protocols are classified into flat networks routing, hierarchical networks routing, and location based routing. In the case of protocol operation, the routing protocols are classified into negotiation based routing, multi-path based routing, query based routing, Quality of Service (QoS) based routing, and coherent based routing. This paper focuses on the hierarchical routing protocols [4]. Hierarchical routing protocols cluster the network depending on the presence of a node corresponding to all the nodes in its cluster. They are named by a Cluster Head (CH) as shown in Figure 1. This node, CH, collects all the sensed data of the nodes inside its cluster to send them to Base Station (BS). The presence of CH reduces the power consumption of the sensor nodes used to send the data to BS. The popular approaches of hierarchical routing protocols will be discussed and compared with each other in this paper. These protocols are named by Low Energy Adaptive Clustering Hierarchy (LEACH) [5], Threshold Sensitive Energy Efficient Sensor Network Protocol (TEEN) [6], Adaptive Periodic TEEN (APTEEN) [6], An Energy Efficient Weight-Clustering Algorithm [7], and Vice-LEACH protocol (VLEACH) [8], Long Lifetime Hierarchical Routing Protocol (LL-HRP) [9].

The paper is organized as follows: section II introduces survey on hierarchical routing protocols, the performance analysis of these hierarchical routing protocols is discussed in section III, and conclusions are shown at the end of this paper in section IV.

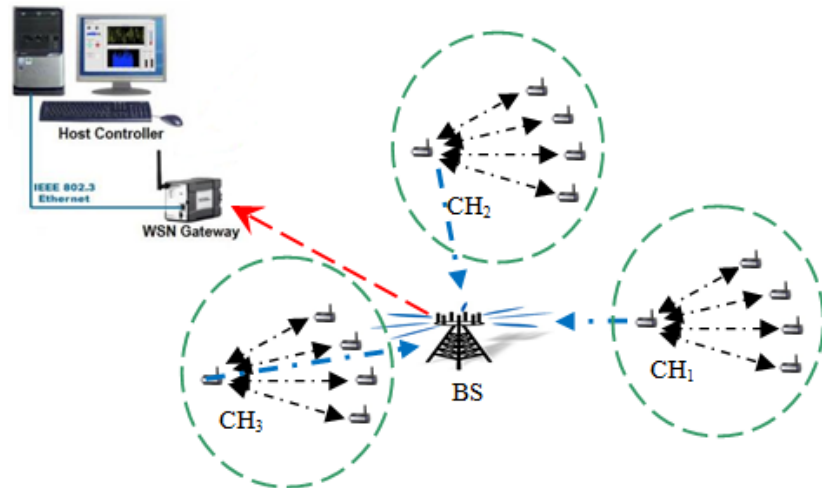


Figure 1: WSN clustering [4]

2. HIERARCHICAL ROUTING PROTOCOLS

A. Low Energy Adaptive Clustering Hierarchy (LEACH)

The sensor nodes are distributed randomly in the network area. Each sensor has a sensor unit and the sensed data must transmit to the network operator to take decision. So, it must specify a route from the sensor node to the network operator. This route is specified by the routing protocols. One of these routing protocol is Low Energy Adaptive Clustering Hierarchy (LEACH) which has a topology like the star topology of the computer network as shown in Figure 1 [5]. LEACH partitions the network area into clusters. Each cluster has a CH and its members from the sensor nodes in its area. The presence of CH reduces the energy consumption of the sensor nodes to send a sensed data to the BS. The sensor node sends its sensed data by limited energy to CH in comparison with the energy dissipation used to communication with BS. CH spends more energy than its members to send all their sensed data to BS. It has been thought to change CH periodically to save its energy as a normal node in the next period. LEACH steps can be explained in two stages or phases which are Set-up phase (Network clustering) and Steady-state phase (data transfer). These two phases are reinstalled periodically or with each round. The choice of CH depends on a generated number comparing with a threshold, T_n . The steps of these two phases are as follows:

• **Set-up phase (Network clustering for CHs determination)**

1. Each sensor node generates a random number in the [0,1] range to send it to BS.
2. For determining the threshold value, BS calculates T_n using equation (1) [5] with each round where p and r are CH proportion and round number respectively as shown in Figure 2. Then, BS compares T_n with the received random numbers of the sensor nodes.
3. The node that its random number less than T_n will be elected as CH [5].

$$T_n = \frac{p}{1 - p \left(r \bmod \left(\frac{1}{p} \right) \right)} \quad (1)$$

4. BS announces the results to the sensor nodes.
5. The elected CHs broadcast their IDs to all the sensor nodes to join with the nearest CH as shown in Figure 3.
6. Each sensor node announces its CH-ID, the nearest to it. So, the CHs will know their members from their IDs according their received messages.
7. CH collects its member IDs to produce a Time Division Multiple Access (TDMA) schedule, and notifies all its members in the cluster.

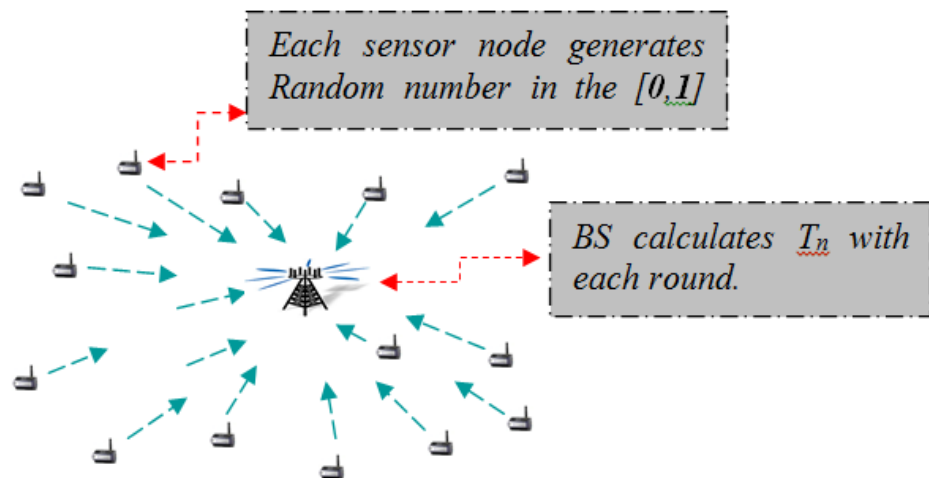


Figure 2: Set-up phase (CHs selection) [5]

- **Steady-state phase (data transfer)**

After the sensor node receives TDMA schedule, it will send data in its own time slots, and remains in the sleep mode otherwise. Then, CH collects all these sensed data of its members to send them to BS as shown in Figure 4 [5].

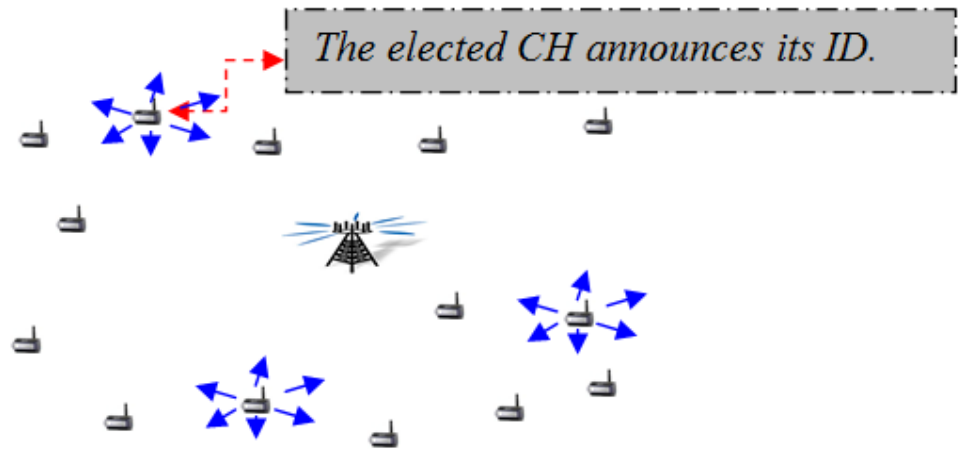


Figure 3: Cluster members selection [5]

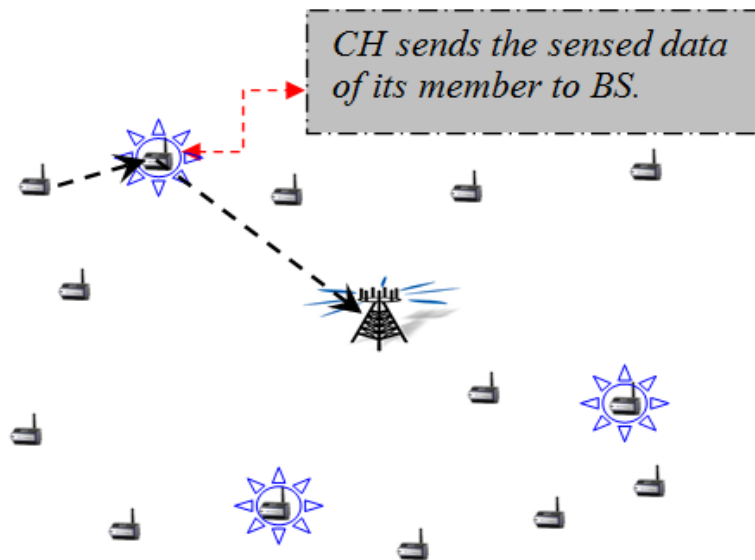


Figure 4: Steady-state phase (data transfer) [5]

B. Threshold Sensitive Energy Efficient Sensor Network Protocol (TEEN)

In TEEN, both set-up phase and steady-state phase are the same as LEACH except the condition of data transfer. TEEN specified two thresholds [6]:

- **Hard threshold (HT)**
It is a threshold value for the sensed attribute.
- **Soft threshold (ST)**
It is a small change in the value of the sensed attribute which triggers the node to switch on its transmitter to transmit its sensed data.

C. Adaptive Periodic TEEN (APTEEN)

In APTEEN, both set-up phase and steady-state phase are the same as TEEN, but the sensor node must transmit its last sensed data to its CH at the end of the round if the sensor node did not send any data along the current round [6].

D. An Energy Efficient Weight-Clustering Algorithm (WALEACH)

In WALEACH, both set-up phase and steady-state phase are the same as LEACH with some modification to the threshold T_n [7] named by T_{nn} in this paper to differentiate it from T_n formula as shown in Eqh. (2) where K_{opt} can be determined as in Eqh. (3) [7].

$$T_{nn} = \left(\frac{p}{1 - p \left(r \bmod \left(\frac{1}{p} \right) \right)} \cdot \frac{E_{residual}}{E_{initial}} \right) \cdot K_{opt} \quad (2)$$

$$K_{opt} = \frac{1}{d_{toBS}^2} \sqrt{\frac{N \epsilon_{fs}}{2\pi \epsilon_{mp}} \cdot A} \quad (3)$$

Where:

- p is CH proportion which indicates the desired number of CHs in WSN.
- r is round number.
- E_{residual} is the residual energy of the sensor node at each round.
- E_{initial} is the initial energy of the sensor node.
- K_{opt} is optimal number of CH.
- d_{toBS} is the distance between the sensor node and BS.
- N is the number of sensor nodes in WSN.
- \mathcal{E} is the amplifier energy of the sensor node transmitter and denoted by \mathcal{E}_{fs} for free space propagation and \mathcal{E}_{mp} for multi-path propagation.
- A is the WSN area.

E. Vice-LEACH protocol (VLEACH)

In VLEACH, both set-up phase and steady-state phase are the same as LEACH with some modification to steady-state phase [8]. VLEACH has suggested to use a vice-CH in each cluster from its members. This vice-CH works as a CH in the case of CH death to avoid lost data along the round as shown in Figure 5 [8].

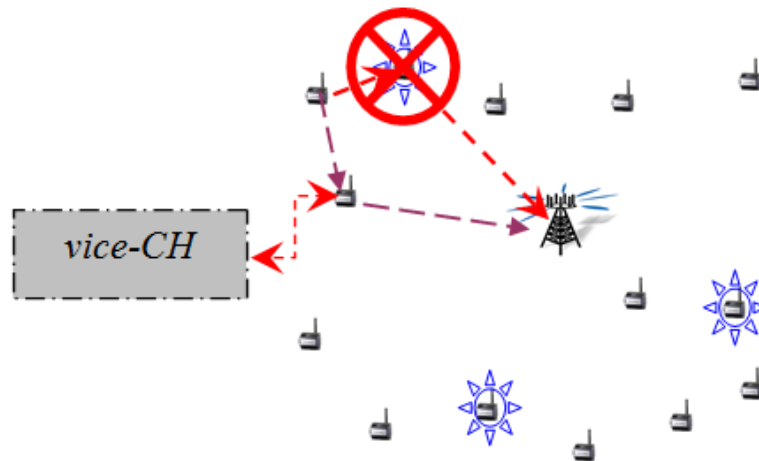


Figure 5: Vice-LEACH protocol

F. Long Lifetime Hierarchical Routing Protocol (LL-HRP)

LL-HRP has suggested to cluster the WSN once and no need to cluster the network periodically [9]. Each cluster has two main points: a Cluster Head (CH) and a Recombination Cluster Head (RCH) as shown in Figure 6. RCH functions like CH functions used in LEACH while CH used LL-HRP manages the operation in the cluster in the case of RCH death only. The presence of both RCH and CH enhance both the security level and WSN lifetime.

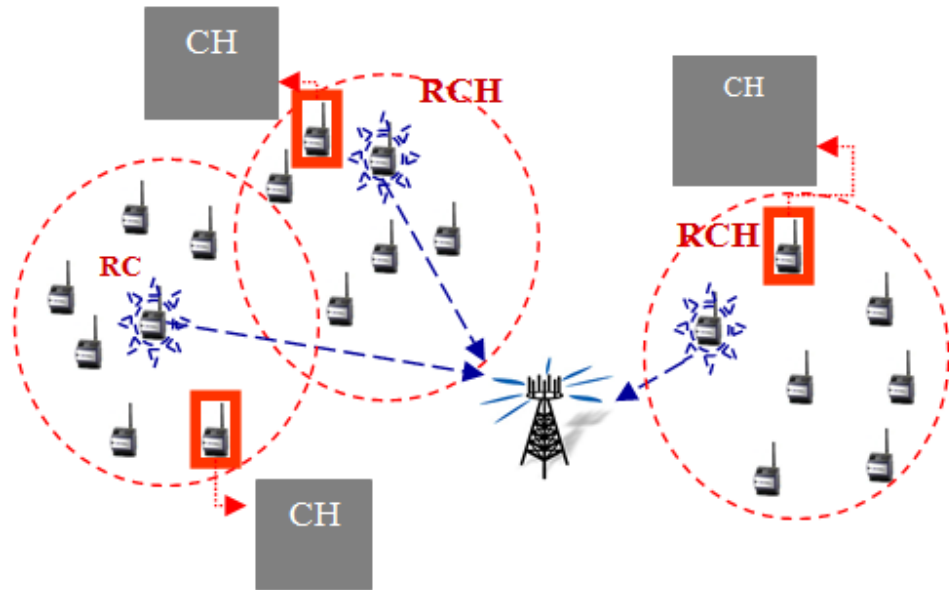


Figure 6: The presence of both RCH and CH in each cluster [9]

- **Set-up phase**

1. At the first time, the nodes are fixed and distributed around BS randomly.
2. The clustering process begins from the nodes by transmitting their IDs to the BS to authenticate its presence in the network.
3. BS measures their Received Signal Strength Indicator (RSSI) and ranks them in descending order. then, BS partitions these RSSI into equal groups (3-5 groups).

4. The maximum RSSI from each group will be elected as RCH as in Figure 7.
5. After RCH election, BS will announce the IDs of the elected RCHs to all nodes.
6. Each sensor node will start to detect the nearest RCH.
7. If the sensor node detects no RCH close to it, then the sensor node will send a message to BS for RCH election by repeating the previous procedures as in Figure 8.
8. Repeat step 7 as shown in Figure 9 until all the sensor nodes join with a RCH as shown in Figure 10.

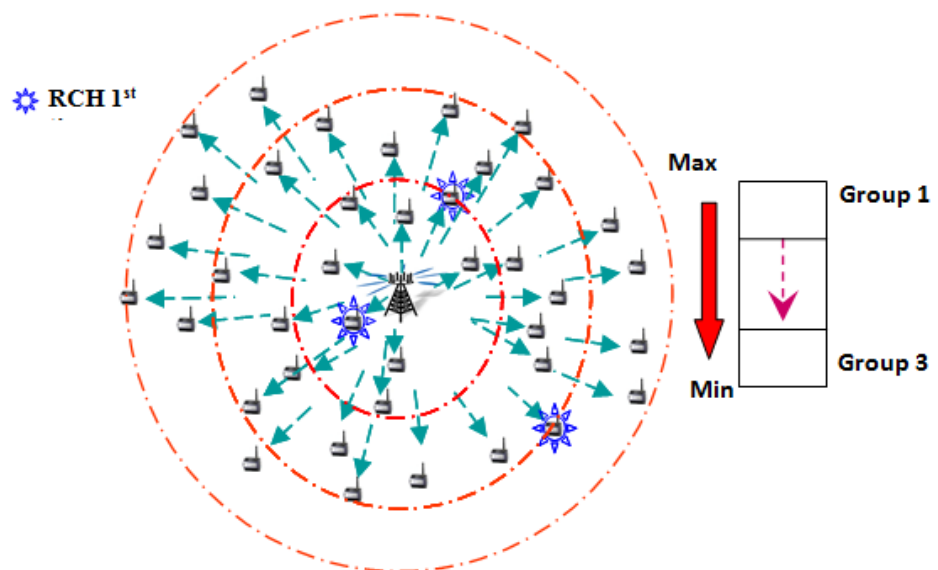


Figure 7: WSN clustering using LL-HRP [9]

- **Steady-state phase**

LL-HRP depends on soft threshold, ST . If SD_{n+1} and SD_n are the current sensed data and the previous one respectively, then the sensor node will send its sensed data, SD_{n+1} , when $|SD_{n+1}-SD_n|>ST$. The reduction in RCH energy to some level means another new RCH election process where RCH will send a notification message to CH. Then, CH will test the power level of each node in the cluster and elect the highest one to be RCH. Finally, both CH and new elected RCH will announce this election. By the same way, the reduction in CH energy to some level means another new

CH election process where CH will send a notification message to RCH and the members in the cluster to elect the highest one to be CH. Finally, both RCH and new elected CH will announce this election.

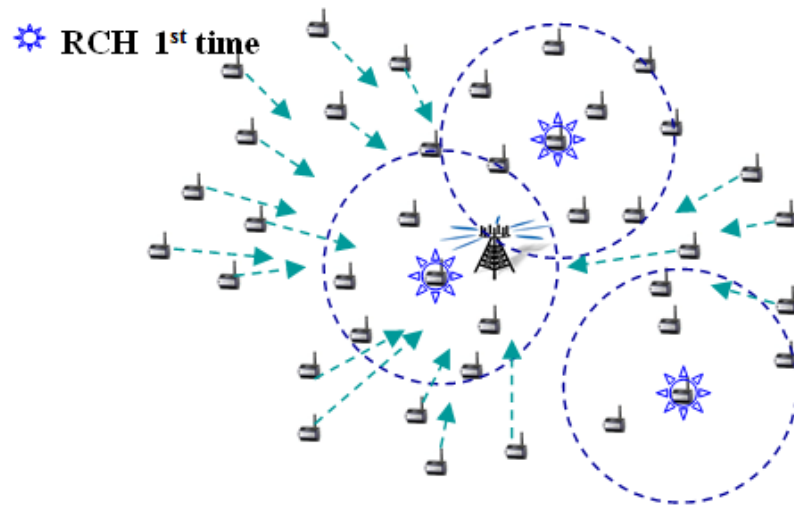


Figure 8: Repeating the procedures of Figure 7 for the sensors who detect no RCH near to them [9]

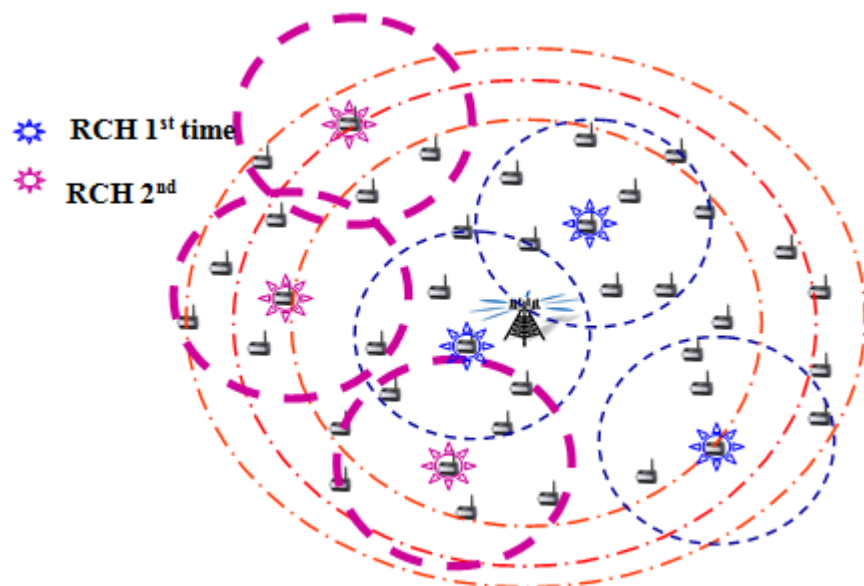


Figure 9: Clustering process for the second time [9]

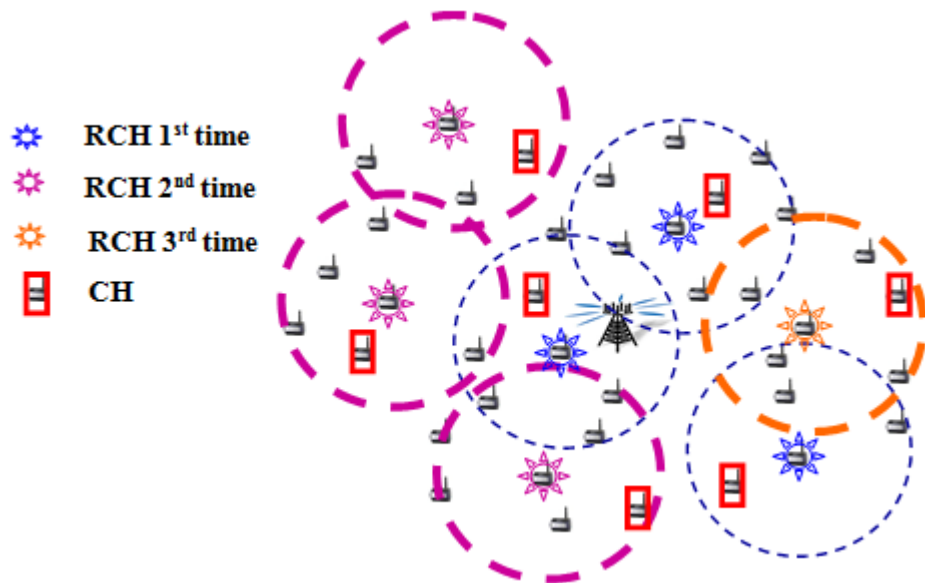


Figure 10: WSN clusters using LL-HRP [9]

3. RESULTS AND DISCUSSIONS

WSN is composed of multiple battery-operated sensor nodes and a Base Station (BS). These sensor nodes are distributed randomly as shown in Figure 11. Number of sensor nodes used in our estimations is 100 nodes and these nodes are in an area 50x50 m². This area gives the sensor nodes the ability to communicate with BS which is located at the center or at (25, 25). The specifications of the network will be shown in tables, tables 1 and 2, with the comparisons and they are standards. LL-HRP is compared with the other protocols using the following metrics [10]:

- A. Sensor nodes distribution during set-up phase (Network clustering).
- B. Energy consumption:
 - 1. in the case of set-up phase only.
 - 2. in the case of both set-up phase and steady-state phase.
- C. Number of alive nodes in each round (First dead node and Last dead node):

1. in the case of set-up phase only.
2. in the case of both set-up phase and steady-state phase.

D. Number of lost sensed data.

The sensed data is lost due to CH death. So, the sensor nodes in this cluster unable to send their data to the BS.

E. Throughput.

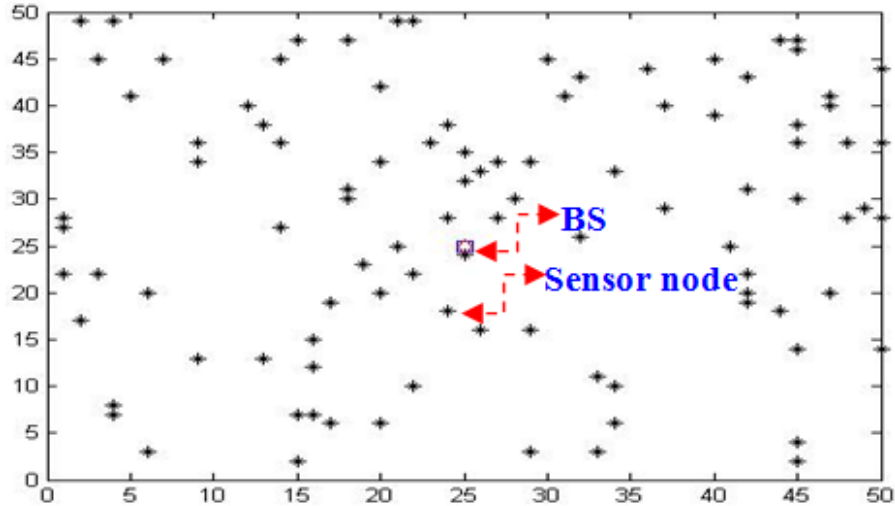


Figure 11: Sensor nodes distribution in WSN

A. Network clustering

- LEACH, TEEN, and APTEEN suffer from some drawbacks which are:

1. The probability of all nodes become CHs can occur.

All sensor nodes become CHs as shown in Figure 12 when all sensor nodes generate random numbers less than T_n , at $T_n=1$, or at certain values of r as shown in Figure 13.

2. The probability of no CHs can occur.

No CHs occurs when all sensor nodes generate random numbers greater than T_n only because T_n does not equal 0 as shown in Figure 14.

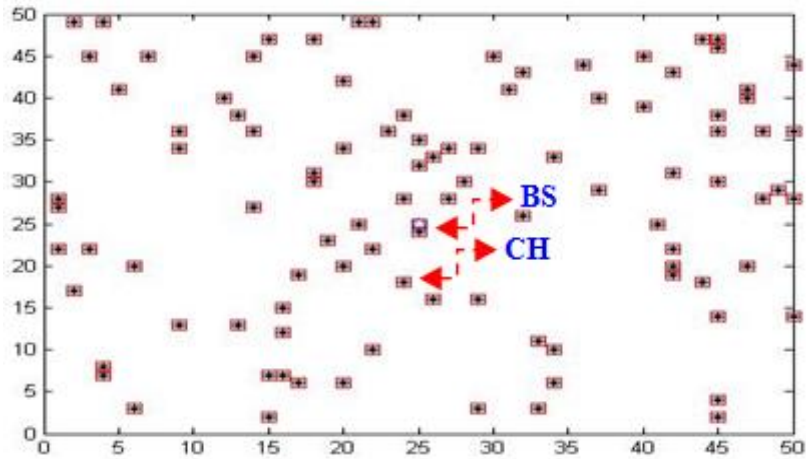


Figure 12: The probability of all nodes become CHs

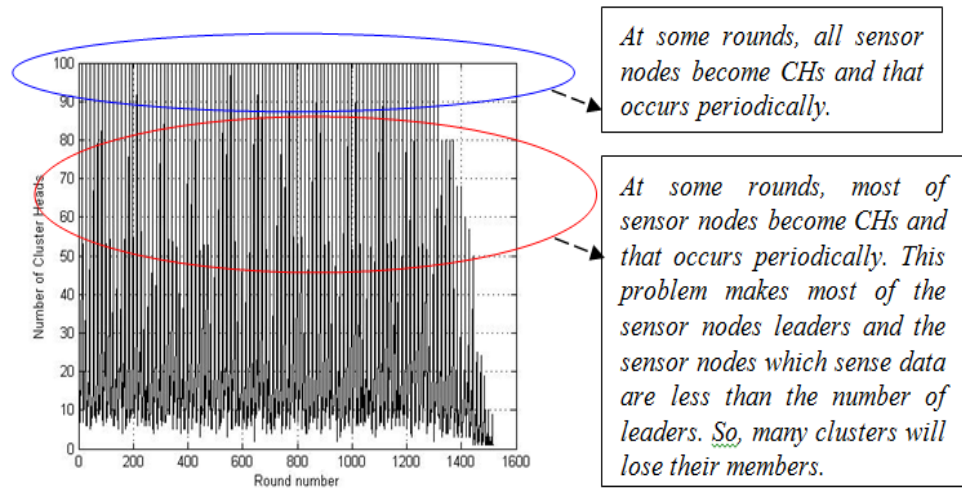


Figure 13: Number of CHs vs. round number r

3. The probability of unfair distribution.

BS may elect all CHs in one side of the network and may leave the other sides without CHs. So, the unfair distribution will reduce the sensors lifetime because the distance between some of the sensor nodes and their CHs become more than the distance between BS and these sensor nodes as shown in Figure 15. The unfair distribution gives a probability of a CH without members as shown in Figure 16.

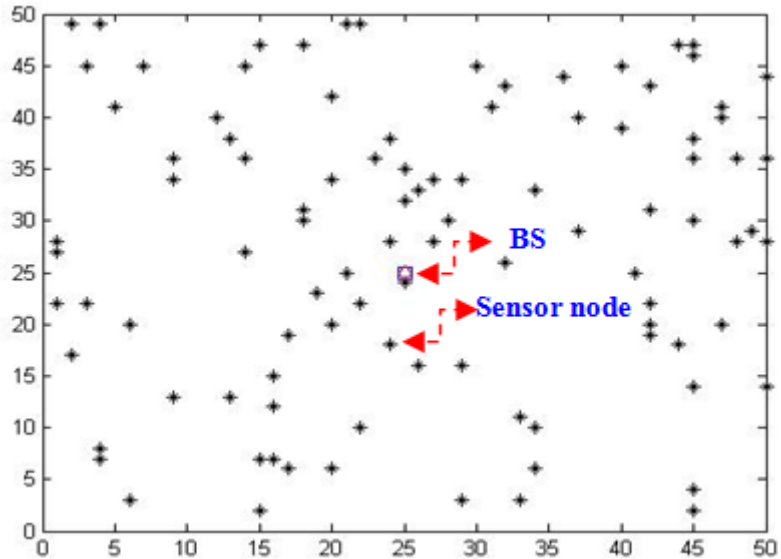


Figure 14: The probability of no CH

4. The sensor nodes with low remnant energy have the same priority to be a CH as the node with high remnant energy.

The CH death can occur before the end of the round as shown in Figure 17 causing lost sensed data and exhausting the batteries of the members due to multiple ACK which reduces the network lifetime.

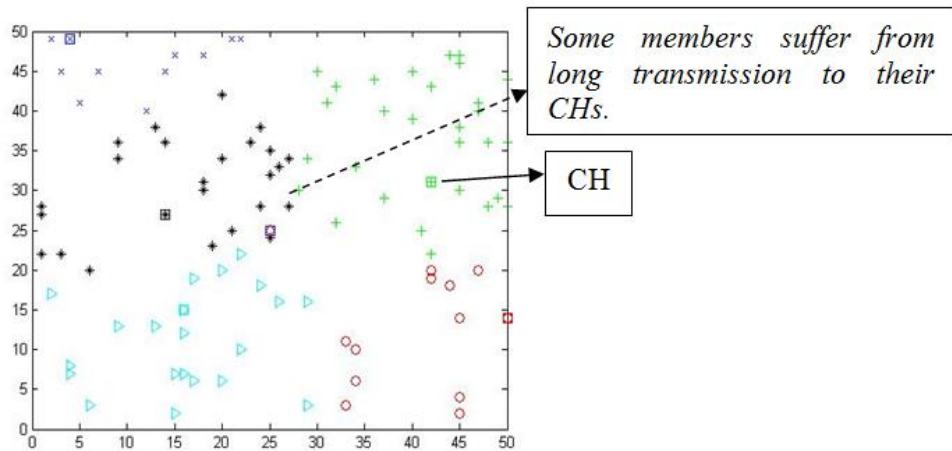


Figure 15: Unfair distance between the sensor nodes and their CHs in comparison with BS

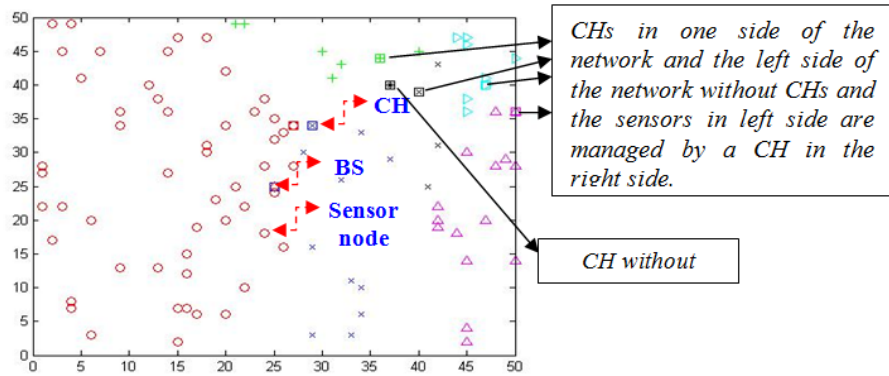


Figure 16: The probability of unfair distribution

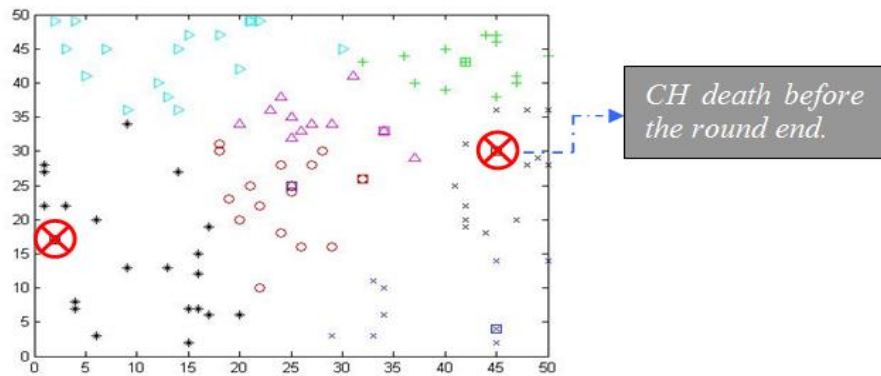


Figure 17: The probability of CH death

- An Energy Efficient Weight-Clustering Algorithm (WALEACH)
 1. $E_{\text{residual}}/E_{\text{initial}}$ term does not solve the drawback of LEACH, TEEN, and APTEEN which is “The nodes with low remnant energy have the same priority to be a cluster head as the node with high remnant energy” because it does not prevent the probability to generate a random number less than T_{nn} (CH election condition) but, it reduces T_{nn} value which reduces only the number of CHs in the network.
 2. K_{opt} can increase T_{nn} to be greater than 1 which increase the probability of “all nodes become CHs can occur” to be 1 as shown in Figure 18. This problem can reduce the lifetime of the network rapidly because of the communication with BS directly without clustering. Therefore, the probability of unfair distribution becomes 1.

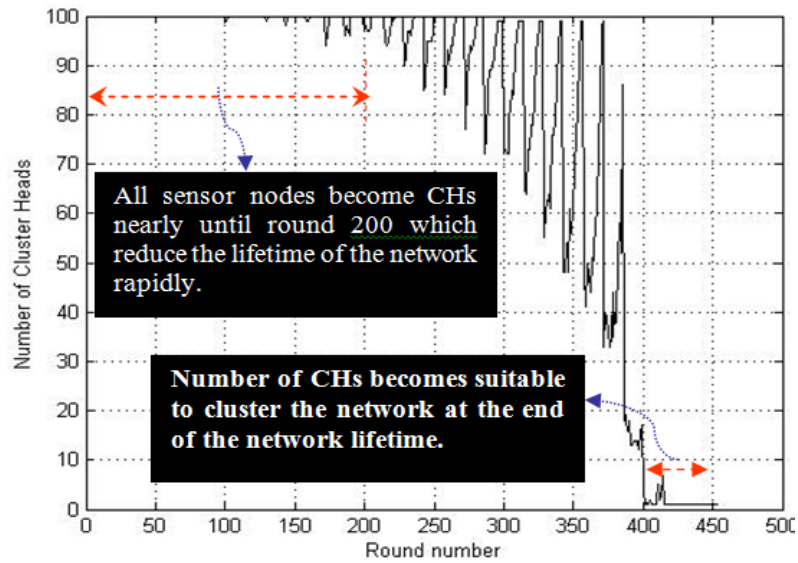


Figure 18: Number of CHs in each round of An Energy Efficient Weight-Clustering Algorithm

The deletion of K_{opt} term from T_{nn} formula enhances the algorithm performance (it reduces the probability of all sensors become CHs in comparison with LEACH, TEEN, and APTEEN) as shown in Figure 19 in comparison with Figure 18, but the drawbacks of the LEACH, TEEN, and APTEEN still exist

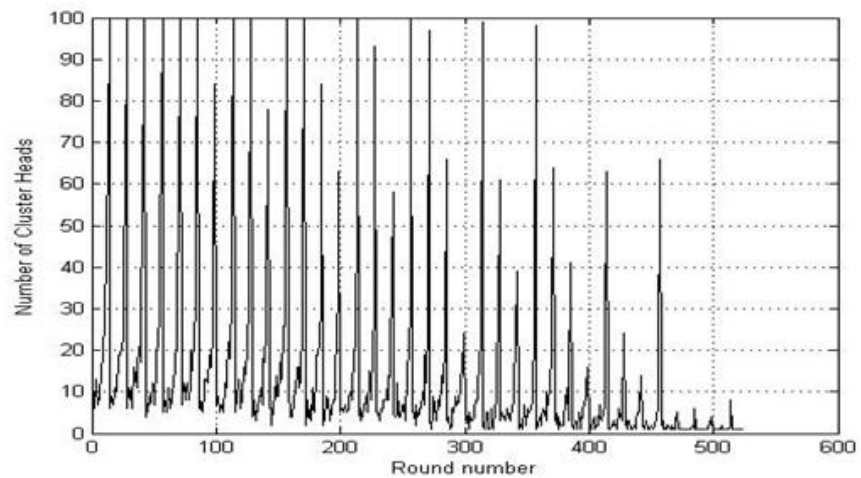


Figure 19: Number of CHs in each round of WALEACH after The deletion of K_{opt} term from T_{nn} formula.

- VLEACH

VLEACH remedies the probability of CH death before the round end during steady-state phase, but VLEACH still has the same drawbacks of LEACH, TEEN, and APTEEN at set-up phase (Network clustering). Figure 20 shows VLEACH still has the drawback of LEACH, TEEN, and APTEEN which is all sensor nodes become CHs at some rounds or conditions as shown later.

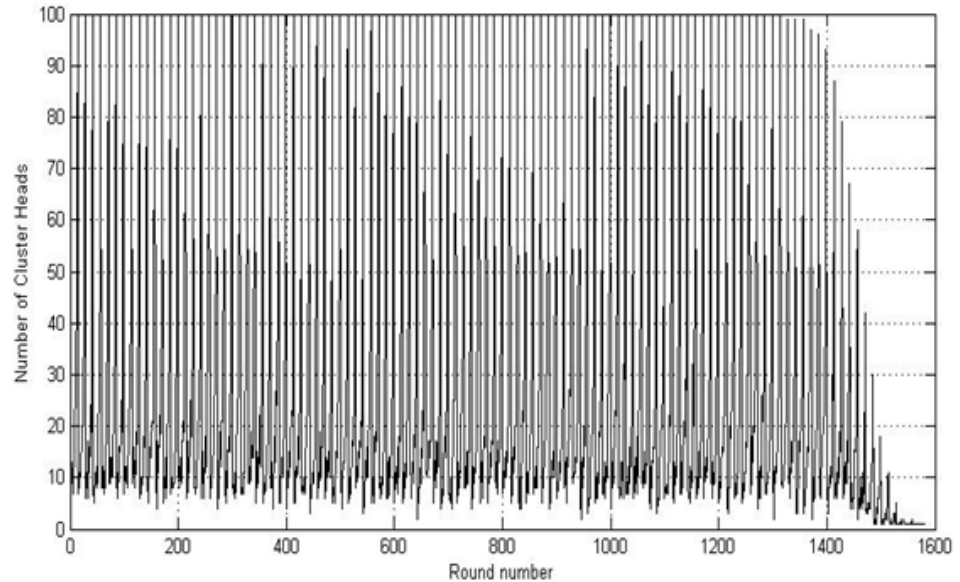


Figure 20. Number of CHs in each round of VLEACH

- LL-HRP

LL-HRP overcomes the drawbacks of the previous protocols. It clusters the network once during set-up phase as shown in Figure 21 and the change of both CH and RCH depends on their lifetime during steady-state phase only as shown in Figure 22. So, no probability of:

1. all sensor nodes become CHs
2. no CHs exist.
3. unfair distribution.
4. the nodes with low remnant energy have the same priority to be a cluster head as the node with high remnant energy.

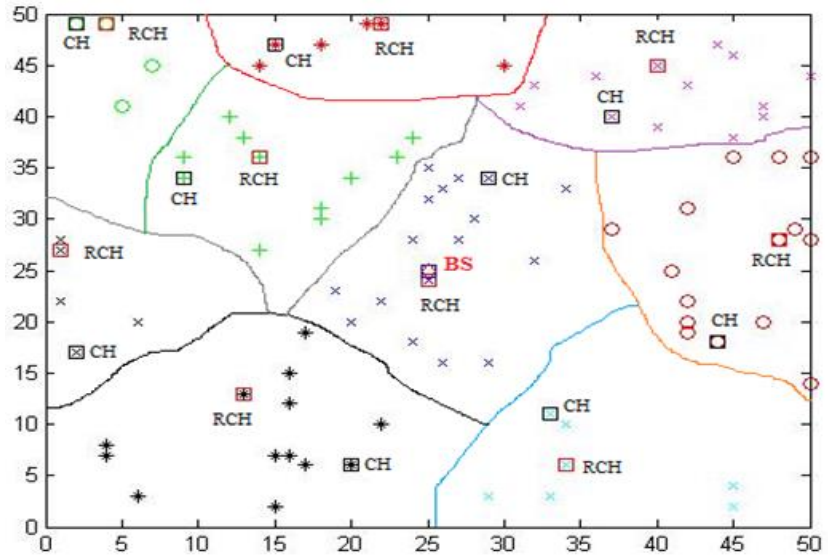


Figure 21: WSN clustering using LL-HRP

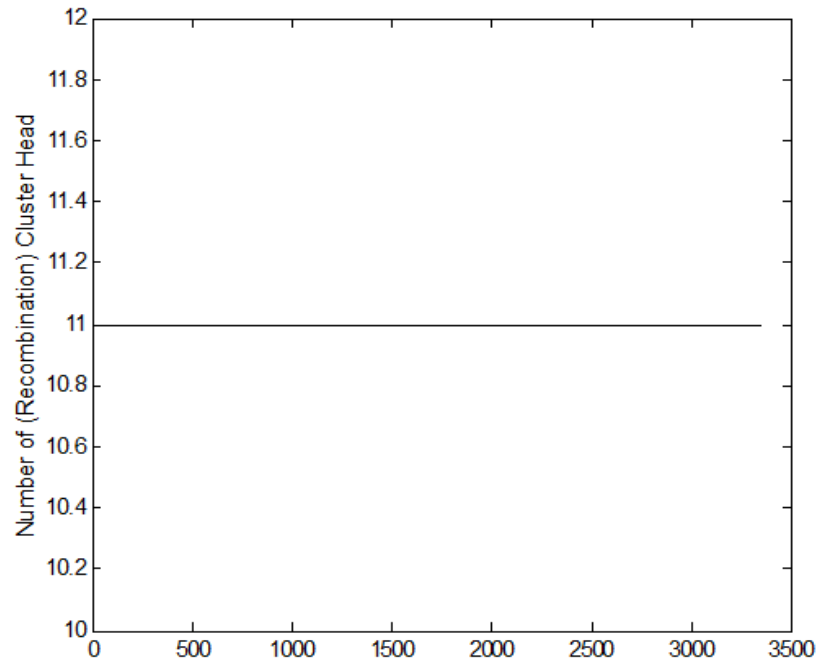


Figure 22: Number of CHs in each round of LL-HRP

B. Energy consumption

The design of algorithms for WSN is governed by the energy consumption which is a main metric used to differentiate and compare between different algorithms in WSN. The energy consumption depends on the radio energy dissipation model of the sensor node as a transmitter and as a receiver as shown in Figure 23 and its symbols definitions and values are shown in table 1 which are standards [11]. The energy consumption estimation depends on the propagation type between the transmitter and the receiver. The propagation type is specified by d and d_0 where d_0 can be calculated as shown in Eqh (4) [11].

$$d_0 = \sqrt{\frac{\epsilon_{fs}}{\epsilon_{mp}}} \quad (4)$$

For free space propagation: $d \leq d_0$, $\gamma=2$, and $\epsilon=\epsilon_{fs}=10\text{pJ/bit/m}^2$ while multi-path propagation: $d > d_0$, $\gamma=4$, and $\epsilon=\epsilon_{mp}=0.0013\text{pJ/bit/m}^4$. Also, the energy estimation depends on the routing protocols parameters shown in table 2 which are used in the simulation. The suggested sensed data used in our simulation is shown in Figure 24 until 500 values only to be clear in the figure, but the total number of the sensed data used in our simulation are until two millions values.

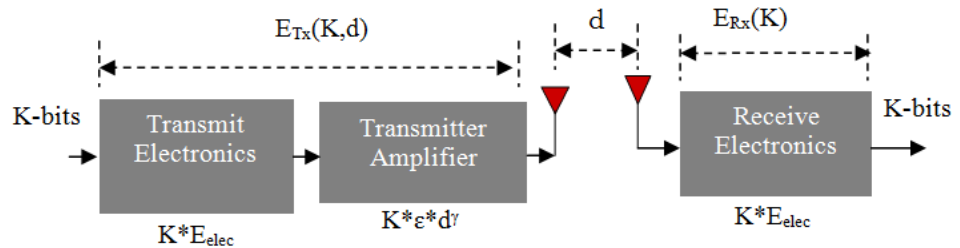


Figure 23: Radio energy dissipation model [11]

Figure 25 shows the comparison between different routing protocols without data transmission in each round to show how the periodic CH election process spends more energy consumption without data transmission. As expected, WALEACH exhausted the battery of the sensor nodes more than the other protocols causing the death of WSN quickly in comparison with the others. The suggested enhancement, the deletion of K_{opt} term from T_{nn} formula, denoted by (WALEACHenhanced)

as shown in Figure 25 prolongs the lifetime of the network more than the other protocols except LL-HRP. LL-HRP does not suffer from the network death as the other protocols. The change of CH/RCH periodically spends more energy and delay time to send the sensed data, but the LL-HRP does not obey to this rule. So, the network lifetime cannot be estimated from the set-up phase for LL-HRP because of the dependence on the steady-state phase rather than set-up phase to elect a new CH/RCH. The energy consumption rate of VLEACH is the same as LEACH, TEEN, and APTEEN which exhausted the sensor nodes of the WSN after WALEACH but VLEACH prolongs the network lifetime more than them as shown in Figure 25.

Table 1. The symbols definitions and values of radio energy dissipation model [11]

<i>Symbol</i>	<i>Definition</i>	<i>Value</i>
K	Number of bits	4000 bits
E_{elec}	Energy dissipation in Transmit and Receive Electronics stages	50 nJ/bit
d	Distance between Tx and Rx	Variable
E_{ini}	Initial Energy (Full Battery)	2 J
γ	Propagation constant	2 or 4
ϵ	Energy dissipation in T_X amplifier.	10 pJ/bit/m ² or 0.0013 pJ/bit/m ⁴
E_{DA}	Data Aggregation	5 nJ/bit

Table 2: The symbols definitions and values of the parameters used in the routing protocols for network specifications [11]

<i>Symbol</i>	<i>Definition</i>	<i>Value</i>
p	cluster portion used in equation (1)	0.07
N	Number of sensor nodes	100
A	Network Area	50x50 m ²
H_T	Hard Threshold for both TEEN and APTEEN	0.5
	Hard Threshold for proposed protocol	1st sensed data
S_T	Soft Threshold	0.15
M	Number of sensed data per round	4
(x_{BS}, y_{BS})	BS coordinates	(25, 25)
d_{max}	Maximum distance between RCH and its members	15 m

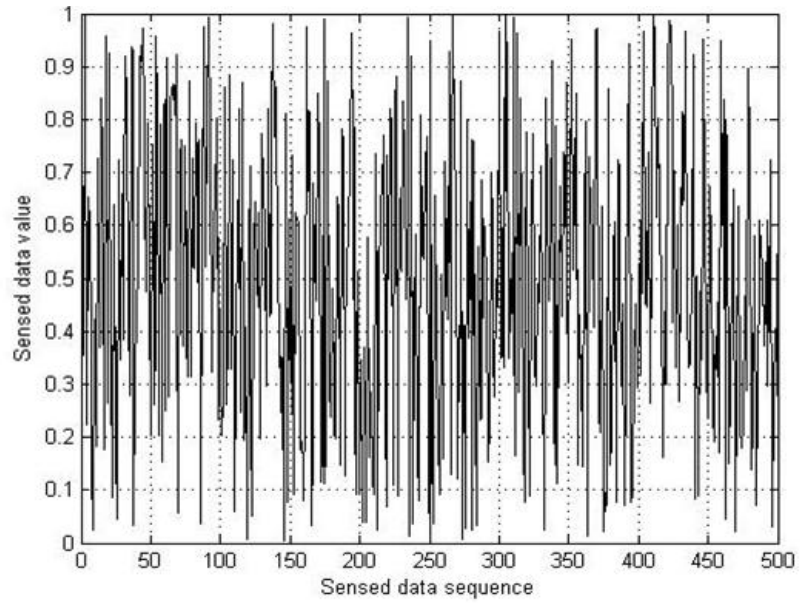


Figure 24: Sensed data values used in our simulation

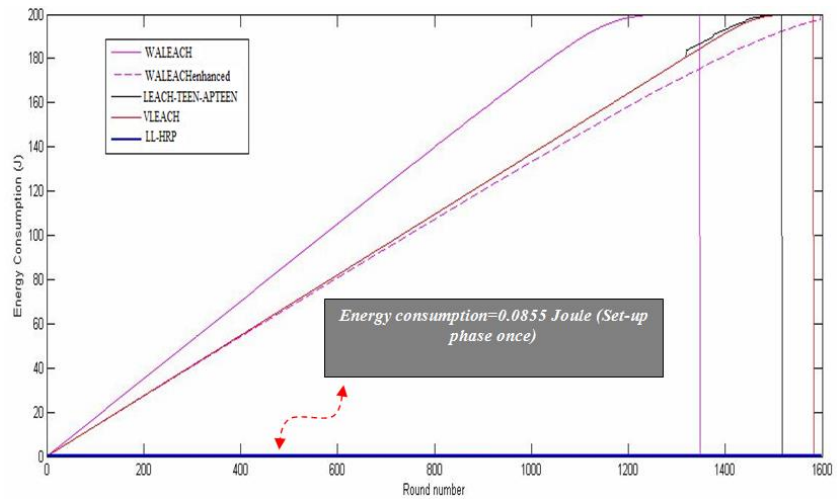


Figure 25: Energy consumption comparison in the case of set-up phase only

Figure 26 shows the comparison between different routing protocols in the case of both periodic CH election process and data transmission in each round. WALEACH scores the highest energy consumption rate while LL-HRP scores the least one. And also, The network lifetime is the shortest in the case of WALEACH and the longest in the case of LL-HRP. Both

TEEN and APTEEN prolongs the network lifetime in comparison with LEACH, VLEACH, and enhanced WALEACH in the case of both energy consumption rate and WSN death. TEEN prolongs the network lifetime in comparison with APTEEN although they have the same energy consumption rate. And also, VLEACH prolongs the network lifetime in comparison with both LEACH and enhanced WALEACH although they have the same energy consumption rate. Finally, the enhanced WALEACH prolongs the network lifetime in comparison with both WALEACH and LEACH

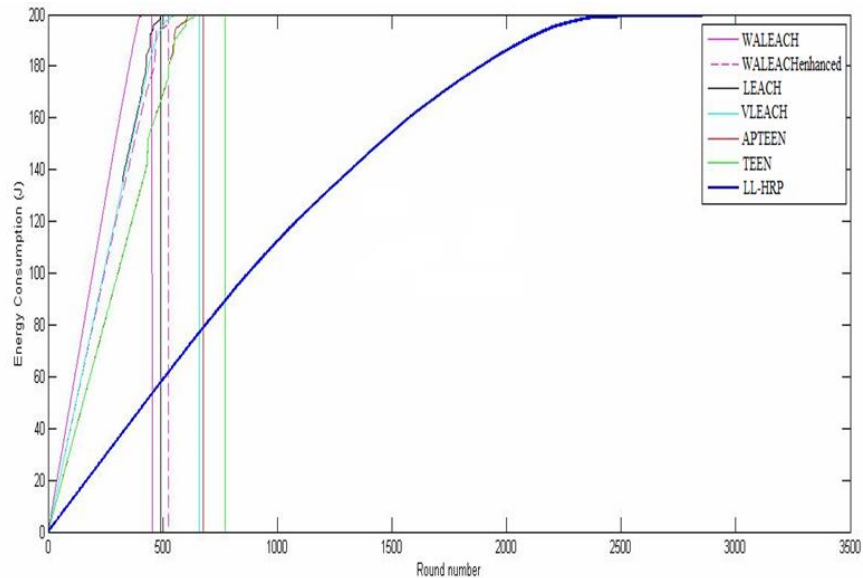


Figure 26: Energy consumption comparison in the case of both set-up phase and steady-state phase

C. Number of alive nodes per round

Number of alive nodes per round is a metric used to show how many sensor nodes in the network can sense the data from the surroundings in each round. This metric indicates the rate of the sensor nodes death as shown in Figure 27. In the case of set-up phase only, LL-HRP keeps all sensor nodes without death which means that no lost data as shown in Figure 27. WALEACH has higher rate of the sensor nodes death than the others while its enhancement prolongs the sensor nodes more than the others except LL-HRP. In the case of both set-up phase and steady-state phase, the routing protocols except LL-HRP are close to each other with

respect to number of nodes per rounds as shown in Figure 28 while LL-HRP prolongs the sensor nodes to a high level. The round number of both first dead node and the last dead node are written down in table 3. It is so clear from table 4 that LL-HRP does not suffer from the problem of sensor nodes death in the case of set-up phase while the others suffer from this problem. And also, LL-HRP prolongs the sensor node lifetime more than the others in the case of both set-up and steady state phases.

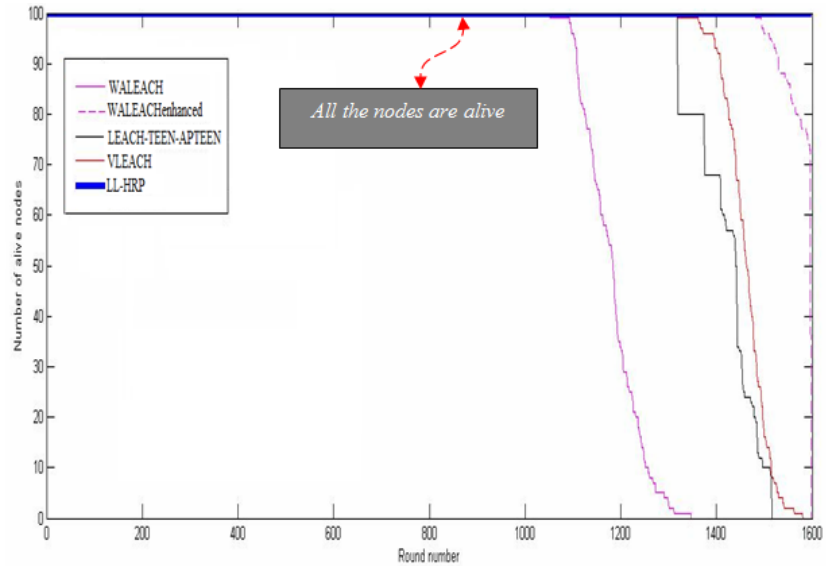


Figure 27: Number of alive nodes per round in the case of set-up phase only

Table 3: Number of alive nodes per round comparison

<i>Routing Protocol</i>	<i>In the case of set-up phase only</i>		<i>In the case of both set-up phase and steady state phase</i>	
	<i>First dead node</i>	<i>Last dead node</i>	<i>First dead node</i>	<i>Last dead node</i>
LEACH	1319	1516	326	490
TEEN	1319	1516	434	772
APTEEN	1319	1516	434	676
WALEACH	1052	1347	299	453
Enhanced WALEACH	1480	1597	418	523
VLEACH	1319	1581	326	660
LL-HRP	0	0	452	3359

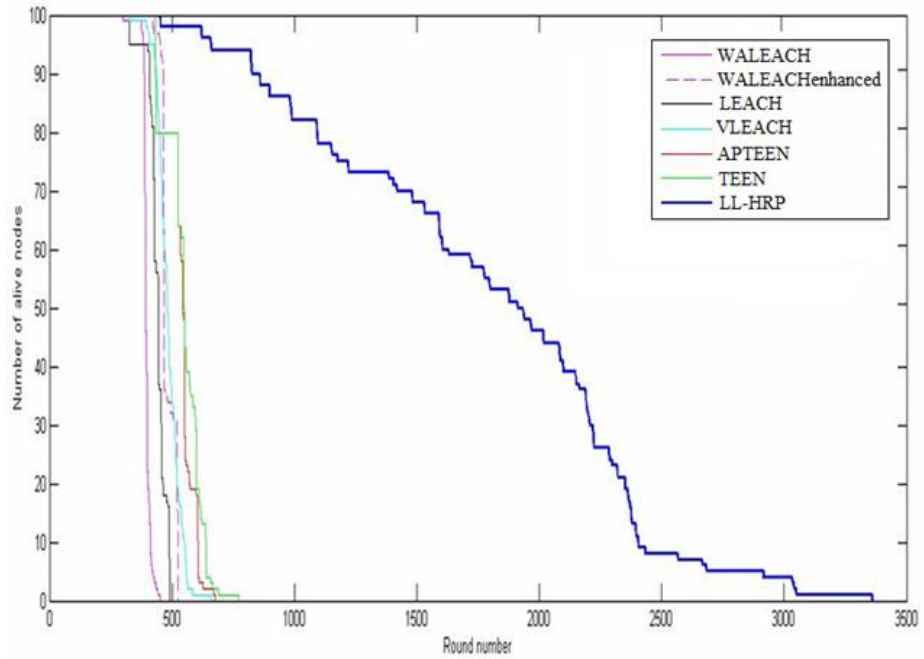


Figure 28: Number of alive nodes per round in the case of both set-up phase and steady-state phase

D. Number of lost sensed data

One of the metrics used in the comparison between routing protocols is number of lost sensed data. The lost data occur during steady-state phase because of CH/RCH death before the round end. Table 4 shows number of times of each routing protocol lost data. These numbers do not refer to number of bits, but they refer to how many times the network lost sensed data from the sensor nodes due to CH death before the round end. Both VLEACH and LL-HRP do suffer from this problem. VLEACH has remedied this problem by using another node to send the sensed data of the cluster in the case of CH death. LL-HRP has remedied this problem in the cluster as shown later. WALEACH lost few data in comparison with LEACH, TEEN, APTEEN, and enhanced WALEACH because all the sensor nodes become CHs most of the time and no members in their clusters. Although WALEACHenhanced is the enhancement of WALEACH, it suffers from higher number from lost data than WALEACH as shown in table 4.

Table 4: Number of lost sensed data comparison

<i>Routing protocol</i>	<i>Number of times the data lost (no unit)</i>
LEACH	330
TEEN	404
APTEEN	238
WALEACH	181
Enhanced WALEACH	344
VLEACH	0
LL-HRP	0

E. Throughput

Throughput is the ratio of total transmitted data sent successfully to BS to the lifetime of the network. So, the throughput is the average number of bits per round. The round number of the last dead node will be used instead of the lifetime of the network. All the discussed routing protocols do not depend on a threshold to send the data except TEEN, APTEEN, and LL-HRP which scores the least throughput as shown in Figure 29.

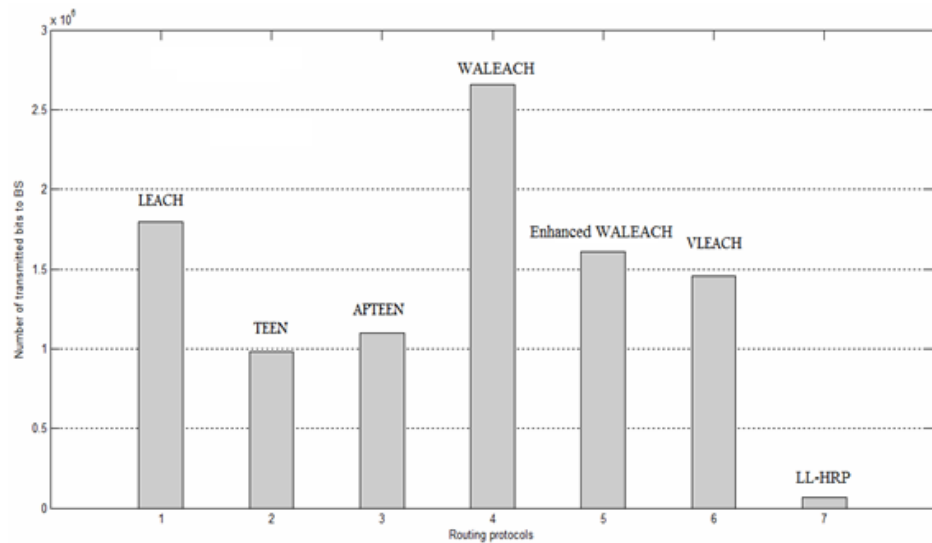


Figure 29: Throughput comparison in the case of both set-up phase and steady-state phase

It is so clear the effect of network lifetime on the throughput estimation as shown in Figure 29. The throughput estimation refers to the data traffic in each round. LL-HRP is the least one while TEEN scores less throughput than both LEACH and APTEEN. WALEACH scores the highest one while its enhancement scores higher throughput than VLEACH and less throughput than LEACH.

4. Results discussion

The metrics used in the performance comparison are sensor nodes distribution during set-up phase (Network clustering), energy consumption, number of alive nodes in each round (First dead node and Last dead node), number of lost sensed data, and throughput. The comparison results show that LL-HRP overcomes the drawbacks of the previous protocols. Also, the network lifetime is the shortest in the case of WALEACH and the longest in the case of LL-HRP. LL-HRP does not suffer from the problem of sensor nodes death in the case of set-up phase while the others suffer from this problem. In addition, LL-HRP prolongs the sensor node lifetime more than the others in the case of both set-up and steady state phases. Finally, LL-HRP does not suffer from the lost data problem due to CH death while the other routing protocols except VLEACH suffer from this problem. So, LL-HRP approach enhances the network performance. It enhances the clusters distribution and remedies the drawbacks of the others. Although some of the discussed protocols have compared with another protocols which are not discussed in this paper, the public drawbacks of hierarchical routing protocols are not cared except by LL-HRP.

5. CONCLUSIONS

The paper discussed different approaches used in the design of hierarchical routing protocols. All these approaches introduced the periodic CHs election except one which suggested to elect another CH depending on the CH lifetime. These approaches are compared with each other in the case of both set-up and steady state phases. The paper introduces performance analysis for these protocols. The results show the

preference of LL-HRP approach than the other approaches. LL-HRP remedies the drawbacks of the periodic CHs election and enhances the network lifetime

References

- [1] S. Tarannum, S. Srividya, D. Asha, and K. Venugopal, "Dynamic Hierarchical Communication Paradigm for Wireless Sensor Networks: A Centralized Energy Efficient Approach", *Wireless Sensor Network Journal*, vol. 1, pp. 340-349, 2009.
- [2] S. Anand and S. Chandel, "Comparison of Routing Protocols in Wireless Sensor Networks: A Detailed Survey", *International Journal of Engineering and Science (IJES)*, vol. 3, no. 12, pp. 20-27, December 2014.
- [3] L. Almazaydeh, E. Abdelfattah, M. Al-Bzoor, and A. Al-Rahayfeh, "Performance Evaluation of Routing Protocols in Wireless Sensor Networks", *International Journal of Computer Science and Information Technology*, vol.2, no. 2, April 2010.
- [4] G. Indhumathi and J. Gnanambigai, "Optimization of Energy Consumption for Hierarchical Routing Protocol in WSNs", *International Conference on Engineering Trends and Science & Humanities (ICETSH-2015)*, pp. 196-201, 2015.
- [5] M. Handy, M. Haase, and D. Timmermann, "Low Energy Adaptive Clustering Hierarchy with Deterministic Cluster-Head Selection", 4th IEEE Conference on Mobile and Wireless Communications Networks, Stockholm, September 2002.
- [6] P. Kaur and M. Katiyar, "The Energy-Efficient Hierarchical Routing Protocols for WSN: A Review", *International Journal of Advanced Research in Computer Science and Software Engineering*, vol. 2, no. 11, pp. 194-199, November 2012.
- [7] A. Thakkar and K. Kotecha, "WALEACH: Weight Based Energy Efficient Advanced LEACH Algorithm", *Computer Science & Information Technology (CS&IT)*, pp. 117-130, 2012.
- [8] M. Yassein, A. Al-zou'bi, Y. Khamayseh, and W. Mardini, "Improvement on LEACH Protocol of Wireless Sensor Network (VLEACH)", *International Journal of Digital Content Technology and its Applications*, vol. 3, no. 2, June 2009.
- [9] A. Kishk, N. Messiha, N. El-Fishawy, A. Alkafs, and A. Madian, "Proposed Hierarchical Routing Protocol with Simple Nodes Locating Algorithm for Authenticated Nodes in Wireless Sensor Network", 2nd International IEEE conference on Engineering and Technology (ICET 2014), 2014.

- [10] K. Latif, M. Jaffar, N. Javaid, M. Saqib, U. Qasim, and Z. Khan, "Performance Analysis of Hierarchical Routing Protocols in Wireless Sensor Networks", 7th IEEE International Conference on Broadband and Wireless Computing, Communication and Applications (BWCCA 2012), Victoria, Canada, 2012.
- [11] S. Mitra and M. Naskar, "Comparative Study of Radio Models for Data Gathering in Wireless Sensor Network", International Journal of Computer Applications, vol. 27, no. 4, pp. 49-57, August 2011.

الملخص باللغة العربية

الشبكات الاستشعارية اللاسلكية هي تتكون من العديد من المجسات الاستشعارية التي تخدم نقل البيانات المحسة إلى مشغل الشبكة. هذه المجسات الاستشعارية تعتمد على البطارية كمصدر طاقة. فلذلك تصميم التقنيات مبني على توفير الطاقة الاستهلاكية. وأيضاً اختيار بروتوكول لتنظيم نقل البيانات داخل الشبكة عامل مؤثر في عمر الشبكة نظراً لاعتمادها على البطارية كمصدر طاقة. هناك العديد من البروتوكولات المقترحة في هذا الشأن وتم دراسة الأفكار المختلفة التي تبنى عليها تصميم هذه البروتوكولات ومقارنتها مع بعضها البعض في هذا البحث.

تم توضيح الأفكار المختلفة بشرح البروتوكولات المشهورة التي تستخدمها وتم مقارنتها مع بعضها البعض باستخدام القياسات المشهورة. هذه الأفكار تعتمد على تقسيم الشبكة إلى مساحات وكل مساحة يوجد مدير منتخب من أحد أعضائها. هذا المدير ينقل البيانات المحسة من قبل الأعضاء إلى المشغل الرئيسي للشبكة. عمل التقسيم وطرق نقل المعلومات وشروط نقلها تختلف من بروتوكول لآخر. فمنهم من يعتمد على توليد رقم عشوائي في تقسيم الشبكة ومنهم من يعتمد على مدى بعد المجسات اللاسلكية عنها. فمن خلال المقارنات تبين أفضلية البروتوكول المعتمد على الطاقة المستقبلة عن استخدام الأرقام العشوائية. وأيضاً علاج العيوب المشهورة في البروتوكولات المستخدمة للأرقام العشوائية.

Two Efficient Unit Cell Designs for Polarization Independent 5-G Reflectarrays

**Rania Elsharkawy¹, A.R. Sebak², Moataza Hindy¹, Osama M. Haraz³,
Adel A. Saleeb⁴, and El-Sayed M. El-Rabaie⁴**

¹ Electronics Research Institute, Dokki, Giza, Egypt.

² ECEDepartment, Concordia University, Montreal, Quebec, Canada

³ Electrical Engineering Dept., Assiut University, Assiut 71515, Egypt

⁴ Faculty of Electronic Engineering, Menoufia University, Menouf, 32952, Egypt.

(Received: 15-November-2015 – Accepted: 05-Januray-2016)

Abstract

This paper presents two different polarization independent unit cells for reflectarray antenna that are suitable for 5-G mobile base-station applications and compares between them. The first unit cell is composed of two concentric rings and a cross loop inside and the second one contains three circular rings for bandwidth enhancement. These reflectarrays are designed around 28 GHz with $10\lambda \times 10\lambda$ aperture dimensions. The unit cells dimensions are $0.5\lambda \times 0.5\lambda$. A pyramidal horn antenna is used for the feeding purpose. The F/D ratio is taken as one. All the simulation stages are carried on the CST microwave studio. The simulation results show that the design with the UC₂ gives a better performance than the design with UC₁ from the aperture efficiency and the side-lobe level perspectives. Both designs offer a good cross-polarization level.

1. Introduction

With the advances of printed circuit technology, microstrip antennas have invaded the field of electromagnetics in the last decades. Microstrip reflectarray antennas have been developed to take place of large reflector antennas depending on printed circuit technology. The reflectarrays have several advantages compared to the traditional reflector antennas [1]. Reflectarrays have low profile, weight, and cost. They allow beamforming

in different directions. They can be adapted for several applications in different frequency bands.

The main idea of reflectarrays depends on phase adjustment of discrete elements. The design of a reflectarray antenna is based on the selection of an appropriate unit cell of certain size to achieve the required polarization [1]. The unit cell should be composed of some discrete elements that resonate at closely related frequencies to span the required bandwidth. The primary step to design a reflectarray is to create a phase diagram relating the unit cell size or relevant controlling parameter to the phase of the reflection coefficient by varying the unit cell size or controlling parameter and calculating the phase using the infinite array approach. The resulting phase diagram should preserve linearity as much as possible so that the phase change will not be overly sensitive to the element change to minimize the overall phase error in the array design [1]. The phase curve must span at least 360° to make sure that the unit cell is suitable for the design of a reflectarray antenna.

The reflectarray antenna consists of either a flat or a slightly curved reflecting surface and an illuminating feed antenna. The feed to reflectarrays is mostly performed with horn antennas. When the wave impinges upon the reflectarray surface, each element performs a certain phase shift corresponding to its size or geometry. The overall reflected components from the surface now form the collimated beam in a certain direction considered in the design process of the reflectarray. The efficiency of the designed reflectarray depends on the horn aperture, the array aperture, and the achieved gain [8]. This efficiency can be increased largely with large arrays [2], but the problem reduces again to an optimization process between the required specifications and the array size.

Circular rings are frequently used in reflectarray antennas. Li et al. presented an X-band reflectarray composed of 81 elements. The unit cell in this array consists of two rings. It is a polarization independent array [3]. Kalil et al. presented an Ultra-Wide Band (UWB) reflectarray antenna for tag localization in Radio Frequency Identification (RFID) applications. This array consists of unit cells with two circular rings [4]. It works at 2.2 GHz. The array consists of 10×10 unit cells, and it achieved a high gain pencil beam. Han et al. built a circular polarized high-gain X/Ka band reflectarray composed of two layers with varying elements [5]. Their unit cell is composed of a fixed-size single open-ring. The phase adaptation in

the different unit cells is performed with the rotation of open rings. Bialkowski et al. investigated the use of circular and square rings in the unit cells [6]. They proved that circular rings give better phase responses than square rings in terms of linearity. In addition, they proved that the use of a single ring may not achieve the required 360° phase range. This problem can be solved either with the incorporation of a Frequency Selective Surface (FSS) or the addition of another ring.

This paper presents two solutions to solve this problem. The first one is to use a unit cell with two circular rings with a solid cross inside. The second one is to use three circular rings. Each element resonates at a certain frequency leading to a wide bandwidth structure. The rest of this paper is organized as follows. Section II discusses the reflectarray design rules. Section III presents the unit cells structures. Section IV gives the reflectarray specifications. Section V gives the simulation results. The concluding remarks are given in section VI.

2. Design of Reflectarrays

The design parameters of the reflectarray are selected based on some factors including the required polarization, loss, cost, operating frequency, and required bandwidth. In addition, the required antenna gain is the main parameter that governs the antenna size. Figures 1 and 2 show two circular shapes suggested unit cell structures to build a reflectarray to work at 28 GHz for 5-G applications with loss specifications as shown in Figure 3. Two reflectarrays are built upon these designs of unit cells and compared. The arrangement of unit cells, their sizes and spacings are selected to achieve the required gain and avoid grating lobes.

The circular shape of the unit cells is selected to achieve polarization independence. The focal length of the array F is set to guarantee a 10 dB illumination at the edge elements of the reflectarray [7]. The ratio between the focal length and the antenna array edge F/D is the key factor that determines both the taper and spillover efficiencies, [8]. Several design rules are adopted for reflectarray design, one of which is the infinite array design rule. In this design rule, each array element must satisfy the following rule [1]:

$$k_o(R_i - \vec{r}_i \cdot \hat{r}_b) - \gamma_i = 2N\pi \quad (1)$$

Where, k_o refers to the free-space wavenumber, R_i is the spacing between the feed phase center and the reflectarray element center. The vector \vec{r}_i is the position vector that point from the reflectarray surface center to the the reflectarray element center. The unit vector \hat{r}_b points to the direction of the collimated beam. The integer number N is arbitrarily selected. The phase shift achieved by each element is γ_i .

Phase curves are designed by varying the unit cell size and studying the corresponding phase. From the designed phase curves the required unit cell with appropriate size is selected at each position. Operation on the linear regions of the phase curves shown in Figures 4 and 5 guarantees constant delays for reflected wave from each element. This, in turn, achieves phase collimation.

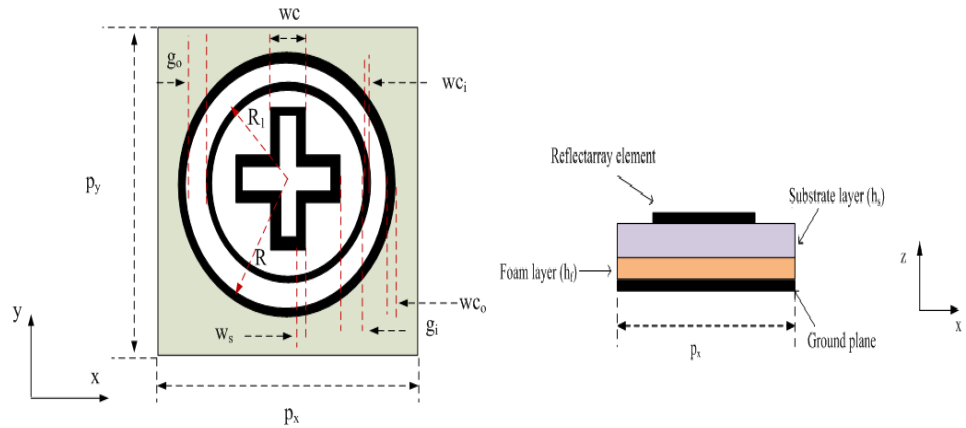


Figure 1: A UC_1 configuration of RA. The dimensions of UC_1 are (all in mm): $P_x = P_y = 10.7/2$, $R_i = R - g_o$, $w_{ci} = 0.2$, $w_{co} = 0.086$, $w_s = 0.086$, $g_o = 0.214$, $g_i = 0.214$, $h_s = 3.175$, $h_f = 2.95$ and $\epsilon_r = 2.2$ (Rogers RT 5880). UC refers to unit cell.

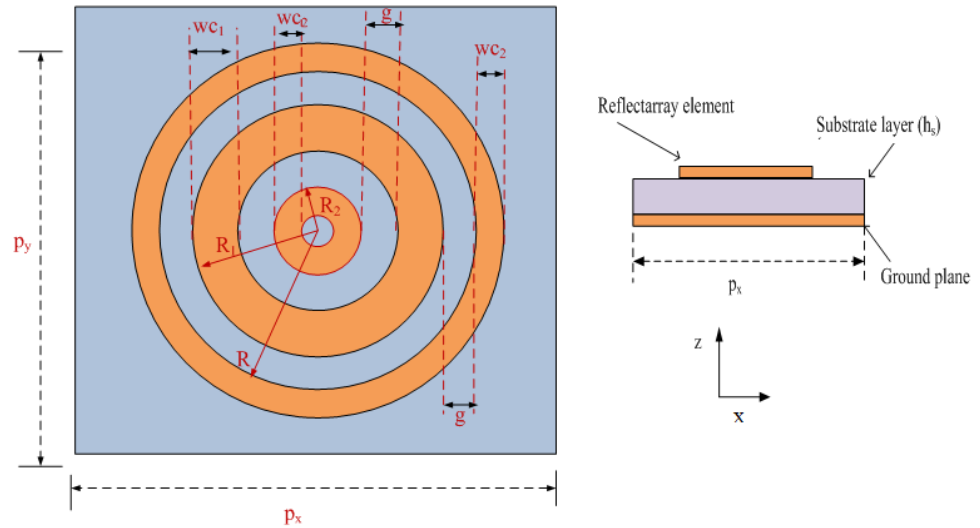


Figure 2: UC₂ configuration of the reflectarray. The dimensions of UC₂ are all in mm, $P_x = P_y = 10.7/2$, $R_1 = R - g$, $R_2 = R_1 - g - W_{c1}$, $W_{c1} = 0.2$, $W_{c2} = 0.1714$, $g = 0.214$, $h_s = 1.6$ and $\epsilon_r = 2.2$ (Rogers RT 5880).

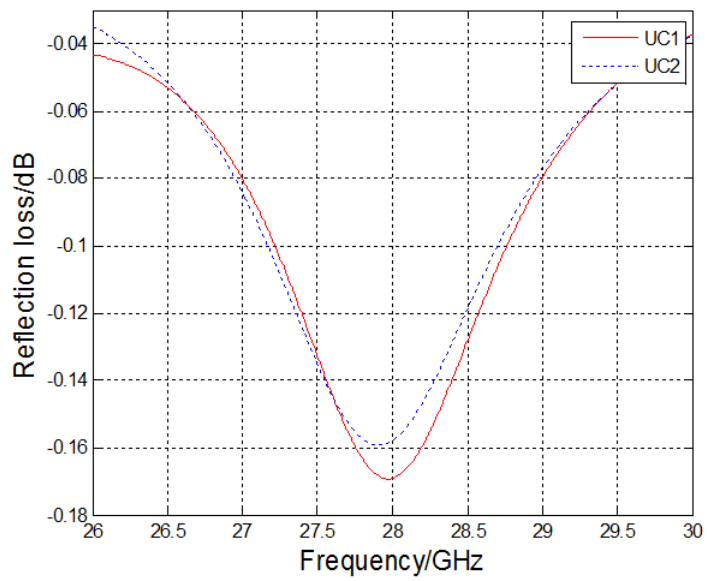


Figure 3: Reflection loss versus frequency for both UC₁ and UC₂

3. Unit cell structure

Some attempts have been presented to design polarization independent unit cells. One of such attempts was that of Niroo-Jazi et al., who developed a reflectarray containing polarization independent unit cells to work at 12 GHz [7]. This paper presents an extension to this unit cell that works at 28 GHz in addition to another simpler design of a circular unit cell to work at the same frequency. The first unit cell based on Niroo-Jazi design contains two circular rings with a cross loop as shown in Figure 1, but the substrate is thick containing two layers with a foam layer also. The suggested design to work at the same frequency range is simpler in the substrate and it contains three rings eliminating the cross in the first design (See Figure 2). The resonance frequencies of all elements, which are very close to each other, govern the operating bandwidth.

In both designs, the sizes of the unit cells are selected from the linear phase curves obtained for both *TE*- and *TM*-polarized waves with incidence angles up to 30°. Figure 3(a) shows the reflection loss versus frequency for both unit cells. From this figure, we can obtain the 10% and 20% bandwidths to be 612 and 917 MHz for UC₁ and 665 and 998 MHz for UC₂. UC₂ gives a wider bandwidth than UC₁, which is an important factor for comparison. The dimensions of the unit cells are optimized for linear phase variation for both *TE*- and *TM*-polarized incident angles up to 30°. The simulated phase of the reflection coefficient versus *R* in Figure 4 and Figure 5 shows a good linearity and insensitivity to polarization for both unit cells.

4. Reflectarray Specification

The designed reflectarray contains 400 cells and its area is $10\lambda \times 10\lambda$. The size of each unit cell is $\lambda/2 \times \lambda/2$. The type of feeding adopted is center feeding with $F/D = 1$, which means that the feeding source is put 10λ away from the array surface. The feed horn used is a pyramidal horn with aperture dimensions of (14×12.4×25) mm. The feeding waveguide is WR28 waveguide. The horn gain is 12.1 dB at 28 GHz as shown in Figure 6. The *E*- and *H*-plane half-power beam-widths are 43.8° and 48.2°, respectively. The simulation has been conducted with the CST Microwave studio [9].

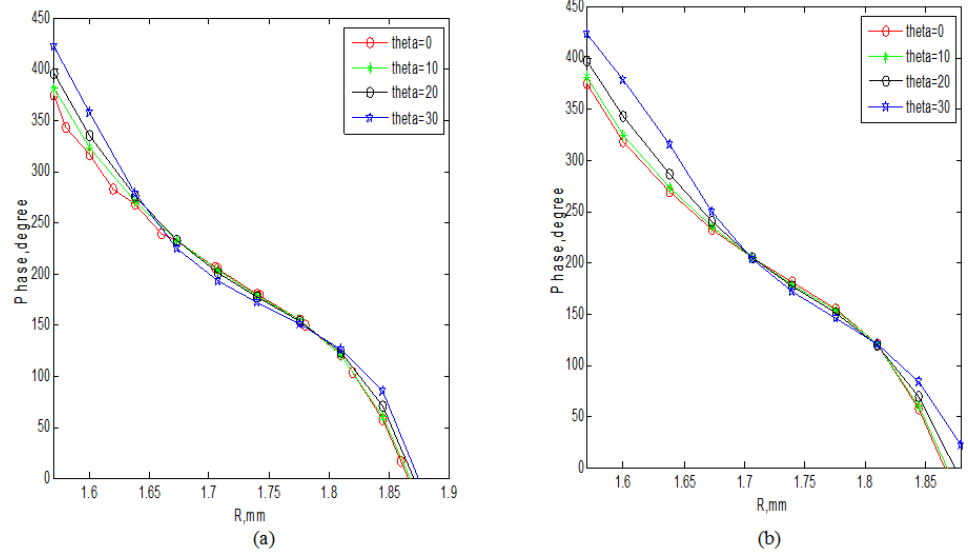


Figure 4: The reflection phase response of the UC₁ in case of (a) *TE*-incidence, (b) *TM*-incidence.

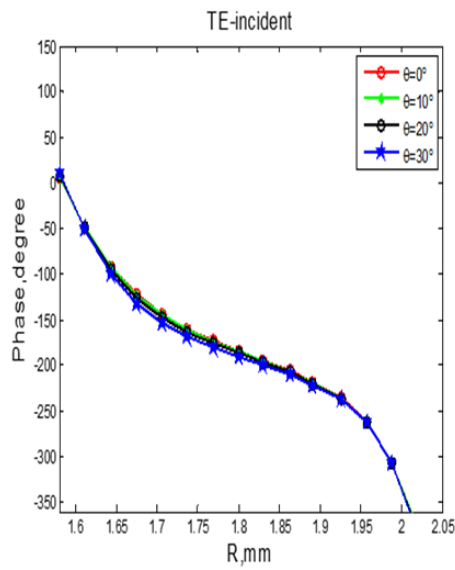


Figure 5: The reflection phase response of the UC₂ in case of *TE*-incidence

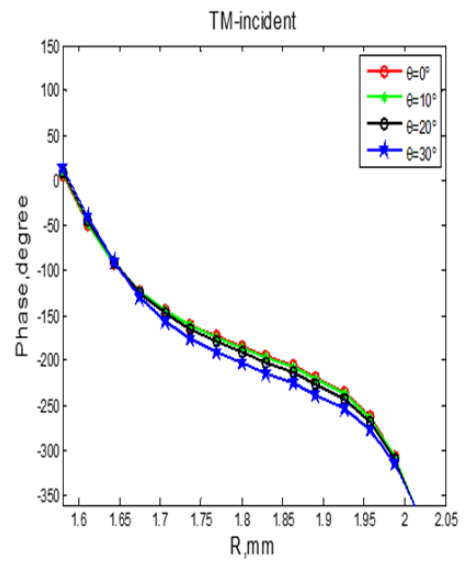


Figure 5: The reflection phase response of the UC₂ in case of *TM*-incidence

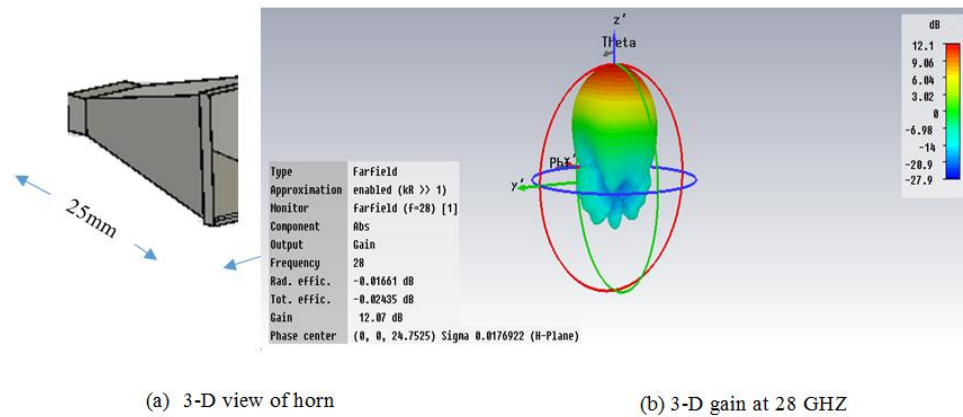


Figure 6: The geometry of linear polarized horn and the 3D gain at 28 GHZ

5. Simulation Results

Figures 7 and 8 illustrate E - and H -planes of the radiation pattern of the two designed reflectarray antennas at frequencies ranging from 26 to 29 GHz. These figures show that both designs offer a good cross polarization level. Figure 9 shows the gain variation with frequency over the frequency range of interest. This figure reveals a slight variation of the gain from 26 to 29 GHz. Table 1 and Table 2 summarize all arrays characteristics of the frequency band.

6. Conclusions

The paper presented two polarization independent reflectarray antennas suitable for 5-G mobile applications. These arrays have been built based on the infinite array approximation approach with variable-size unit cells. Simulation results revealed high gain-bandwidth product for both arrays due to the use of rings resonating at closely spaced frequencies. The designed reflectarray with UC_2 gives better results from the side-lobe levels and the aperture efficiency perspectives. Moreover, the design with UC_2 is simpler than the design with UC_1 as it has a single layer substrate, which makes the realization easier.

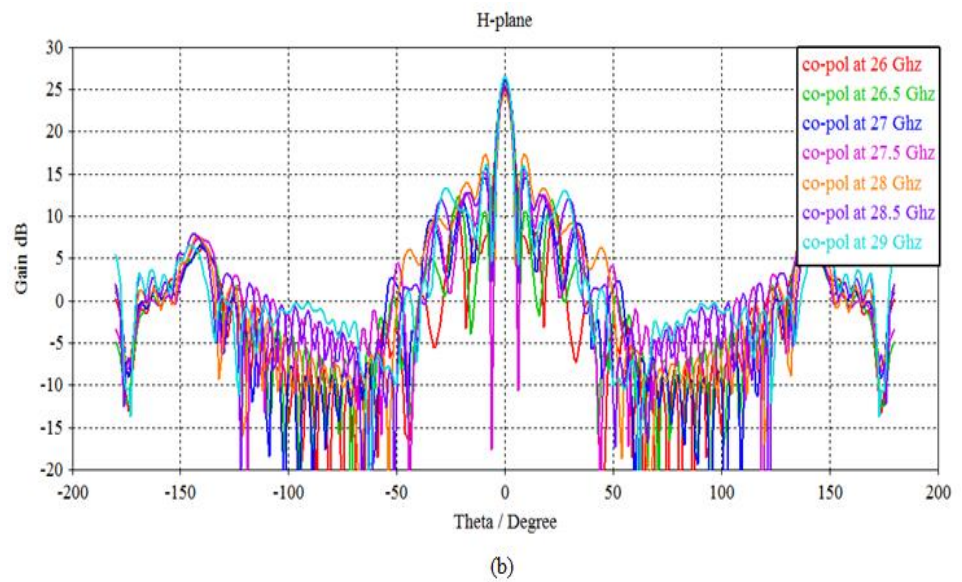
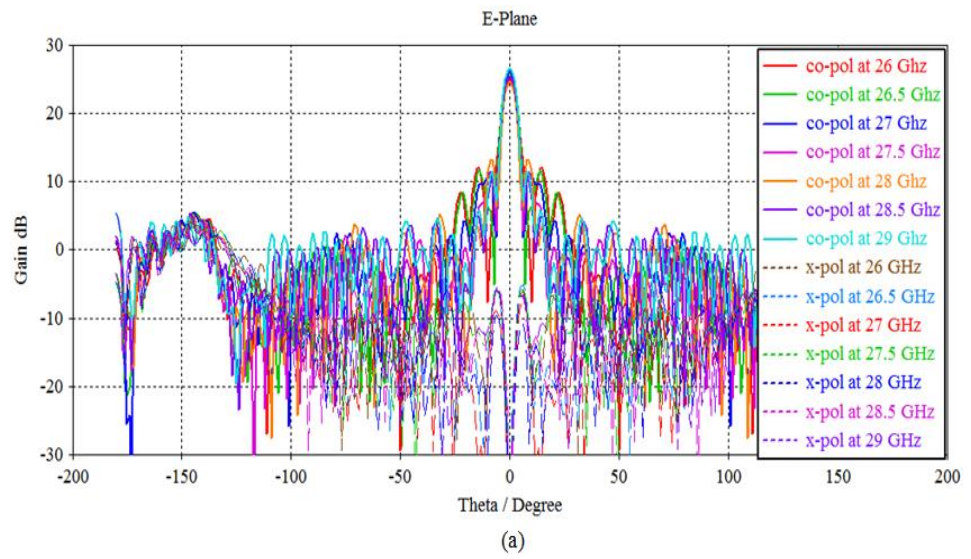


Figure 7: Radiation pattern of the RA antenna with UC₁ from 26 GHz to 29GHz
(a) E-plane (b) H-plane

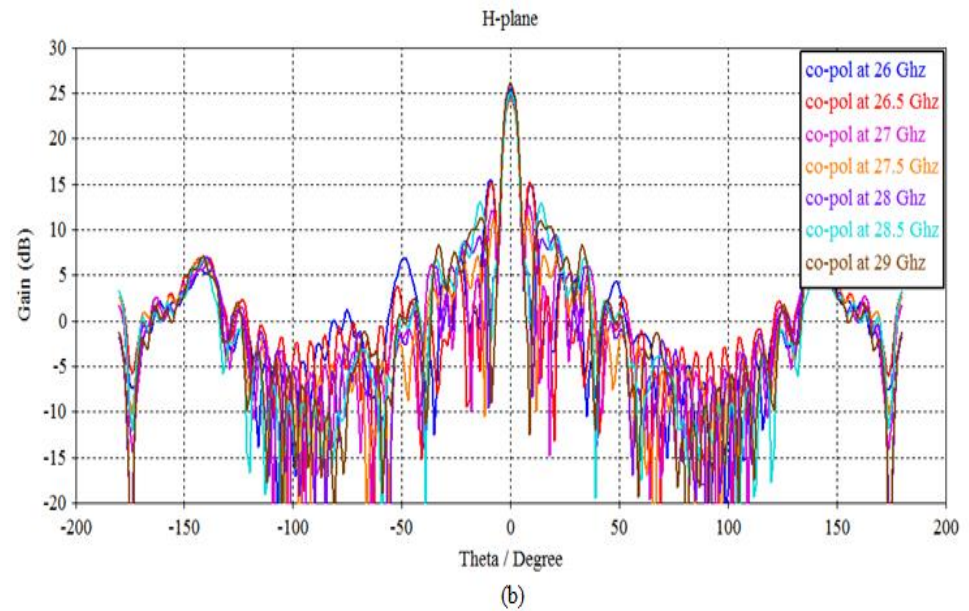
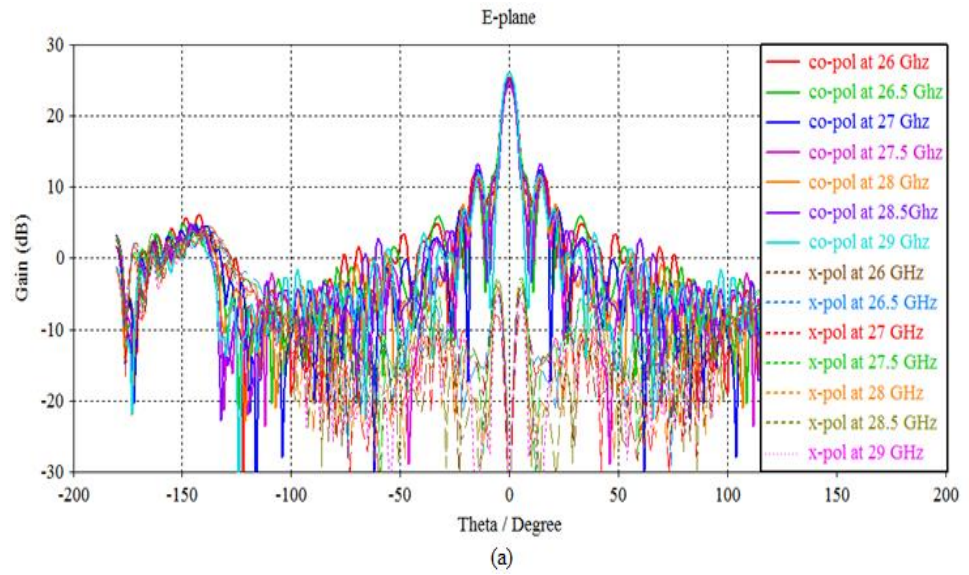


Figure 8: Radiation pattern of the RA antenna with UC₂ from 26 GHz to 29 GHz
(a) E-plane (b) H-plane.

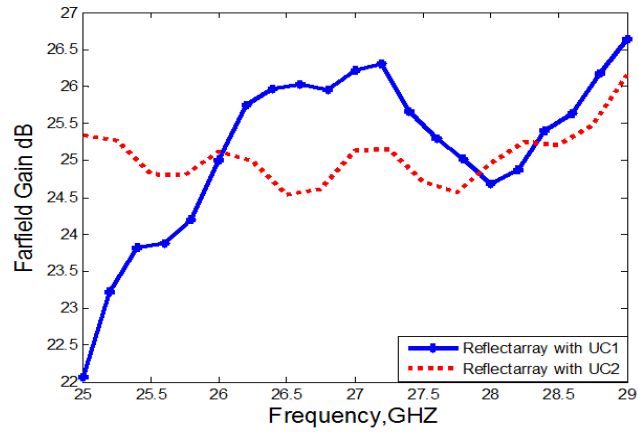


Figure 9: Realized gain of the RA antenna over the frequency band

Table 1: Radiation Pattern Characteristics for the reflectarray with UC₁

Frequency	SLL E-plane dB	SLL H-plane dB	Aperture Efficiency %	3dB HPBW E-plane	3dB HPBW H-plane	Gain (dBi)
26 GHz	-13	-14	37	6°	6.1°	25
26.5 GHz	-14.4	-13.7	45	5.7°	5.8°	26
27 GHz	-14.8	-11.7	45.5	5.4°	5.4°	26.2
27.5 GHz	-13.9	-10.3	36.5	5.2°	5.3°	25.4
28 GHz	-11.4	-7.3	29.9	5°	4.9°	24.7
28.5 GHz	-15	-9.7	34.7	5.3°	5°	25.5
29 GHz	-15.2	-10.4	43	5.1°	4.9°	26.6

Table 2: Radiation Pattern Characteristics for the reflectarray with UC₂

Frequency	SLL E-plane dB	SLL H-plane dB	Aperture Efficiency %	3dB HPBW E-plane	3dB HPBW H-plane	Gain (dBi)
26 GHz	-13.6	-10	41.8	5.7°	5.2°	25.5
26.5 GHz	-13.5	-9.6	34.25	5.5°	5.1°	24.8
27 GHz	-12.8	-12.5	36.18	5.2°	5°	25.2
27.5 GHz	-13.7	-13.1	29.68	5.1°	5°	24.5
28 GHz	-13.3	-15.5	31.39	5.2°	5.1°	24.9
28.5 GHz	-12	-12	32.47	5°	5°	25.2
29 GHz	-14.4	-14.9	39.48	5.2°	5°	26.2

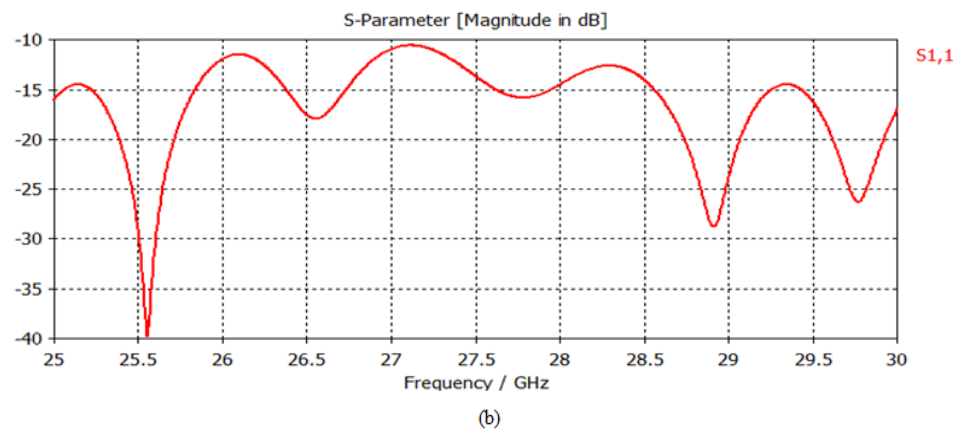
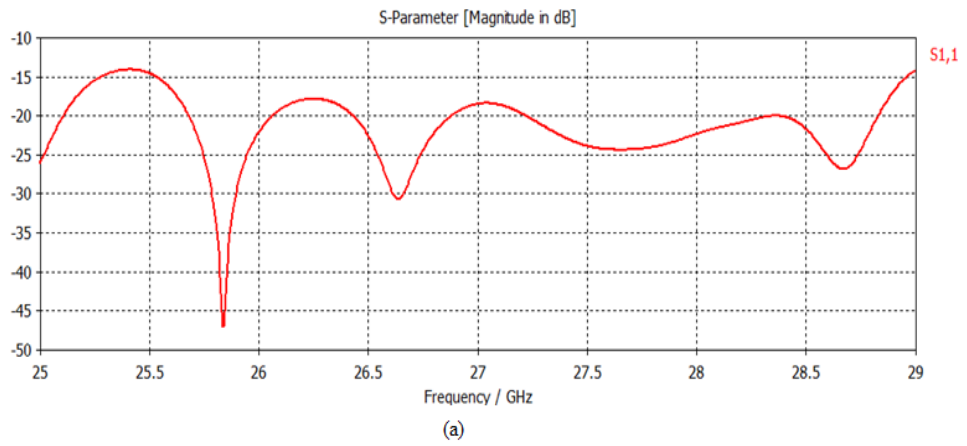


Figure 10: Reflection coefficient for the reflectarray antenna.
(a) Antenna with UC1 (b) Antenna with UC2.

References

- [1] J. Huang, J. A. Encinar, Reflectarray Antennas, A John Wiley & Sons, Inc., Publication, 2008.
- [2] C. Balanis, Antenna Theory Analysis and Design 3rd edition, A John Wiley & Sons, Inc., Publication, 2005.
- [3] Y. Li, M. E. Bialkowski, K. H. Sayidmarie, N. V. Shuley, “ 81-element single-layer reflectarray with double-ring phasing elements for wideband applications,” IEEE Antennas and Propagation Society International Symposium (APSURSI), Toronto, pp. 1-4, July, 2010.

- [4] M. Khaliel, A. Fawky, M. El-Hadidy, T. Kaiser, “ UWB Reflectarray Antenna for Chipless RFID Applications,” 31st National Radio Science Conference of Egypt, pp. 17-20, April, 2010.
- [5] C. Han ; J. Huang, K. Chang, “ A high efficiency offset-fed X/ka-dual-band reflectarray using thin membranes,” IEEE Transactions on Antennas and Propagation, Vol. 53, No. 9, pp. 2792 – 2798, September, 2005.
- [6] M. E. Bialkowski, Khalil H. Sayidmarie, “Investigations Into Phase Characteristics of a Single-Layer Reflectarray Employing Patch or Ring Elements of Variable Size,” IEEE Transactions on Antennas and Propagation, Vol. 5, No. 11, pp. 3366– 3372, November, 2008.
- [7] M. Niroo-Jazi, M. R. Chaharmir, J. Shaker, and A. R. Sebak, “ Reflectarray antennas using single layer polarization independent multi-resonant unit cells,” IEEE Antennas and Propagation Society International Symposium (APSURSI), 2014.
- [8] M. Zebrowski, “Illumination and Spillover Efficiency Calculations for Rectangular Reflectarray Antennas,” High Frequency Design, pp. 28-38, December, 2012.
- [9] CST-Computer Simulation Technology, Documentation. Available online: www.cst.com.

الملخص العربي

يقدم هذا البحث تصميمين جديدين لمصفوفات الهوائيات العاكسة للعمل في محطات الاستقبال الخاصة بالجيل الخامس من خدمات الهاتف الخلوى. و قد قدم البحث دراسة للوحدات البنائية لكل من المصفوفتين المقترحتين اعتمادا على عناصر دائرية مطبوعة في شكل دوائر شريطية. و قد أظهرت الوحدات البنائية المقترحة أداء خطيا للطور الخاص بالوحدات البنائية مع تغير أبعاد الوحدة البنائية. و يتسم أحد التصميمين بالبساطة مقارنة بالآخر و قد أظهرت النتائج أداء جيدا لكل من التصميمين من منظور الكفاءة و الكسب مما يؤيد امكانية استخدام التصميم الأبسط في مصفوفات الهوائيات العاكسة في محطات الاستقبال للجيل الخامس من شبكات الهاتف الخلوى لتحسين الأداء.

A Survey of Different Steganography Techniques

E. A. Elshazly*, Safey A. S. Abdelwahab*, R. M. Fikry*, O. Zahran, S. M. Elaraby* and M. El-Kordy****

* Engineering Dep., Nuclear Research Center, Atomic Energy Authority, Cairo, Egypt.

** Electronics and Electrical Communications Engineering Dep., Faculty of Electronic Engineering, Menoufia University, Menouf, Egypt

(Received: 15-November-2015 – Accepted: 06-December-2015)

Abstract

Steganography is defined as the art and science of embedding data in a cover object without leaving a remarkable track on the cover object, in other words it is the study of invisible communications. It is usually dealing with the methods of hiding the existence of data to be transmitted in such a way that, it remains confidential. The main objectives of steganography are high capacity of the hidden data, perceptual transparency (invisibility), temper resistance, undetectability, computation complexity and robustness. It is classified into three categories which are; pure (no key), secret key, public key steganography. According to the type of the cover object, there are different types of steganography which are; image, audio, video, network and text. In the image steganography, the secrecy can be achieved by hiding data into the cover image and generating the stego-image. According to the embedding techniques, there are different techniques of steganography which are those embedding in the spatial domain (substitution method), those embedding in the transform domain (frequency domain), spread spectrum techniques, distortion techniques, masking and filtering techniques, and cover generation techniques. Each of these techniques has its strengths and weaknesses for different algorithms. This paper presents a review of these techniques; the different algorithms, concepts, advantages and disadvantages. The steps of the different algorithms of these techniques will presented in details, with a comparison between all these techniques. The different applications of steganography, the attacks, and the robust image steganography against attacks are presented. Lastly, the future and the novel trends in steganography are presented.

1. Introduction

There are many different digital image processing algorithms whereas; data hiding is considered as one of the most important algorithms. Data hiding is the art of embedding data for various purposes such as; maintaining private data, secure confidential data and so on. The most common techniques that used for data hiding are; steganography and watermarking; steganography is an ancient well-known technology, which has many applications even in today's modern society. It is the art and science of embedding a secret message within a cover media in such a way that, only intended recipient has knowledge about secret message and the extraction of it at its destination. Cover media can be image, audio, video, text or network. It is concerned with transmitting a secret message while embedding its existence. The word "steganography" is derived from the Greek words "steganos" which meaning "**covered**" and "graphie" which meaning "**writing**" that defining it as "**covered writing**" [1, 2].

Watermarking is the process of inserting a low energy signal (the watermark) into a high energy one (visible or invisible), without any effect on the main signal features. A good watermarking technique should satisfy four requirements; robustness, imperceptibility, security and capacity [3, 4]. Cryptography is the science of enabling secure communications between a sender and one or more recipients. It is not concerned with embedding the existence of a message, but it converts the plaintext to cipher text by using encryption key at the transmitter and decrypts the cipher text to plaintext at the receiver. The word cryptography is derived from the Greek word "kryptos", which meaning "**hidden**" [4, 5].

In these days, the communication happens in every growing area. All people wants the particular safety and secrecy of the communicating data. In our lifestyle, many secure pathways like telephone or perhaps internet to transfer and share data are used, but it may not be protected at a certain level. So that to share data in a very much more hidden fashion, cryptography and steganography approaches should be used [6]. In cryptography, an encryption key which is known to both transmitter and receiver is used to modify the data to an encrypted form. This data cannot be accessed in anyplace without making use of the particular encryption key, however the encrypted data transmission may easily arouse attacker's suspicion, and the encrypted data can be intercepted, attacked or perhaps decrypted strongly. So that to overcome the drawbacks of cryptography approaches, steganography approaches are actually used [7]. Table 1

presents a comparison between the steganography, watermarking and cryptography approaches [8]. The main purpose of steganography is actually hiding data in a cover object, so that others will not be capable to identify it, the main purpose of watermarking is actually copyright preserving and the main purpose of cryptography is actually protecting the content of messages [9]. Figure 1 shows the data hiding scheme.

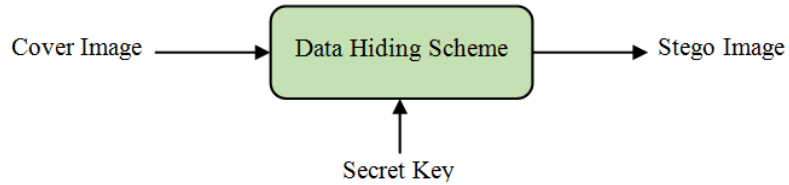


Figure 1: Data hiding scheme

Table (1): Comparison of Steganography, Watermarking and Cryptography

Criterion/Method	Steganography	Watermarking	cryptography
Cover	Any type of digital media	Audio files/ images	Text-based, with some extensions to an image files
Secret message	Payload	Watermark	Plain-text
Key	not necessary		
Input files	At least two inputs		Only one
Authentication	Recovery of all data	Achieved by a cross correlation	Recovery of all data
Objective	Secret communication	Copyright preserving	Protection of data
Detection	Blind	The cover or watermark is needed in recovery stage (informative)	Blind
Output file	Stego-file	Watermarked-file	Cipher-text
Concern	Detectability/ capacity	Robustness	Robustness
Kind of attacks	Steganalysis	Image processing	Cryptanalysis
Visibility	Never	Sometimes	Always
Fails	When it is detected	It is removed/ replaced	De-ciphered
Relation to cover	Not necessarily (the message is more important than the cover object)	An attribute of the cover image (the cover is more important than the message)	N/A
Flexibility	Choice of cover is free (i.e, choose any suitable cover)	Restriction to choose the cover	N/A

The data hiding applications of the systems ranges over a broad area of military, intelligence agencies, online elections, internet banking, medical-imaging and so on. These varieties of applications make the steganography to be an important topic to be studied. The cover object is usually chosen with taking into consideration, the size and the type of a secret message and the different formats of carrier file that can be used.

The remaining of this paper is organized as follows; Section 2 introduces the basic structure of steganography; the types, the terminologies, and the factors affecting on the steganography. Section 3 presents the different categories of steganography. Section 4 discusses the various techniques of steganography. Section 5 presents the different applications of steganography. Section 6 discusses the robustness of image steganography against attacks. Section 7 presents the future and a novel trend for steganography techniques. Finally, section 8 introduces the conclusions

2. Basic Structure of Steganography

The steganography is not only the art of embedding data, but also embedding the fact of sending of the secret data. It embeds the secret data in another file in such a way that only the recipient knows the existence of message [11].

The main equation of steganography is:

$$\text{Stego object} = \text{Cover object} + \text{Secret message} + \text{Stego key} \quad (1)$$

The hidden data is the secret message that one wishes to send secretly. The stego key is used to control the embedding process to restrict the detection and /or the recovery of the hidden data to parties who know it. Figure 2 describes the different branches of steganography in security domain [8, 10].

2.1 Types of Steganography

According to the type of the cover object, there are five types of steganography techniques [12]. Figure 3 shows the types of steganography.

1. **Image Steganography:** In this technique, the cover object is an image, and the pixel intensities of this image are used to hide the secret message [13].
2. **Video Steganography:** In this technique, the digital video is used as a cover object to hide any kind of files or information. Generally, the Discrete **Cosine** Transform (DCT) alters the values which are used to embed the data in each frame in the video, which are not detected by the human eye. The video formats that used in video steganography

are H.264, Moving Picture Experts Group (MPEG), Mp4, AVI or any other formats [13, 14].

3. **Audio Steganography:** In this technique, the audio is used as a cover object for data hiding. Due to the voice over IP (VOIP) popularity, the audio has become very significant medium. The digital audio formats like AVI, WAVE, MPEG, or MIDI can be used for audio steganography [13, 15].
4. **Text Steganography:** In this technique, the text is used as a cover object for data hiding. Hiding **data** in a text is a most important method of steganography. The method is used to embed a secret message in every n^{th} letter of every word of a cover text. Because the text files have a small amount of redundant data, text steganography is not used very often [13, 16].
5. **Network Steganography:** In this technique, the network protocol is used a cover object, and this type is known as a network protocol steganography. In the Open Systems Interconnection (OSI) network layer model, the steganography can be performed in unused header bits of Transmission Control Protocol/Internet Protocol (TCP/ IP) fields [17].

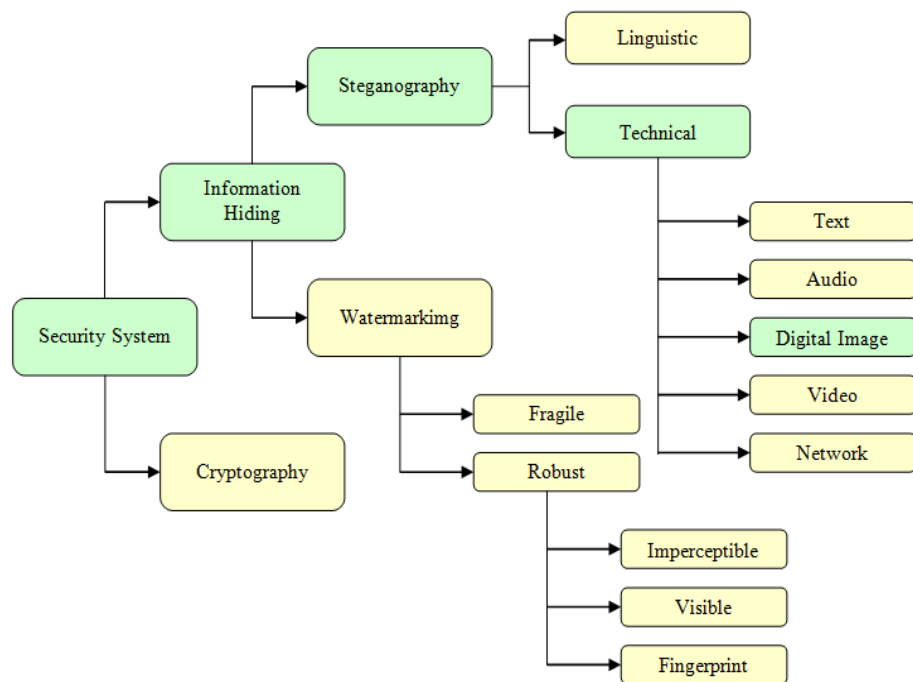


Figure 2: Steganography in Security Domain

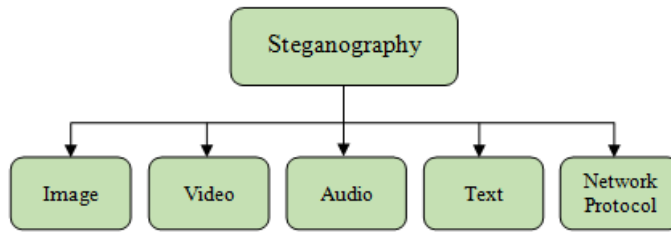


Figure 3: Types of Steganography

2.2 Terminologies of Steganography

Steganography consists of two main terms; a secret message and a cover object. Secret message is the secret data to be hidden, while cover object is the carrier that embeds the secret message in it. Figure (4) shows the basic steganography diagram [18]. After embedding the secret message into the cover object, the resultant object is known as a stego-object, while key used for hiding or extracting the secret messages from cover objects and stego-objects, is called a "stego key".

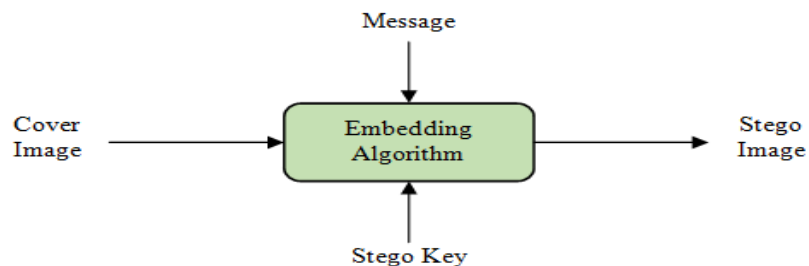


Figure 4: Steganography Diagram

2.3 Factors Affecting on the Image Steganography Techniques

The effectiveness of image steganography approaches is determined by comparing the stego-image with the cover image. The actual factors determine the efficiency of an image steganography approaches are generally [18, 19]:

1. **Robustness:** The ability of hidden information to keep intact regardless of whether the stego-image undergoes transformations.

For example, sharpening, linear and non-linear filtering, addition of random noise, blurring, scaling, shifts, rotations, decimation, cropping, or even lossy compression.

2. **Imperceptibility:** This describes the invisibility of an image steganography and the ability of the steganography approaches to be able to embed messages in an undetected way in which there is no-one to view almost any visible distortions or even artifacts inside the carrier file. This therefore helps prevent drawing suspicions along with obscures the fact that a secret communication is usually occurring. Because it is the first and foremost requirement, since the strength of steganography lies in its capability to possibly be undetected by the human eye.
3. **Payload Capacity:** It refers to the amount of secret data which might be embedded inside the cover object without damaging or even distorting it. In image steganography, it is very important to hide as much as possible data inside the carrier image devoid of which makes it blurry, devoid of raising its brightness, along with devoid of changing its size. This has to be a key element in making the embedded information imperceptible and the carrier image innocent along with unsuspecting. Watermarking normally hides only a small amount of copyright data, whereas, steganography focuses on embedded communication and therefore have sufficient hiding capacity.
4. **Computational Complexity:** This describes the computational cost of hiding and recovering of the secret data.
5. **Mean Square Error (MSE):** It is defined as the mean squared difference between a new stego-image and a cover image. The actual image steganography approach is usually more efficient, as the MSE is smaller. MSE can be computed by taking summation of the squared differences of all pixels and then dividing by the total amount of pixels. If I_C and I_S are the cover image and stego-image respectively, the MSE is calculated using the following equations [19]:

$$MSE = \frac{1}{M \times N} \sum_{i=0}^{N-1} \sum_{j=0}^{M-1} [I_S(i, j) - I_C(i, j)]^2 \quad (\text{For Grayscale Images}) \quad (2)$$

$$MSE_{RGB} = \left[\frac{MSE(R) + MSE(G) + MSE(B)}{3} \right] \quad (\text{For color Images}) \quad (3)$$

Where M is the number of rows and N is the number of columns in the cover image.

- 6. Peak Signal to Noise Ratio (PSNR):** It is defined as the quality measurement between the cover image and stego-image. The greater values of PSNR represent the better quality of the stego-image. The value of the PSNR is computed using the following equation [19]:

$$PSNR = 10 \log_{10} \left(\frac{C_{\max}^2}{MSE_{RGB}} \right) \quad (4)$$

Where C_{\max} holds the maximum value in the original images.

- 7. Normalized Cross-Correlation (NCC):** It can be used as a metric to evaluate the degree of similarity (or dissimilarity) between the stego-image and the cover image. The NCC is calculated using the following equation [20].

$$NCC = \frac{\sum_{i=0}^{N-1} \sum_{j=0}^{M-1} C(i, j) \cdot S(i, j)}{\sum_{i=0}^{N-1} \sum_{j=0}^{M-1} C^2(i, j)} \quad (5)$$

Table 2 summarizes the best image steganography measures [18, 19].

Table 2: Measures of Image Steganography Algorithm

Measures	Advantage	Disadvantage
Robustness	High	Low
Imperceptibility	High	Low
Payload Capacity	High	Low
Computation Complexity	Low	High
MSE	Low	High
PSNR	High	Low
NCC	High	Low

3. Categories of Steganography

Steganography can be classified into 3 categories which are [21]:

- 1. Pure steganography (or No Key Steganography - NKS):** It is the simplest and weakest category of steganography in which, the secret message is directly hidden into the cover object without any encryption.

The success of this hidden communication depends on the assumption that, parties other than the intended receivers (attackers) are not aware of the existence of the secret message [22]. Figure (5) shows the pure steganography.

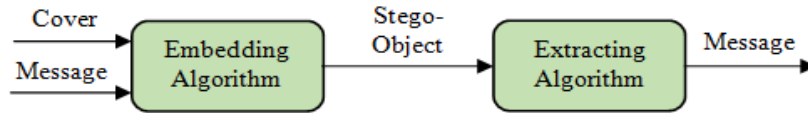


Figure 5: Pure Steganography

- 2. Secret key steganography (SKS):** In this form of steganography, both the receiver and sender have common agreed secret keys. The secret message is hidden into and extracted out of the stego-image using these keys. The keys can be separately shared between both parties using some confidential channel prior to the actual transmission starts. The strength of this system is its higher security. Parties other than the intended receiver cannot retrieve the secret message or require a very high computational time and maximum power to retrieve it applying some brute force methods, in the case that they suspect the presence of the secret information. The robustness of this system lies with the secrecy of the keys and the difficult part in this method is about, how to share the keys between the sending and receiving parties maintaining their secrecies [22]. Figure (6) shows the secret key steganography.

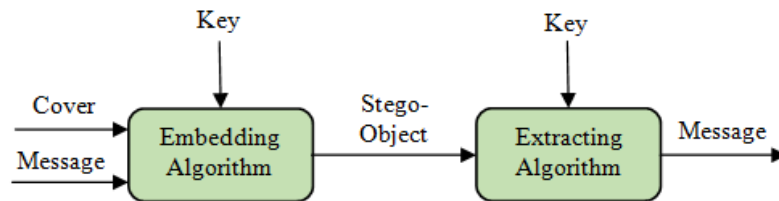


Figure 6: Secret Key Steganography

- 3. Public Key Steganography (PKS):** This methods use both public and private keys to hide the secret information. The key benefits of this system are its robustness as well as it is an easy key management. The method is robust because the parties other than the intended receivers need to know both the private and public keys used for embedding in addition to the encryption algorithms used, in order to be able to extract the hidden information [22].

Table (3) summarizes a comparison between different categories of steganography [23].

Table 3: Comparison between Different Steganography Categories

Technique		Capacity	Robustness	Security	Invisibility	Key management/ Complexity of Embedding
NKS	OBS	Low	medium	Low	Very High	Not required /Low
	MBS	High			Very High	Not required /Low
PKS	OBS	Low	Medium	High	Very High	Easy / Low
	MBS	High			Very High	Easy / Low
SKS	OBS	Low	medium	Very High	Very High	Difficult / Low
	MBS	High			Very High	Difficult / Low

OBS: One Bit Substitution

MBS: Multiple Bit Substitution

4. Techniques of Image Steganography

Techniques of image steganography are divided into the following techniques [24, 25]:

- 1. Substitution methods:** the redundant parts of a cover can be substituted with a secret data.
- 2. Transform domain techniques:** hide a secret message in a transform domain of the image.
- 3. Spread spectrum techniques:** follow the ideas of spread spectrum communication.
- 4. Distortion techniques:** embed data by signal distortion and then measure the deviation from the cover object in the decoding stage.
- 5. Masking and Filtering:** embed data by marking the cover image. These techniques hide the data in the more significant regions than embedding it into the noise level.
- 6. Cover generation methods:** do not embed messages in a randomly chosen cover-objects, but create covers that fit a message that need to be hidden.

These steganography techniques will be explained in more details as follows:-

1. Substitution methods:

These methods are known as "a spatial domain methods". There are different algorithms of these methods, all directly change the redundant bits in the image pixel values in embedding the secret message. The Least significant bit (LSB) based steganography can be considered as one of the most important algorithms that embeds a secret message in the LSBs of pixel values without leaving any perceptible distortions. The changes in the LSBs of the pixels are imperceptible for human eyes [26]. These techniques are classified into the following algorithms:

- A. Least significant bit (LSB):** The Least Significant Bit (LSB) is most well-known algorithm to hide a secret text in an image. The LSB embedding algorithm replaces the LSBs of the pixels of the cover image by the bit stream of the secret text to be hidden. The stego-image is almost similar to the cover image because the change in the LSBs of image pixels does not introduce too much difference in the image [27]. If the LSB of the pixel value $I_C(i, j)$ is equal to the message bit m to be embedded, $I_C(i, j)$ remain unchanged; if not, the LSB of $I_C(i, j)$ is set to m . The stego-image is obtained according to the following formula [28].

$$I_S(i, j) = \begin{cases} I_C(i, j) - 1 & \text{LSB}(I_C(i, j)) = 1 \text{ and } m = 0 \\ I_C(i, j) & \text{LSB}(I_C(i, j)) = m \\ I_C(i, j) + 1 & \text{LSB}(I_C(i, j)) = 0 \text{ and } m = 1 \end{cases} \quad (6)$$

where $\text{LSB}(I_C(i, j))$ stands for the LSB of $I_C(i, j)$ and m is the next bit to be embedded. In the case of 24-bit images, three bits can be embedded in each pixel by changing a bit in each color component. Given three adjacent pixels (9 bytes) with the RGB encoding as follows [28].

```
10010101 00001101 11001001
10010110 00001111 11001011
10011111 00010000 11001011
```

To embed the number 400, with a binary representation is (110 010 000), into the LSBs of the above part of the image (9 bytes), we get the following new 9 bytes:

```
10010101 00001100 11001001
10010110 00001111 11001010
10011110 00010000 11001010
```

The number 400 is hidden into the grid, only 4 bits need to be changed according to the message to be embedded. This means that, only 50% of pixels of an image are needed to be modified to embed a secret message in the case of full capacity (the number of bits in the secret message equals to the number of pixels in the cover image). Using the human eye, it will be hardly to notice the difference between the cover image and the stego-image [28].

B. Pixel value differencing (PVD): Based on the fact that the human vision is sensitive to the slight changes in the smooth regions, while in the edge regions it can be tolerate more severe changes. The PVD-based algorithm is used to enhance the embedding capacity without leaving obvious visual distortions or artifacts into stego-images. In this method, two consecutive pixels (the pixel and its neighbor) are selected for hiding the secret message. The larger the difference between the two consecutive pixels, the more secret bits can be hidden. Usually, PVD-based approaches can achieve more imperceptible results compared with those typical LSB-based approaches with the same capacity of embedding. Payload can be determined by checking the difference between the two consecutive pixels and it serves as basis for identifying whether the two pixels belongs to an edge area or smooth area. Based on extensive experiments and analysis, the most existing PVD based algorithms perform bad in resistance to some statistical analysis even with a low embedding capacity [29, 30].

Firstly, the cover image is segmented straight into non-overlapping blocks, each has two consecutive pixels (p_i and p_{i+1}). In each block, the difference value d_i can be computed by subtracting p_i from p_{i+1} . All difference values are range from -255 to 255. Therefore, the absolute of difference values $|d_i|$ range from 0 to 255. The blocks with large difference values locate in the sharp edged area, while the blocks with small difference values are in smooth area. In the PVD algorithm, a range table has been designed with n contiguous ranges R_k (where $k=1,2,\dots,n$), and the range is 0 to 255. The upper and lower bound are denoted as u_k and l_k respectively, then $R_k \in [l_k, u_k]$. The actual width of R_k is computed as $w_k = u_k - l_k + 1$. w_k , decides how many bits can be embedded in a pixel block. For security purpose R_k is kept as a variable. Therefore, the original range table is required to extract the hidden data. The actual steps of the embedding algorithm are as follows [29, 30]:

1. Compute the difference value (d_i) of the two consecutive pixels p_i and p_{i+1} for every block in the cover image, this is given by $d_i = |p_{i+1} - p_i|$.
2. Calculate the optimal range, where the difference lies in the range table by utilizing d_i . This is calculated as $R_i = \min (u_k - d_i)$, where $u_k \geq d_i$ for all $1 \leq k \leq n$.
3. Calculate the number of bits (t) to be embedded in a pixel block which can be defined as $t = \lfloor \log_2 (w_i) \rfloor$, where w_i is the width of the range in which, the pixel difference d_i is actually that belong.
4. Read t bits from binary secret message as well as convert it directly into its decimal value b . For instance if $t=011$, then $b=3$.
5. Compute the new difference value (d_i') which can be given by $d_i' = l_i + b$.
6. Modify the values of p_i and p_{i+1} , using the following formula:

$$(p_i', p_{i+1}') = \begin{cases} (p_i + \lceil m/2 \rceil, p_{i+1} - \lfloor m/2 \rfloor), & \text{if } p_i \geq p_{i+1} \text{ and } d_i' > d_i \\ (p_i - \lfloor m/2 \rfloor, p_{i+1} + \lceil m/2 \rceil), & \text{if } p_i < p_{i+1} \text{ and } d_i' > d_i \\ (p_i - \lceil m/2 \rceil, p_{i+1} + \lfloor m/2 \rfloor), & \text{if } p_i \geq p_{i+1} \text{ and } d_i' \leq d_i \\ (p_i + \lfloor m/2 \rfloor, p_{i+1} - \lceil m/2 \rceil), & \text{if } p_i < p_{i+1} \text{ and } d_i' \leq d_i \end{cases} \quad (7)$$

Where, $m = |d_i' - d_i|$. The pixel pair (p_i', p_{i+1}') will be acquired soon after hiding the secret message directly into pixel pair (p_i, p_{i+1}) . Step 1 – 6 are usually repeated until all secret message are hidden into the cover image, and the stego-image is formed.

When extracting the actual embedded data from the stego-image, the original range table is needed. Firstly, the stego-image is actually segmented into pixel blocks, each contains two consecutive non-overlapping pixels. The difference value is actually calculated for each block as $d_i' = |p_i' - p_{i+1}'|$. Then, the particular range R_i of d_i' can be found, and b' can be obtained by subtracting l_i from d_i' . By converting b' into its binary of ' t ' bits, where $t = \lfloor \log_2 (w_i) \rfloor$, these t bits which might be the actual inserted data are generally obtained from the actual pixel block (p_i', p_{i+1}') [29, 30].

- C. Edges based data embedding method (EBE):** Canny edge detection algorithm embeds secret data into the pixels, which can make in the extracted edges of the cover image. The secret message might be

almost any type and they are basically hidden into the three LSBs of the pixels of the cover image, and not in all pixels, only within the pixels that are part of the edges that detected by the algorithm of edge detection [31]. The actual edge area can tolerate more changes than smooth area, so the robustness will increase using this technique but the payload capacity is less because non-edge area pixels are not used for embedding data. To improve payload capacity hybrid edge detector technique is developed in which the combination of both canny and fuzzy edge detection techniques is used. In this technique, different amount of data bits are embedded to edge-pixels and non-edge pixels but this technique is applied only to gray scale image [31].

- D. Random pixel embedding method (RPE):** In this algorithm, the data is embedded randomly i.e., the data is embedded in some pixels, selected randomly for increasing robustness against attack. Last two bits of each random position pixel are used for embedding the message. These random pixels are generated by using Fibonacci algorithm [32].
- E. Mapping pixel to hidden data method (PMM):** This technique is utilized to map the data (not hide or embed it) through adapting the particular the gray level values of the image pixels. This method uses the idea of even and odd numbers to map the message within an image, which is a one-to-one mapping between the selected pixels in an image and the binary data. A set of pixels from a given image are selected depending on a numerical perform. The gray level values of these pixels are generally reviewed along with weighed against the particular bits which is to be mapped inside the image [33].
- F. Labeling or connectivity method:** The morphological processing starts at the peaks in the marker image in addition to spreads throughout the remaining of the image in line with the connectivity of the pixels. The connectivity defines which pixels are connected to other pixels. A group of pixels that connected depended on connectivity types is called an object [34].
- G. Pixel intensity based method:** In this particular method, the hiding pixels are generally determined depend on any exact function which in turn is dependent upon the pixel intensity value of the seed pixel as well as the 8 neighbors are generally determined in counter clockwise path. Just before hiding, a verification may be carried out to find out

whether the determined hiding pixels or even their neighbors lies in the boundaries of the image or even certainly not. Information hiding is carried out simply by mapping each two or even four bits of the secret data within each of the neighbor pixel depended on some features of that pixel [35].

H. Texture based method: In this technique, the secret and host images are divided into blocks of specific size and each block in secret image is taken as a texture pattern for which the most similar block is found among the blocks of the host image. The embedding procedure is carried on by replacing these small blocks of the secret image with blocks in host image in such a way that least distortion would be imposed on it [36, 37].

I. Histogram shifting methods: In this method, the crucial information is embedded into the image histogram. Pairs of peak points and zero points are used to achieve low hiding distortion with respect to providing low data hiding capacity [39, 40].

In [27], the author used the histogram and statistical analysis methods to possibly identify an image with embedded data. The existing LSB steganography algorithms embed the secret message into the cover image by replacing directly the LSBs of the cover image by the bits of secret message. For increasing the hiding capacity, two or more bits in each value can be used to embed messages without introducing a detectably degradation of the cover image. Although there are several types of LSB hiding methods, these LSB steganography methods have certain limitation, the embedded data is converted into another format which causes the embedded data to be lost.

In [28], the authors present a novel steganography approach to increase the security of the data embedded in a color image. They have used LSB insertion method that hides the bits of a secret message into the LSBs in the red channel of the pixels within a cover image. The pixels are selected by using a random number generator. It is commonly seen that the changes in the LSBs of the color cannot be detected due to noise that is presented in the digital images by the human visual system. The central idea of the proposed method is to increase security, so that, the data is hidden only into the red channel of the image. They have also explained the method that extracts the hidden message at the receiving end using a key. The proposed method combines both the preferences and the

resistance to the visual and statistical attacks for a large size of data to be hidden in a cover image.

In [29], the authors firstly analyze the common limitations of the original PVD and its modified versions, and then propose a more secure steganography algorithm based on a content adaptive scheme. In this method, a cover image is firstly partitioned into small squares. Each square is then rotated by a random degree of 0, 90, 180 or 270. The resulting image is then divided into non-overlapping embedding units with three consecutive pixels, and the middle one is used for data embedding. The number of hidden bits is depending on the differences among the three pixels. To preserve the local statistical features, the sort order of the three pixel values will remain the same after data hiding. Furthermore, the new method can firstly use sharper edge regions for data hiding adaptively, while preserving other smoother regions by adjusting a parameter. The experimental results which are evaluated on a large image database, show that their method achieves much better security compared with the previous PVD-based methods.

In [30], the authors have used PVD method for secret message hiding in the red, green and blue components of every pixel in the color image, although after they utilize the PVD algorithm as image steganography scheme, the pixel values in the stego-image may perhaps exceed the range 0~255. This overflow problem has been eliminated for every component pixel. Additionally, the authors have utilized different number of bits in different pixel channels for giving a lot more security. It will be very hard to trace, what is the number of bits are hidden in a pixel of the stego-image. The results obtained in the proposed algorithm provide excellent visual quality of stego-image compared to the traditional PVD algorithm.

In [31], the author suggests an image steganography algorithm in line with the Canny edge detection algorithm. That algorithm is designed to embed a secret message within the pixels of a cover image that comprise the limits associated of objects discovered in the image. Additionally specifically, the three LSBs of each color channel of the pixels found by the Canny edge detection algorithm as part of the edges in the cover image are replaced by the bits of the secret message. The algorithm will be parameterized through several variables: the size of the Gaussian filter, a low tolerance value, along with a high tolerance value. These variables can certainly generate different results for the same input image and secret message. The effects involving trials demonstrated some sort of

simulation tool code known as GhostBit, which in turn intended to cover and uncover secret message using this algorithm.

In [32], the authors have proposed some new techniques of embedding a text message in an image based on randomization. They also have compared the actual and embedded images with histograms and computed the MSE and PSNR.

In [33], the authors proposed an enhanced technique that provides a better PSNR with good embedding capacity and better imperceptible quality. The proposed approach is based on four modules; mapping rules, set classifier method, pixel selection method, and minimum differencing function to hide data within an image. This method works by selecting a set of pixels; map secret data into these selected pixels according to mapping rules and produces new stego pixel value after mapping secret message according to the minimum pixel difference function. This integrated proposed approach provides more security to secret data, as without knowing the mapping rules and locations of pixels, no one could extract the secret data.

In [34], the authors have presented an algorithm of steganography in the gray image. This particular algorithm converts each character of the message into binary, finds the black locations of the gray image (dark) by transforming the original image into binary image intended for labeling all physical objects of the image through thinking about the 8 connectivity, and then changes these images to RGB images in order to find black locations. Because each collection associated with a gray color turns into RGB color, in addition to black degree of gray image is located, if the gray image is very lighting, the histogram will be modified manually to get the black locations. Finally, every 8 pixels associated with black locations has become considered as a byte and the binary value of each character has become put in low bit of each byte which has recently been developed manually by through black locations pixels to increase the security of the steganography algorithm.

In [35], the authors have improved the Modified Kekre's Algorithm (MKA) which is based on LSB method. The improved scheme increases the embedding capacity while retaining the good quality of stego-image as good as MKA. Experimental results show that, the improved scheme outperform the original comparative scheme especially in capacity of hidden data bits.

In [36], a new algorithm for image steganography based on the texture of the cover image have been introduced. The algorithm consists of two stages; in the first stage, the authors divide the cover image into an isolated regions and then cluster these regions to determine the parts with the highest frequencies, and then these parts are used as a region to hide the message. The authors proposed a new algorithm to embed each byte of message individually in each row of that region. In the second stage (extraction stage), they divide the stego-image and clustering the parts to determine the highest frequencies and then apply the extracting algorithm to extract the message.

In [37], the authors present a steganography algorithm which allows the image process to recognize the segments of the cover image which might be fewer probable to discover the embedded message using visual attacks. The selected regions are classified as the segments as their feel is actually inhomogeneous, this is due to these segments are originally noisy and too difficult to detect the additional data. Since, the pixels, where the message is embedded, depend on the features of the cover image, and also the steganography algorithm turns into adaptive.

In [38], the histogram shift-based steganography uses the peak point of the cover image to embed the secret message. The authors propose a steganalysis method based on an effective peak location algorithm (PLA) to detect the histogram shift-based steganography. In the proposed method, three effective features were first derived from the four consecutive bins of the histogram of the test image. The minimum sum of the proposed features is compared with a predefined threshold to determine where an image is stego or cover.

In [39], a novel prediction-based reversible steganography scheme based on image inpainting was used. In the proposed system, the reference pixel is chosen adaptively according to the distribution characteristics of the image content. In the existing systems, only one secret image was hidden in the original image, but in this system, firstly the cover image was divided into two blocks of pixels such as b1 and b2. In the first block (b1) secret image was embedded and in the second half (b2) a secret text was hidden. After hiding the secret data in the two blocks the corresponding blocks are merged together and the stego-image is formed.

The general advantages of spatial domain techniques are [18]:

1. Low degradation of the cover image.
2. More information can be hidden in an image; this means high hiding capacity.
3. Less Complex.

The general disadvantages of spatial domain techniques are [18]:

1. The hidden data can be lost with image manipulation; this means less robust.
2. Simple attacks can easily destroy the hidden data.
3. The hidden message may be segmented on a part of image.
4. Depends on the format of the image.

Table (4) summarizes the performance comparison of different spatial domain techniques [40].

Table 4: Performance Comparison of Different Spatial Domain Techniques.

Spatial Domain Tehnique	Capacity	Visibility	Detectability	Robustness	Complexity	Comments on Technique
LSB	High	Low	High	Low	Low	Independent of image format and texture
PVD	Medium	Low	Medium	Low	Low	Suitable for high contrast images
EBE	Low	Low	Medium	Low	Low	Preffered for images with objects
RPE	High	Medium	Low	Low	Low	Provides better security of information leakage
PMM	Medium	Low	Low	Medium	Medium	N/A
Labeling or connectivity	Medium	Low	Low	Medium	Medium	Preffered for mosaic images
Pixel intensity	Medium	Low	Low	Low	Low	Robust hiding for noisy images
Texture based	Medium	Low	Medium	Medium	Medium	Preffered for patterned
Histogram shifting	Low	Low	Medium	Medium	Medium	Limited capacity and hard to detect

2. Transform Domain Techniques:

These techniques are known as "a frequency domain techniques". These techniques tend to be difficult strategies of embedding data in an image. Various transformations on image and many algorithms are used to embed data in it. In these kinds of methods, the secret message is hidden in the transform domain of the image. Transform domain hiding might be termed

as a domain of hiding techniques for which often numerous algorithms are already proposed [41]. The process of hiding data in the transform domain of a signal is quite a bit stronger than hiding in the spatial domain. Right now, a lot of the steganography methods operate within the frequency domain. These techniques, offer an advantage over a substitution techniques as they embed data in regions of the image which have been much less encountered to image processing, cropping, and compression. Some of the frequency domain techniques may well outrun lossless and lossy format conversions, this means the independency on the image format. Different transformations and algorithms are utilized on the image to order to embed data in it. Transform domain techniques are classified into [42, 43].

A. Discrete Cosine Transformation Technique (DCT): The particular DCT is definitely an orthogonal transform with regard to digital image processing and signal processing with strengths like high compression ratio, very good information integration capacity, smaller bit error rate, and also agood synthetic effect of calculation complexness. The particular DCT makes it possible for an image to become partitioned into various frequency bands that is the high, the middle and also the low frequency bands thus, turning it into easier to choose the band in which the secret message will be inserted. The previous work reveals that, typically the middle frequency bands are selected due to the fact that hiding the information in a middle frequency band doesn't scatter the secret message to most visual important parts of the image i.e. the lower frequencies and also it do not overexpose them to eliminate through compression and noise attacks where the higher frequency components are targeted. Although a number of the steganography techniques hide the secret message in the DC component, many techniques use the comparison of middle band DCT coefficients to hide a single bit of data into a DCT block [44, 45]. The DCT is similar to the particular Fourier transform, however it utilizes simply real arithmetics. Additionally, it possesses simply real frequency domain coefficients in addition to incorporates totally positive frequencies. The 2D DCT $S(u,v)$ for an image $s(x,y)$ of size $M \times N$ can be given by [44, 45]:

$$S(u, v) = \frac{2}{\sqrt{MN}} C_u C_v \sum_{x=0}^{M-1} \sum_{y=0}^{N-1} s(x, y) \cdot \cos\left(\frac{\pi(2x+1)u}{2M}\right) \cos\left(\frac{\pi(2y+1)v}{2N}\right) \quad (8)$$

$$C_u = C_v = \begin{cases} 1/\sqrt{2} & u = v = 0 \\ 0 & \text{otherwise} \end{cases} \quad (9)$$

where $x, u = 0$ to $M - 1$ and $y, v = 0$ to $N - 1$, $s(x, y)$ is the pixel intensity at the image location (x, y) , and $S(u, v)$ is the DCT coefficient at the transform position (u, v) .

- B. Discrete Fourier Transformation Technique (DFT):** The DFT based technique is similar to the DCT based technique but it utilizes the Fourier transform instead of cosine transform which makes it lack resistance to strong geometric distortions. Although, it increases the overall complexity of the process [45, 46]. The DFT of time domain value $f(x, y)$ for the image of size $M \times N$ can be defined as [45, 46]:-

$$F(u, v) = \frac{1}{\sqrt{MN}} \sum_{x=0}^{M-1} \sum_{y=0}^{N-1} f(x, y) \cdot e^{-j2\pi(\frac{ux}{M} + \frac{vy}{N})} \quad (10)$$

where $u = 0, 1, 2, \dots, M - 1$ and $v = 0, 1, 2, \dots, N-1$. Similarly, the inverse DFT (IDFT) is used to convert frequency component to the time domain value, and can be defined as [45, 46]:-

$$f(x, y) = \frac{1}{\sqrt{MN}} \sum_{u=0}^{M-1} \sum_{v=0}^{N-1} F(u, v) \cdot e^{j2\pi(\frac{ux}{M} + \frac{vy}{N})} \quad (11)$$

The Fourier transform makes a complicated number valued output image and this can be exhibited with two images, often with the real and also imaginary part or perhaps with magnitude and phase.

- C. Discrete Wavelet Transformation Technique (DWT):** A wavelet is a small wave which often oscillates in addition to decays in a time domain. The DWT is a computationally productive method in computer science. Wavelet analysis will be effective since it performs local analysis in addition to multi-resolution analysis. To analyze a signal at various frequencies with multi-resolutions is referred to as "multi-resolution analysis" (MRA). This technique transforms the item within wavelet domain, processes the particular coefficients after which it works inverse wavelet transform to represent the original format of the stego-object [47, 48].
- D. Integer Wavelet Transformation Technique (IWT):** Since the DWT enables independent processing of the resulting components without significant perceptible interaction concerning these, for this reason it truly is anticipated to create the process of imperceptible

hiding more effective. Nonetheless, the particular utilized wavelet filters have floating point coefficients. So, if the input message includes sequences of integers (as in the case for images), the particular resulting filtered results don't contain integers, which won't let best reconstruction of the cover image. Nonetheless, with the introduction of wavelet transforms that map integers to integers the particular result might be fully characterized with integers [49 – 51].

E. Discrete Curvelet Transform Technique (DCVT): Curvelet transform may be the new member of the evolving family of multiscale geometric transforms. Since it represents the edges better than wavelet, Curvelet transform has a powerful strategy to the issues linked to image steganography using wavelets in addition to DCT [52].

In [43], the frequency domain methods embed data in insensitive areas of the cover image that make them more robust against attacks. DCT/DWT is used to transform cover image from spatial domain to frequency domain. The secret image or information is then hidden into the transform domain coefficients. Different wavelet filters can be used for embedding secret image in these frequency components. This paper compares hybrid transform domain techniques for different wavelet filters for embedding secret image into cover image. The algorithms are compared for PSNR which is a measure of the difference between the cover image and the stego-image.

In [44], the DCT based steganography approach is suggested which provides a high impedance against the image processing attacks like JPEG compression, rotation, noise, translation, etc. In this method, the secret message is hidden in the middle frequency band of the DCT blocks, which carry the low frequency components while the higher frequency sub-band components remain unutilized. Secret message is concealed by modifying the DCT coefficients of the image and by utilizing the secret key. Secret message can be recovered using the same secret key without any knowledge of the cover image. The performance analysis shows that this technique of steganography is robust.

In [45], it is suggested to utilize the Discrete Fractional Fourier transform (DFrFT) as a main tool in image processing for data embedding approach. A comparative study of steganography in spatial domain and frequency

domain based on DFT, DCT, and DFrFT is made. PSNR and MSE of cover image and stego-image are used as performance index and it is found that among three frequency domain methods DFrFT based steganography gives better results in terms of PSNR and MSE and also provide more security for communication. The results show that, the suggested approach provides more security, better PSNR and lower MSE of cover image and stego-image.

In [46], the authors suggested an approach to collect the characteristics of both image enhancement and image steganography. Tests have been implemented on various still images.

In [47], an excessive capacity and also safety steganography utilizing the DWT is suggested. The wavelet coefficients of both the cover and message images are generally fused into one image utilizing hiding toughness parameters alpha and also beta. The cover and message images are generally pre-processed to reduce the actual pixel range to make certain that, the message can be extracted accurately at the desired destination. It is observed that, the capacity and also safety are generally increased with acceptable PSNR in the suggested algorithm compared to the current algorithms.

In [48], authors proposed a technique to hide a secret image with larger size than that of a cover image securely. The main aim here is the absolute invisibility of the large size secret image. The secret image is firstly, scrambled by using Arnold transformation. Haar DWT is then applied on the cover image and transformed the secret image, followed by Alpha blending operation, then the Haar IDWT is applied to obtain the stego-image. At the receiver side, firstly the cover image is obtained from the stego-image, then the Haar DWT is applied on the cover image and the stego-image followed by an alpha blending operation. The Haar IDWT is applied on the resulting image, then the secret image is obtained. The proposed method does not require the sender to send the cover image to the receiver for obtaining the secret image. The performance of the suggested method is investigated by computing the PSNR, the MSE and the NCC between the cover image and the stego-image. The experimental results demonstrate that the effectiveness and accuracy of the suggested method.

In [49], integer wavelet transform can be performed on a grayscale cover images and in turn hides the message bitstream into the LSB's of the coefficients of the IWT of the image. The main purpose of this work is to improve the hiding ability and minimize the distortions that occurring to the stego-image. The refinement of the algorithm plays an important role for accomplishing higher embedding capacity and low distortion rate. The experimental results prove that, the performance metric like the PSNR can be improved in a high manner, also the proposed algorithm has a very good invisibility and a high capacity.

In [51], the secret messages are usually hidden in the 1-level Haar IWT utilizing the coefficient difference scheme which is acquired through a PVD technique. The secret messages are usually hidden on the difference values of the two adjacent wavelet coefficients. The experimental results show that, the suggested method can easily provide better performance than the current methods which usually employ the Haar IWT and the PMM in term of the maximum capacity as well as the imperceptibility.

In [52], the authors suggested an adapted high-capacity image steganography algorithm depended on the curvelet transform with an acceptable levels of invisibility as well as distortion in the cover image and the high level of overall safety.

The general advantages of transform domain techniques are [18]:

1. Less chance for removal or loss of the hidden data.
2. Information is distributed over the whole image.
3. Provides much higher flexibility for hiding data.
4. Typically independent of the image format.

The general disadvantages of transform domain techniques are [18]:

1. Greater understanding of the embedding domain required.
2. Careful selection of embedding coefficients is required as it can cause degradation of image.
3. Higher computational complexity.
4. Relatively low embedding capacity.

Table (5) summarizes a performance comparison of different transform domain techniques [40].

Table 5: Performance Comparison of Different Transform Domain Techniques

Transform Domain Tehnique	Capacity	Visibility	Detectability	Robustness	Complexity	Comments on Technique
DCT	Medium	Low	Low	Medium	Medium	Simplest in the transform domain
DFT	Medium	Low	Low	Medium	Medium	Involves the complex calculations
DWT	Medium	Low	Low	High	High	Closely matches with human visual perception
IWT	Medium	Low	Low	High	High	Overcomes the rounding off losses
DCVT	Medium	Low	Low	High	High	Improves the degradations at edge areas

3. Spread spectrum techniques:

The spread spectrum encoder can be considered as the core of the spread spectrum image steganography (SSIS). The function of these devices is to modulate the narrow band signal over a carrier. The frequency of the carrier will be continuously shifted using a pseudorandom noise generator feed with a secret key. In this way, the spectral energy of the signal will be spread over a wide band, thus decreasing its density, usually under the level of noise. To recover the hidden message, the receiver ought to use the same secret key and the noise generator to tune on the right frequencies and detect the original signal. A casual observer won't be able even to recover the embedded communication, since it is under the noise level [53].

The general advantages of spread spectrum techniques are:

1. They are usually quite robust.
2. They are widely utilized in military applications because of its robustness against detection.
3. High capacity as well as a low ease of detection.

The general disadvantages of spread spectrum techniques are:

1. Less security.
2. Provides only image steganography.
3. Fewer users friendly.
4. Does not provides compression and file security.

4. Distortion Techniques:

These techniques need some knowledge of the cover image throughout the detecting process where the decoder operates to check for dissimilarities between the cover image and the distorted cover image in order to hide the secret data. The encoder gives a sequence involving alterations to the cover image. Thus, data will be identified as being hidden simply by signal distortion. Employing this approach, a stego-object is created by making use of a sequence involving modifications towards the cover image. This sequence of modifications is utilized to check the secret data that required to be sent [54]. The information will be encoded on pseudo-randomly picked pixels. If the stego-image is different from that of the cover image at a given information pixel, the bit is a "1", otherwise, the bit is a "0." The encoder could modify the "1" value pixels ordinary way that will, the statistical properties of the image will not be impacted. Even so, the necessity for transmitting the cover image limits the advantages of this approach. In a steganography technique, the cover image should never be utilized more than once. In the event that an attacker tampers while using the stego-image by scaling, cropping, or rotating the receiver can be easily extract it. Occasionally, if the data is encoded with error correcting information, the change could even be reversed and the original information can be extracted [54].

The general advantages of distortion techniques are:

1. Improved embedding efficiency.
2. Good imperceptibility.

The general disadvantages of distortion techniques are:

1. Sending the cover image along with stego-image is needed.
2. Less security and robustness.
3. Low embedding capacity.

5. Masking and Filtering Techniques:

These techniques embed data by marking the image, in the same way as to the paper watermarks. These techniques hide the message in the more significant areas than just embedding it into the noise level. The embedded data is more integral to the cover image. Steganography techniques can be

utilized without the fear of image destruction due to the lossy compression as they will be more incorporated into the image [54].

The general advantages of masking and filtering techniques [18, 55]:

1. Much more robust than LSB replacement with respect to compression, since the data is embedded in only the visible parts of the image.

The general disadvantages of masking and filtering techniques [18, 55]:

1. These techniques applied only on the gray scale images (8-bits) and restricted to the color images (24- bits).

6. Cover Generation Techniques:

In contrast to almost all hiding techniques presented above, when secret data is added to a specific cover object by applying a hiding algorithm, some steganography applications can generate a digital object only to be a cover object for secret communication [23].

The general advantages of cover generation techniques are:

1. High imperceptibility.
2. High embedding capacity.

The general disadvantages of cover generation techniques are:

1. Less robustness.

Table (6) summarizes a comparison between all image steganography techniques in terms of different factors or measures which affecting on the different techniques.

Table 6: A Comparison of Different Steganography Techniques

Algorithm Measures	Spatial Domain	Transform Domain	Spread Spectrum	Masking and Filtering techniques	Distortion techniques	Cover Generation Techniques
Imperceptibility	High	High	High	Medium	Low	High
Robustness	Low	High	Medium	Low	Low	Low
Capacity	High	Medium	High	Low	Low	High

5. Applications of Steganography

Steganography can be utilized in various applications such as [27]:

1. Copyright Protection, where a secret copyright notice can be hidden inside an image to recognize it as intellectual property. Furthermore, when the image is distributed or sold, a recognition of the recipient and time stamp can be hidden to recognize potential pirates. Example of copyright protection is the smart ID cards, where the personal data are hidden in the image itself for copyright control of materials.
2. Medical imaging, where the details of a patient can be hidden within an image to achieve a protection of the private data of the patient and to minimize the time and cost of transmission.
3. Online voting system, making the online election being safe as well as robust against a variety of fraudulent behaviors, regarding data embedding in nations around the world wherever cryptography is actually disallowed.
4. Secret Communications, in numerous scenarios, sending some sort of a cryptographic information attracts undesirable attention. The utilization of cryptographic technologies might be not allowed or perhaps constrained for legal reasons. Nevertheless, using steganography does not advertise covert communication and therefore avoids critique on the sender, message, and also the recipient.
5. Feature Tagging, time stamps, where captions, annotations, and also the additional illustrative aspects can be embedded inside an image, including regions in a map or some names of individuals in a photo. Copying the stego-image also copies each of the embedded features and only the parties who contain the decoding stego-key should be able to recover in addition to check out these features.
6. Defense organizations for secure circulation of secret message, and military and intelligence agencies.
7. Improving mobile banking safety.
8. Tamper proofing to prevent or perhaps detect the unauthorized adjustments.

6. Robust Image Steganography Against Attacks

6.1 Attacks

Attacks on images can be possible in image steganography like image manipulation attacks, statistical attacks, visual attacks etc. The well-known attacks on stego-images are compression attack, cropping of stego, resizing the stego, noise addition, brightness attack can be possible in steganography. Attacks are mainly categorized into six types, which are [56]:

- i. Stego-only attack:** the stego-image is only available for analysis.
- ii. Known cover attack:** the cover image and stego-image are both available.
- iii. Known message attack:** at some point, the particular embedded data becomes recognized to the attacker. Analyzing the stego-image for patterns that are corresponding to the hidden data may be beneficial for future attacks against that system. Even with the message, this may be very hard and could even be regarded corresponding to the particular stego-only attack.
- iv. Chosen stego attack:** the steganography algorithm and stego-image are known.
- v. Chosen message attack:** the actual stego expert creates a new stego-image by a number of steganography algorithms from a selected data. The goal in this particular attack is always to decide matching patterns in the stego-image which could specify the utilization of a particular steganography algorithms.
- vi. Known stego attack:** the steganography technique is known and also both the cover image and stego-image are also available.

6.2 Robust Image Steganography

As explained in sections 1 and 2, both the steganography and cryptography are data hiding techniques that used for a secure communications over insecure channel. In a robust image steganography, the combination of both (steganography and cryptography) is used for

obtaining a much higher security. The cryptography is used inside the steganography process, so it's called as dual steganography [57]. Firstly, the text message is encrypted into cipher text and then this cipher text is embedded into an image by any of the image steganography techniques which are explained in section 4.

The basic model of a robust image steganography is shown Figure (7). Here, the secret data is firstly converted into encrypted form and then this encrypted information is used as secret data, which will be hidden inside the cover image with the help of an embedding algorithm and finally the stego-image is formed which is same as a cover image in human perceptible way. The common cryptography algorithms used are RSA (Rivest Shamir Adelman), DES (Data Encryption Standard), AES (Advanced Encryption Standard), and Diffie Hellman. Sometimes a stego-key is also used to make the communication more secured. This key can directly be given by the sender and used during the embedding algorithm. The stego-key must be known at both transmitter and receiver side. Thus using cryptography along with steganography, secret information can be easily communicated with high security, which is more secured way of using steganography [58].

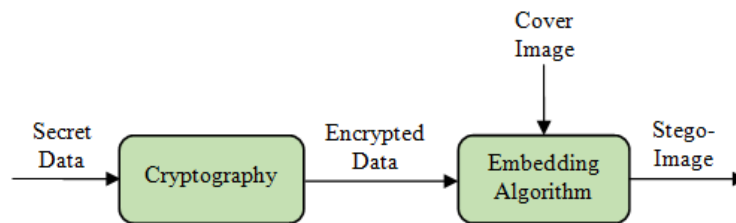


Figure 7: Robust Image Steganography Model

7. The Novel Trends for Steganography Techniques

The new trends in Steganography include the following topics:

- Still efforts have to be made to increase the embedding capacity and maintain secrecy.
- Efforts can be made to hide text files having more size than image size.
- Security of the scheme can be improved by using advanced cryptography techniques and also improve the efficiency by using data compression techniques.

- Steganography techniques based on model-preserving principles which are designed by finding a model for cover images, and embedding modifications are done in such a way that this model is preserved.
- Embedding technique known as pixel value difference technique (PVD). In this technique, the image is divided into non-overlapping blocks of adjacent pixels which are randomly selected, and data is embedded into each of its pixels.
- Adaptive edge LSB technique.
- In hiding behind corners (HBC) technique, corner pixels are used to contain hidden data. Data is embedded by using simple LSB substitution.
- Edge adaptive image steganography technique is based on LSB matching revisited.
- Achieve the above cases by hardware implementation using FPGA.

8. Conclusions

There are many different digital image processing algorithms whereas; data hiding is considered as one of the most important algorithms. Data hiding is the art of hiding data for various purposes such as; maintaining private data, secure confidential data and so on. The different securities and data hiding techniques are used to achieve image steganography. This paper reviews the most common steganography techniques, presenting a survey of these techniques; different embedding and extracting algorithms, concepts, and the advantages and drawbacks of each algorithm. The considered techniques are; spatial domain, Transform domain, spread spectrum, masking and filtering, distortion and cover generation techniques. The steps of the different algorithms of these techniques are presented in details, with a comparison between the algorithms of each technique, and a final comparison between all the techniques is presented. The wide range of image steganography applications are considered. The different attacks are presented in addition to presenting a robust image steganography technique which called "dual image steganography" that based on both cryptography and steganography. The new trends in steganography are also introduced.

References

- [1] S. Deepa and R. Umarani, "A Study on Digital Image Steganography", *International Journal of Advanced Research in Computer Science and Software Engineering (IJARCSSE)*, Vol. 3, Issue 1, pp. 54 – 57, January 2013.
- [2] H. Al-Bahadili, "A Secure Block Permutation Image Steganography Algorithm", *International Journal on Cryptography and Information Security (IJCIS)*, Vol. 3, No. 3, pp. 11 – 22, September 2013.
- [3] K. D. Megha, N. P. Vaidya and K. Patel, "Digital Watermarking: Data Hiding Techniques using DCT-DWT Algorithm", *International Journal of Advanced Research in Computer and Communication Engineering (IJARCCE)*, Vol. 2, Issue 6, pp. 2397 – 2402, June 2013.
- [4] G. Kaur and K. Kaur, "Digital Watermarking and Other Data Hiding Techniques", *International Journal of Innovative Technology and Exploring Engineering (IJITEE)*, Vol. 2, Issue 5, pp. 181 – 184, April 2013.
- [5] K. Challita and H. Farhat, "Combining Steganography and Cryptography: New Directions", *International Journal on New Computer Architectures and Their Applications (IJNCAA)*, Vol. 1 Issue 1, pp. 199 – 208, 2011.
- [6] O. C. Abikoye, K. S. Adewole and A. J. Oladipupo, "Efficient Data Hiding System using Cryptography and Steganography", *International Journal of Applied Information Systems (IJ AIS)*, Volume 4, No. 11, pp. 6 – 11, December 2012.
- [7] M. K. I. Rahmani, K. Arora and N. Pal, "A Crypto-Steganography: A Survey", *International Journal of Advanced Computer Science and Applications (IJACSA)*, Vol. 5, No. 7, pp. 149 – 155, 2014.
- [8] A. Cheddad, J. Condell, K. Curran and P. M. Kevitt, "Digital Image Steganography: Survey and Analysis of Current Methods", *Signal Processing, Elsevier*, Vol. 90, Issue 3, pp. 727 – 752, March 2010.
- [9] M. Juneja and P. S. Sandhu, "Data Hiding with Enhanced LSB Steganography and Cryptography for RGB Color Images", *International Journal of Applied Research*, Vol. 3, No. 5, pp. 118 – 120, May 2013.
- [10] C. P. Sumathi, T. Santanam and G. Umamaheswari, "A Study of Various Steganographic Techniques Used for Information Hiding", *International Journal of Computer Science & Engineering Survey (IJCSSES)*, Vol. 4, No. 6, pp. 9 – 25, December 2013.
- [11] J. Kour and D. Verma, "Steganography Techniques –A Review Paper", *International Journal of Emerging Research in Management & Technology*, Vol. 3, Issue 5, pp. 132 – 135, May 2014.
- [12] F. M. Shelke, A. A. Dongre and P. D. Soni, "Comparison of Different Techniques for Steganography in Images", *International Journal of*

- Application or Innovation in Engineering & Management (IJAIEM), Vol. 3, Issue 2, pp. 171 – 176, February 2014.
- [13] M. Umamaheswari, S. Sivasubramanian and S. Pandiarajan, "Analysis of Different Steganographic Algorithms for Secured Data Hiding", International Journal of Computer Science and Network Security (IJCSNS), Vol. 10, No. 8, pp. 154 – 160, August 2010.
- [14] R. G. Bal and P. Ezhilarasu, "An Efficient Safe and Secured Video Steganography Using Shadow Derivation", International Journal of Innovative Research in Computer and Communication Engineering (IJRCCE), Vol. 2, Issue 3, pp. 3251 – 3258, March 2014.
- [15] A. Chadha, N. Satam, R. Sood and D. Bade, "An Efficient Method for Image and Audio Steganography using Least Significant Bit (LSB) Substitution", International Journal of Computer Applications (IJCA), Vol. 77, No. 13, pp. 37 – 45, September 2013.
- [16] M. Nosrati, R. Karimi and M. Hariri, "An Introduction to Steganography Methods", World Applied Programming, Vol. 1, No. 3, pp. 191 – 195, August 2011.
- [17] T. Handel and M. Sandford, "Hiding Data in the OSI Network Model", Proceedings of the 1st International Workshop on Information Hiding, pp. 23 – 38, June 1996.
- [18] M. Hussain and M. Hussain, "A Survey of Image Steganography Techniques", International Journal of Advanced Science and Technology, Vol. 54, pp. 113 – 124, May 2013.
- [19] E. Dagar and S. Dagar, "Comparative Study of Various Steganography Techniques", International Journal of Emerging Engineering Research and Technology (IJEERT), Vol. 2, Issue 2, pp. 30 – 36, May 2014.
- [20] S. Singh and T. J. Siddiqui, "A Security Enhanced Robust Steganography Algorithm for Data Hiding", International Journal of Computer Science Issues (IJCSI), Vol. 9, Issue 3, No. 1, pp. 131- 139, May 2012.
- [21] A. A. El-Zoghabi, A. H. Yassin and H. H. Hussien, "Public Key Steganography using LSB Method with Chaotic Neural Network", International Journal of Computer Engineering and Technology (IJCET), Vol. 5, Issue 8, pp. 118 – 129, August 2014.
- [22] Z. Kh. AL-Ani, A. A. Zaidan, B .B. Zaidan and H. O. Alanazi, "Overview: Main Fundamentals for Steganography", Journal of Computing, Vol. 2, Issue 3, pp. 158 – 165, March 2010.
- [23] M. Mishra, P. Mishra and M. C. Adhikary, "Digital Image Data Hiding Techniques: A Comparative Study", ANSVESA, Vol. 7, No. 2, pp. 105-115, 2012.
- [24] Chetan, D. Sharma, "A Survey of Image Compression and Steganography Techniques", International Journal of Advanced Research in Computer Science and Software Engineering (IJARCSSE), Vol. 5, Issue 4, pp. 727 – 730, 2015.

- [25] H. Lakhani, "A Steganography Using Spatial Domain Method for Enhance Data Security", *Journal of Emerging Technologies and Innovative Research (JETIR)*, Vol. 2, Issue 3, pp. 611 – 615, March 2015.
- [26] N. Tiwari, M. Sandilya and M. Chawla, "Spatial Domain Image Steganography based on Security and Randomization", *International Journal of Advanced Computer Science and Applications (IJACSA)*, Vol. 5, No. 1, pp. 156 – 159, 2014.
- [27] V. Vijayalakshmi, G. Zayaraz, and V. Nagaraj, "A Modulo Based LSB Steganography Method", *International Conference on Control, Automation, Communication and Energy Conservation*, pp. 1 – 4, 4 – 6 June 2009.
- [28] S. A. Laskar, and K. Hemachandran, "Steganography Based on Random Pixel Selection for Efficient Data Hiding", *International Journal of Computer Engineering & Technology (IJCET)*, Vol. 4, Issue 2, pp. 31 – 44, March – April 2013.
- [29] W. Luo, F. Huang and J. Huang, "A More Secure Steganography Based on Adaptive Pixel-value Differencing Scheme", *Multimedia Tools and Applications*, Springer, Vol. 52, Issue 2 – 3, pp. 407 – 430, April 2011.
- [30] J. K. Mandal and D. Das, "Colour Image Steganography Based on Pixel Value Differencing in Spatial Domain", *International Journal of Information Sciences and Techniques (IJIST)*, Vol. 2, No. 4, pp. 83 – 93, July 2012.
- [31] Y. Bassil, "Image Steganography Based on a Parameterized Canny Edge Detection Algorithm", *International Journal of Computer Applications*, Vol. 60, No. 4, pp. 35 – 40, December 2012.
- [32] O. A. Rawashdeh and N. A. M. Al-Saiyed, "A Novel Approach for Integrating Image Steganography and Encryption", *International Journal of Computer Technology & Applications*, Vol. 5, Issue 6, pp. 1917 – 1923, Nov – Dec 2014.
- [33] P. K. Panjabi and P. Singh, "An Enhanced Data Hiding Approach Using Pixel Mapping Method with Optimal Substitution Approach", *International Journal of Computer Applications*, Vol. 74, No. 10, pp. 36 – 43, July 2013.
- [34] H. Motameni, M. Norouzi, M. Jahandar and A. Hatami, "Labeling Method in Steganography", *International Journal of Computer, Control, Quantum and Information Engineering*, Vol. 1, No. 6, pp. 1574 – 1579, 2007.
- [35] M. Hussain and M. Hussain, "Pixel Intensity Based High Capacity Data Embedding Method", *International Conference on Information and Emerging Technologies (ICIET)*, IEEE, pp. 1 – 5, 14 – 16 June 2010.
- [36] T. A. Al-Asadi and A. A. M. Baker, "A Novel Method for Image Steganography Based on Texture Features", *European Academic Research*, Vol. 2, Issue 1, pp.193 – 203, April 2014.
- [37] D. R. Herrera-Moro, R. Rodríguez-Colín and C. Feregrino-Uribe, "Adaptive Steganography Based on Textures", 17th International

- Conference on Electronics, Communications and Computers (CONIELECOMP'07), IEEE, 2007.
- [38] S. Saini and K. Brindha, "Improved Data Embedding into Images Using Histogram Shifting", *International Journal of Emerging Research in Management & Technology*, Vol. 3, Issue 5, pp. 83 – 86, May 2014.
- [39] R. Keerthana and M. Chanderkumar, "An Efficient Way of Data Hiding Using Histogram Shifting Mechanism", *International Journal of Computer Science and Mobile Computing (IJCSMC)*, Vol. 3, Issue 11, pp. 447 – 454, November 2014.
- [40] A. Tiwari, S. R. Yadav, and N. K. Mittal, "A Review on Different Image Steganography Techniques", *International Journal of Engineering and Innovative Technology (IJEIT)*, Vol. 3, Issue 7, pp. 121 – 124, January 2014.
- [41] G. Kaur and A. Kochhar, "Transform Domain Analysis of Image Steganography", *International Journal for Science and Emerging Technologies with Latest Trends*, Vol. 6, Issue 1, pp. 29 – 37, 2013.
- [42] S. Hemalatha, U. D. Acharya, A. Renuka and P. R. Kamath, "A Secure Color Image Steganography in Transform Domain", *International Journal on Cryptography and Information Security (IJCIS)*, Vol. 3, No. 1, pp. 17 – 24, March 2013.
- [43] M. Goel and R. Goel, "Comparative Analysis of Wavelet Filters on Hybrid Transform Domain Image Steganography Techniques", *International Journal of Advanced Research in Computer Science and Software Engineering*, Vol. 3, Issue 8, pp. 497 – 500, August 2013.
- [44] B. Kaur, A. Kaur and J. Singh, "Steganographic Approach for Hiding Image in DCT Domain", *International Journal of Advances in Engineering & Technology (IJAET)*, Vol. 1, Issue 3, pp. 72 – 78, July 2011.
- [45] A. Kaushal and V. Chaudhary, "Secured Image Steganography using Different Transform Domain", *International Journal of Computer Applications*, Vol. 77, No. 2, pp. 24 – 28, September 2013.
- [46] I. Singh, S. Khullar and S. C. Laroia, "DFT Based Image Enhancement and Steganography", *International Journal of Computer Science and Communication Engineering (IJCSCE)*, Vol. 2 Issue 1, pp. 5 – 7, February 2013.
- [47] H. S. M. Reddy and K. B. Raja, "High Capacity and Security Steganography Using Discrete Wavelet Transform", *International Journal of Computer Science and Security (IJCSS)*, pp. 462 – 472, 2009.
- [48] P. Sehgal and V. K. Sharma, "Eliminating Cover Image Requirement in Discrete Wavelet Transform Based Digital Image Steganography", *International Journal of Computer Applications*, Vol. 68, No. 3, pp. 37 – 42, April 2013.
- [49] M. Vijay and V. VigneshKumar, "Image Steganography Method Using Integer Wavelet Transform", *International Journal of Innovative Research*

- in Science, Engineering and Technology (IJIRSET), Vol. 3, Special Issue 3, pp. 1207 – 1211, March 2014.
- [50] P. Chaturvedi, and R. K. Bairwa, "An Integer Wavelet Transform Based Steganography Technique for Concealing Data in Colored Images", International Journal of Recent Research and Review, Vol. 7, Issue 1, pp. 49 – 57, March 2014.
- [51] N. A. Abu, P. W. Adi and O. Mohd, "Robust Digital Image Steganography within Coefficient Difference on Integer Haar Wavelet Transform", International Journal of Video & Image Processing and Network Security (IJVIPNS-IJENS), Vol. 14, No. 2, pp. 1 – 8, April 2014.
- [52] A. A. Al-Ataby, and F. M. Al-Naima, "High Capacity Image Steganography Based on Curvelet Transform", Developments in E-systems Engineering (DeSE), IEEE, pp. 191 – 196, 6 – 8 Dec. 2011.
- [53] S. Abd Halim and M. F. A. Sani, "Embedding Using Spread Spectrum Image Steganography with GF(2^m)", Proceedings of the 6th IMT-GT Conference on Mathematics, Statistics and its Applications (ICMSA2010), pp. 659 – 666, 2010.
- [54] H. A. Jalab, A. A. Zaidan and B. B. Zaidan, "New Design for Information Hiding with in Steganography Using Distortion Techniques", International Journal of Engineering and Technology (IACSIT), Vol. 2, No. 1, pp. 72 – 77, February 2010.
- [55] P. C. Mandal, "Modern Steganographic Technique: A Survey", International Journal of Computer Science & Engineering Technology (IJCSSET), Vol. 3, No. 9, pp. 444 – 448, Sep 2012.
- [56] S. Thepade and S. S. Chavan, "Appraise Of Multifarious Image Steganography Techniques", International Journal of Engineering Research and Applications (IJERA), Vol. 3, Issue 2, pp. 1067 – 1174, March – April 2013.
- [57] S. M. M. Karim, M. S. Rahman, M. I. Hossain, "A New Approach for LSB Based Image Steganography Using Secret Key", 14th International Conference on Computer and Information Technology, IEEE, December 2011.
- [58] H. S. M. Reddy and K. B. Raja, "High Capacity and Security Steganography Using Discrete Wavelet Transform", International Journal of Computer Science and Security, Vol. 3, pp. 462 – 472, 2009.

مسح للتقنيات المختلفة المستخدمة في إخفاء الرسائل السرية

عماد الشاذلي*، صافى أحمد شحاته*، رفعت محمد فكرى* أسامه زهران**،
سيد العربى*، محمد الكردى**

* القسم الهندسى – مركز البحوث النووية – هيئة الطاقة الذرية
** قسم هندسة الإلكترونيات والاتصالات الكهربائية – كلية الهندسة الإلكترونية – جامعة المنوفية

يعرف علم إخفاء البيانات والمعلومات والرسائل السرية على أنه فن وعلم إخفاء البيانات في غطاء ما دون أن تترك أي أثر ملحوظ على هذا الغطاء، وبعبارة أخرى هو دراسة للاتصالات غير مرئية. إخفاء البيانات والمعلومات عادة ما تتعامل مع طرق إخفاء وجود للبيانات المرسلّة بالطريقة التي تحافظ على سرية إنتقالها، أي أنها تحافظ على السرية بين طرفي التواصل. الأهداف الرئيسية لإخفاء المعلومات هي القدرة العالية على إخفاء كمية كبيرة من البيانات، الشفافية، الإدراك الحسي (الخفي)، مقاومة المزاج، عدم امكانية الاكتشاف، تعقيد الحسابات والمتانة. وتصنف هذه التقنيات إلى ثلاثة فئات هي:- النقي، إستخدام مفتاح سري، إستخدام مفتاح عام. بالنسبة لنوع الغطاء المستخدم يوجد أنواع مختلفة هي الصورة والصوت والفيديو والشبكات والنص. في حالة إستخدام الصورة كغطاء لإخفاء المعلومات، يمكن أن تتحقق السرية عن طريق إخفاء البيانات في صورة الغلاف وتوليد الصورة (stego). بالنسبة للتقنيات المختلفة المستخدمة في إخفاء البيانات، هناك تقنيات مختلفة تستخدم لإخفاء المعلومات منها طرق الإخفاء في المجال المكاني (طريقة الاستبدال)، طرق الإخفاء في مجالات التحويل (مجال التردد)، تقنيات الطيف المنتشر، تقنيات تشويه، تقنيات الترشيح، وأيضا تقنيات توليد الغطاء. كل نوع من هذه التقنيات لديه مواضع القوة والضعف لخوارزميات مختلفة لها. يقدم هذا البحث إستعراضا لهذه التقنيات، الخوارزميات المختلفة لكل تقنية، المفاهيم، المزايا والعيوب، خطوات الخوارزميات المختلفة. يقدم البحث أيضا مقارنة بين كل هذه التقنيات، التطبيقات المختلفة لإخفاء المعلومات، الهجمات، الطرق القوية لإخفاء المعلومات ضد الهجمات. وأخيرا يعرض الاتجاهات الجديدة في إخفاء المعلومات.

Maximum Power Techniques of Wind Energy System

Walaa Mohammed and Galal Atlam

Control and Industrial Electronics Eng. Dep., Faculty of Elect., Eng., Menoufia
University, Menouf, EGYPT

(Received: 18-November-2015 – Accepted: 20-December-2015)

Abstract

This paper illuminates how to maximize the power extraction from wind energy system. This paper compare between two techniques for maximization the power. A method is presented based upon power signal feedback using fuzzy controller. The performance of the controllers design methodology is finally presented through a wind energy conversion system to maximize the extraction of power from wind energy (WE) system.

1. Introduction

Huge exhaustion of fuel and growing concern in environment protection from using fossil fuel and nuclear energy sources. A lot of renewable power generation sources like wind energy, solar energy, wave energy, hydro power and more developed systems depend on hydrogen. Wind energy conversion systems is the fastest growing energy technology in the world. Wind energy changes throughout the day. The performance output power depends on the accuracy of tracking the peak power points by the maximum power point tracking (MPPT) controller.

In this paper, we will deal with variable-speed wind energy conversion systems (VS-WECS) with induction machines [1]–[3], squirrel cage induction generator (SCIG) [4], [5], which we will control on it to maximize the power efficiency. To achieve this goal the tip-speed-ratio of turbine must be keep at its desired value, in spite of, variations of wind. We deal with how can extract maximum power from available wind by suitable algorithm, and there is no methodical way for finding sufficient

stability condition and good performance. In the last years, there is significant research effort in control design for wind energy conversion systems [6-11]. Fuzzy logic control of generator speed was used [12]. The advantages in using fuzzy logic controller against conventional PI controllers are pointed out in better response to frequently changes in wind speed. Ref. [6] shows the problem of output power regulation of fixed-pitch variable-speed wind energy conversion systems. Ref. [7] introduced an integral fuzzy sliding mode control. Ref. [8] maximize energy capture by determining the optimal rotor speed. In [9-11] pitch control was employed to capture a maximum energy from the wind.

This paper is organized as follows. In Section II, we introduce the wind energy conversion system model. Two techniques is presented for maximum power in Section III. In Section IV, presents the proposed controller design and its stability considerations. Simulation is concluded in Section V. Finally, Section VI states the conclusions.

2. WIND ENERGY CONVERSION SYSTEM MODEL

This part demonstrates the wind turbine model by presenting the dynamic model of the wind turbine generator unit. Depending on the generation system, the SCIG used as generator in wind turbine. SCIG wind turbines are coupled to the wind turbine rotor via a gearbox and linked to the grid by inverters to match the frequency of the power supply grid and its voltage. A wind energy system can be explained by a model that includes the modeling of the whole wind turbine. The wind energy system model is clarified by the equations of each of the wind turbine-generator units, meaning the turbine, the drive train, the induction generator, the control system and the grid, as is shown in Fig.1. The exhaustive representation of the wind farm elements is given in [13].

A. Wind turbine model

The aerodynamic torque and the mechanical power of the wind turbine are given by [14-16]:

$$T_m = 0.5 C_p (\lambda, \beta) \rho \pi R^2 v s^3 / \Omega_l \quad (1)$$

$$P_m = T_m \Omega_l = 0.5 \rho \pi R^2 v s^3 C_p (\lambda, \beta) \quad (2)$$

Where, ρ is the air density, R is the radius of the turbine, v_s is the wind speed, $C_p(\lambda, \beta)$ is the power coefficient, $\lambda = \Omega_l R / v_s$ is the tip speed ratio and Ω_l is the turbine speed. Seeing as the maximum $C_p(\lambda, \beta)$ is obtained at a nominal tip speed ratio of $\lambda = \lambda_{opt}$, the control system should adapt the turbine speed at λ_{opt} to achieve maximum power. At this rotational speed, the maximum turbine power $P_{m, max}$ and the torque $T_{m, opt}$ result in $C_{p, max}$ being the maximum power coefficient. So Figure 2 shows the relation between λ and $C_p(\lambda, \beta)$. The power extracted from the wind is limited in high wind speeds, by varying pitch of the rotor blades. The maximum power coefficient achieves at bitch angle = 0.

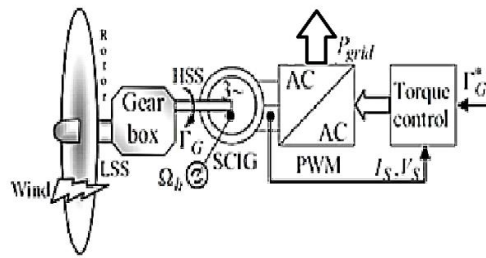


Fig.1: Diagram of the single wind turbine model

parameterised in function of the pitch angle.

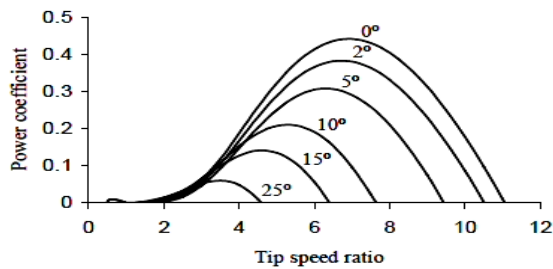


Fig.2. Power coefficient C_p versus tip speed ratio

The control is done with a PI controller which must take into consideration limitations in blades' pitch angle and slew rate and the nonlinear aerodynamic characteristic [17]. The power coefficient C_p is a function of the tip speed ratio λ and the pitch angle of rotor blades β , but for controlling SCIG wind turbines, C_p is a function of only λ , since β stays fixed in these turbines.

B. Drive train model

There are many types of generator as permanent magnet synchronous generators (PMSG), squirrel cage induction generators (SCIG) and doubly fed induction generator (DFIG). We prefer using squirrel cage induction generators (SCIG) in order to these advantageous since it is relatively inexpensive, robust, and require low maintenance. The SCIG connected with the drive train through the gear-box gathering the Low-Speed Shaft (LSS) to the High-Speed Shaft (HSS). By canceling the viscous friction, this interaction can be showed as [13]:

$$J_h \frac{d\Omega_h}{dt} = \frac{\eta_s}{n_g} T_m - T_g \quad (3)$$

$$J_l \frac{d\Omega_l}{dt} = T_m - \frac{n_g}{\eta_i} T_g \quad (4)$$

Where, T_g is the electromagnetic torque, Ω_h is the rotor speed of the generator, $\Omega_h = n_g \Omega_l$, n_g is the gear ratio, η_s is the gear efficiency and J_h and J_l are the inertias at the high-speed shaft and low-speed shafts, respectively, which are computed as

$$J_h = \eta_s (J_1 + J_{wt}) / n_g^2 + (J_2 + J_g) \quad (5)$$

$$J_l = \eta_s (J_1 + J_{wt}) + n_g^2 (J_2 + J_g) / \eta_s \quad (6)$$

Where, J_1 and J_2 are the inertias of the multiplier gears; J_{wt} and J_g are the turbine and generator inertias, respectively.

C. Generator model

The squirrel cage machines work close to the angular synchronous speed with a very small slip. These squirrel cage induction machines are the least expensive and simplest technology comparing with wounded rotor and permanent magnet machines. The electrical equations of a SCIG expressed in a direct (d)-quadrature (q) coordinate reference frame rotating at synchronous speed ω_s are the following [18]:

$$\begin{aligned}
 \frac{di_{sd}}{dt} &= \frac{V_{sd}}{L_s} - \frac{R_s}{L_s} i_{sd} - \frac{L_m}{L_s} \frac{di_{rd}}{dt} + \omega_s \left(i_{sq} + \frac{L_m}{L_s} i_{rq} \right) \\
 \frac{di_{sq}}{dt} &= \frac{V_{sq}}{L_s} - \frac{R_s}{L_s} i_{sq} - \frac{L_m}{L_s} \frac{di_{rq}}{dt} - \omega_s \left(i_{sd} + \frac{L_m}{L_s} i_{rd} \right) \\
 \frac{di_{rd}}{dt} &= -\frac{R_r}{L_r} i_{rd} - \frac{L_m}{L_r} \frac{di_{sd}}{dt} + (\omega_s - \omega) \left(i_{rq} + \frac{L_m}{L_s} i_{sq} \right) \\
 \frac{di_{rq}}{dt} &= -\frac{R_r}{L_r} i_{rq} - \frac{L_m}{L_r} \frac{di_{sq}}{dt} + (\omega_s - \omega) \left(i_{rd} + \frac{L_m}{L_s} i_{sd} \right)
 \end{aligned} \tag{7}$$

Where, i_{sd} , i_{sq} , i_{rd} and i_{rq} are the stator and rotor current (d, q) components, respectively. V_{sd} and V_{sq} are the stator voltage (d,q) components. L_s , L_r , L_m are the stator self-inductance, the rotor self-inductance, and the stator-rotor mutual inductance, respectively. R_s and R_r are the stator and rotor resistances, ω_s is the stator field frequency and $\omega_s = n_p \Omega_h$ is the speed in electrical radians per second where n_p is the number of pole-pairs and Ω_h the rotor's mechanical speed. The electromagnetic torque of the stator windings is:

$$T_g = 1.5 n_p L_m (i_{sd} i_{rq} - i_{sq} i_{rd}) \tag{8}$$

The active and reactive powers of induction generator can be expressed by:

$$P_g = 1.5 (V_{sd} i_{sd} + V_{sq} i_{sq}), \quad Q_g = 1.5 (V_{sq} i_{sd} - V_{sd} i_{sq}) \tag{9}$$

D. Power converter

The power converter is a standard IGBT-based voltage source controller (VSC). The nominal power of the power converter is equal to the nominal power of the generators that it has to control at maximum power point tracking conditions

3. THE MAXIMUM POWER POINT TRACKING TECHNIQUES

In this section we explain the difference between hill-climb search technique and power signal feedback technique for extraction maximum power from wind energy system.

A. Hill-climb search (HCS) control

The HCS technique seeks for the extraction of maximum power of the wind turbine. The tracking method, based on the locality of the operating point and relation between the changes in power and speed, calculate the desired signal to drive the system to the maximum power point. Figure 3 shows the meaning of HCS control for tracking maximum power points.

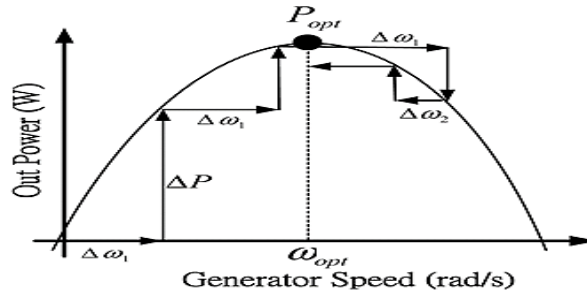


Figure 3: HCS technique for maximum power

HCS control of SCIG WECS are demonstrated in [19, 20]. HCS used a controller for MPPT control. In this method, the controller, using O/P power as input generates at its output the desired rotor speed. The increasing or decreasing in output power due to an increment or decrement in speed is estimated. If change in power is positive with last positive change in speed, the search is continued in the same direction. If, on the other hand, increasing in speed causes decreasing in power obtained, the direction of search is reversed.

B. Power signal feedback (PSF) control

In the PSF control, we must have knowledge of maximum power curve of the wind turbine, and achieve this curve by suitable controller. This curve can be obtained by off-line experiment on individual wind turbines or reference power is generated by using the mechanical power equation of the wind turbine where wind speed or the rotor speed is measured. Figure 4 displays the block diagram of a WECS with PSF controller for maximum power extraction.

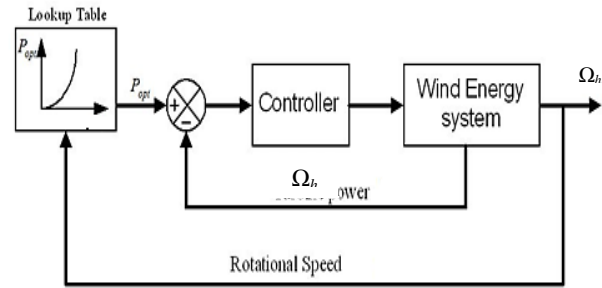


Fig.4. block diagram of power signal feedback

In [21], the turbine maximum power equation is used for obtaining reference power for PSF based MPPT.

$$P_{m(max)} = 0.5C_{p(max)}(\lambda_{opt},\beta) \rho\pi R^2 v_s^3 \quad (10)$$

The PSF control block generates the reference power $P_{m(max)}$ using Eq. (10) which is then applied to the controller. It can be seen that there is a maximum power coefficient $C_{p(max)}$. If $C_{p(max)}=0.48$, the maximum value of C_p is achieved for $\beta=0^\circ$ and λ_{opt} . A variable speed wind turbine follows the $C_p(max)$ to capture the maximum power up to the rated speed by varying the rotor speed to keep the system at λ_{opt} .

4. THE PROPOSED CONTROLLER

Applying fuzzy controller on wind energy conversion system using HCS and PSF technique for more stability under variation of wind speed. We apply the proposed controller on the two previous techniques to clarify which of them gives good result with fuzzy controller.

A. Fuzzy PI controller

Fuzzy logic controllers (FLC) have been lately introduced in the tracking of the MPP in PV systems [21-24]. The fuzzy controller has four main elements:

- i. the “rule-base” supports the knowledge, in the form of a group of rules, of how best to control the system;

- ii. The inference mechanism adjust which control rules are very related at the current time and then decides what is the suitable input.
- iii. The fuzzification interface simply modifies the inputs so that they can be interpreted and compared to the rules in the rule-base.
- iv. the defuzzification interface converts the conclusions reached by the inference mechanism into the inputs to the plant (crisp value) [22].

In our Mamdani controller

- i. We use the error and change of error as inputs. Output is the torque applied on generator
- ii. The second step, inference rules, where the fuzzified variables are compared with predefined sets in order to get the appropriate response.
- iii. The last stage is defuzzication of the rules in order to obtain the crisp values of the duty cycle perturbations.

A.1. Hill climb search technique by fuzzy controller

We use the error of speed and change of error as inputs. Output is reference torque applied on generator.

The variable inputs are expressed as linguistic variables denoted NL(Negative Large), NM(Negative Medium), NS(Negative Small), ZO(Zero), PS(Positive Small), PM(Positive Medium), PL(Positive Large). The fuzzification of the input variables by triangular MFs.

Table 1 shows the fuzzy rules for track the maximum power point.

The input variables and the control O/P for tracking of the maximum power point are illustrated in Figure 5 to Figure 7.

A.2. THE PROPOSED POWER signal feedback by fuzzy control

This technique use error between power reference power and change of error as inputs. Output is reference power.

The variable inputs are linguistic variables as NL(Negative Large), NM(Negative Medium), NS(Negative Small), ZO(Zero), PS(Positive Small), PM(Positive Medium), PL(Positive Large).The fuzzy rules is the same in Table1 and the input variables and the control O/P are like in Figure 6 to Figure 8 with other ranges.

Table 1: Fuzzy rules of HCS method

$\Delta e(t) \backslash e(t)$	NL	NM	NS	ZO	PS	PM	PL
NL	PL	PL	PM	PM	PS	ZO	ZO
NM	PL	PL	PM	PS	PS	ZO	NS
NS	PM	PM	PM	PS	ZO	NS	NS
ZO	PM	PM	PS	ZO	NS	NS	NM
PS	PS	PM	ZO	NS	NS	NM	NM
PM	PS	ZO	NS	NM	NM	NM	NL
PL	ZO	ZO	NM	NM	NM	NL	NL

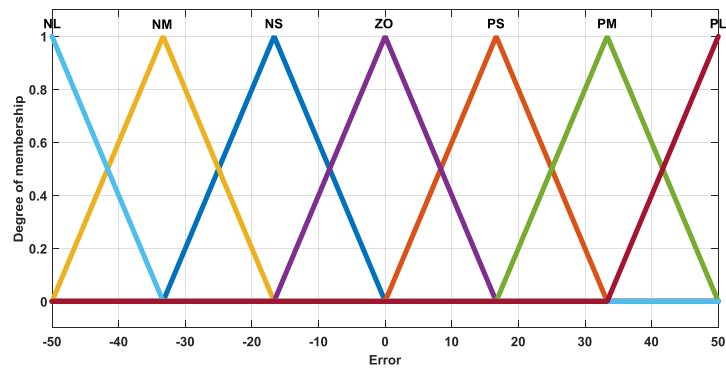


Figure 5: membership function of error

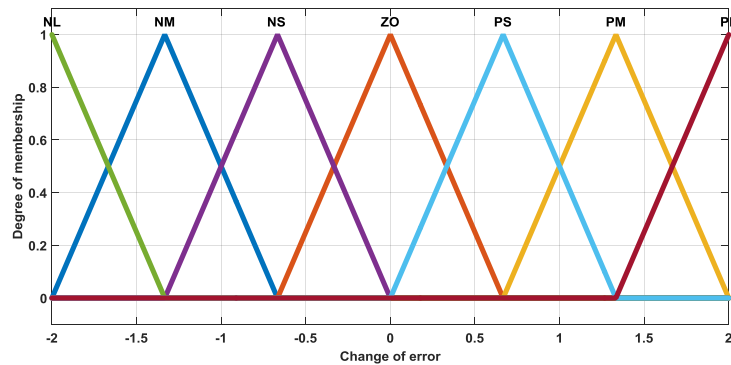


Figure 6: membership function of change of error

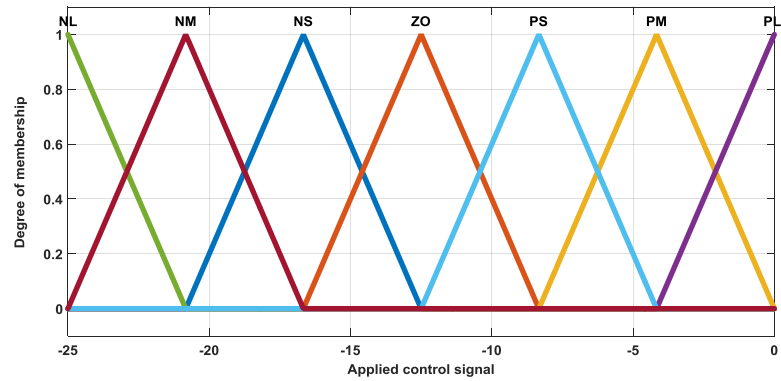


Figure 7: membership function of control signal

5. SIMULATION AND RESULTS

We introduce the comparison between four cases and show which technique approved the maximum power extraction. By applying the wind speed profile in Figure 8. PSF by fuzzy control verify the largest value in power coefficient ≈ 0.48 which displayed in Figure 9.

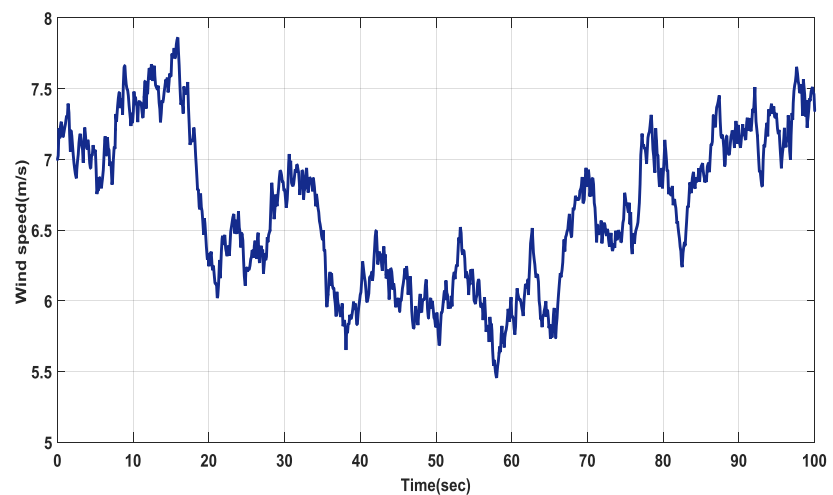


Figure 8: Wind speed profile

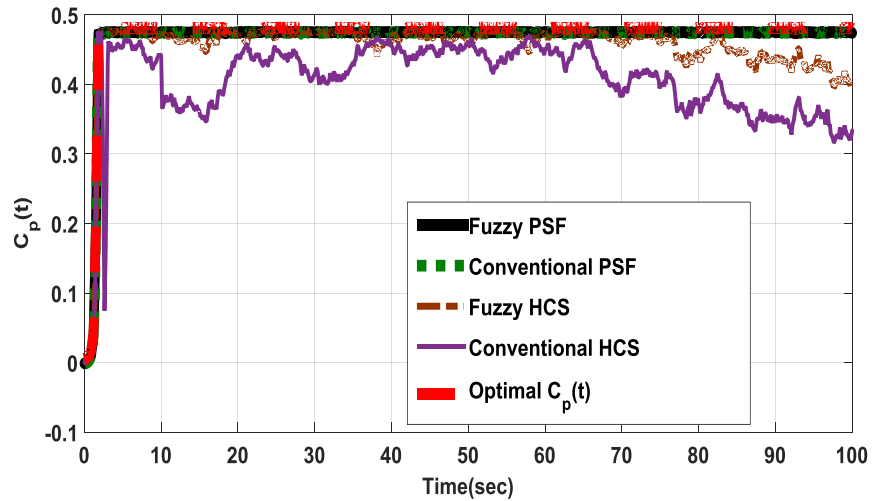


Figure 9: Power coefficient profile

In Figure 10 Tip speed ratio for more stability and maximum value ≈ 7 for PSF by fuzzy controller. Figure 11 and Figure 12 record the rotor rotational speed and generator speed, respectively. The most value of active power extraction clarified in Figure 13. Figure 14 listed the reactive power profile.

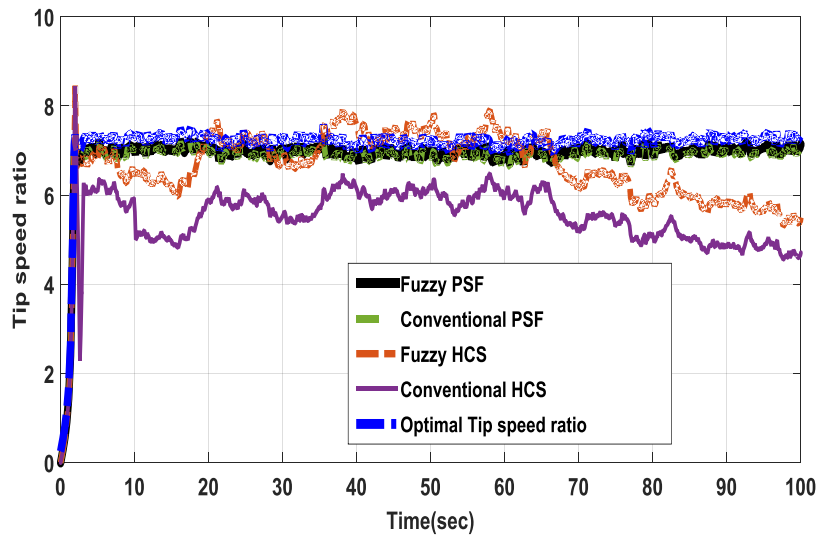


Figure10: Tip speed ratio profile

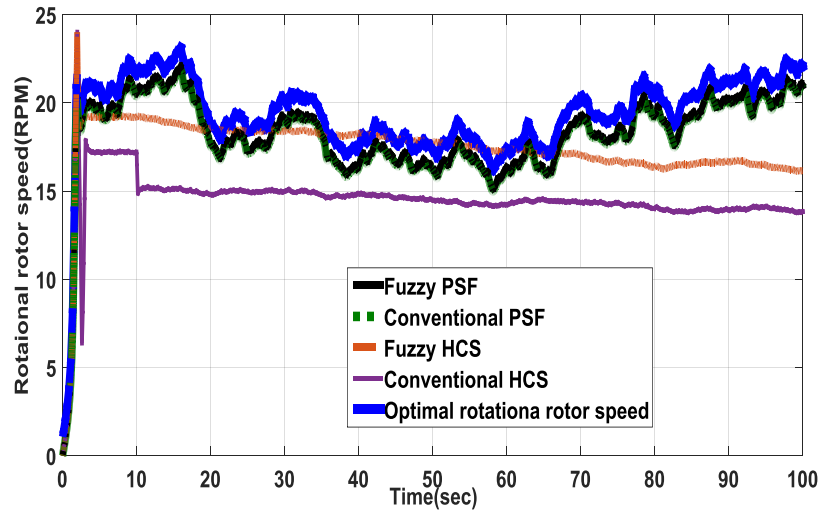


Figure 11: The trajectory of rotational rotor speed

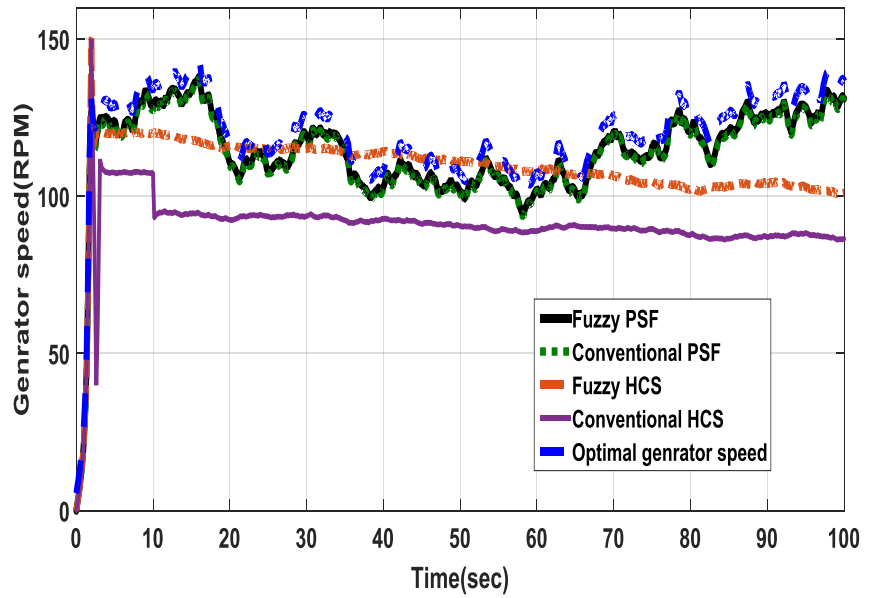


Figure12: The trajectory of generator speed

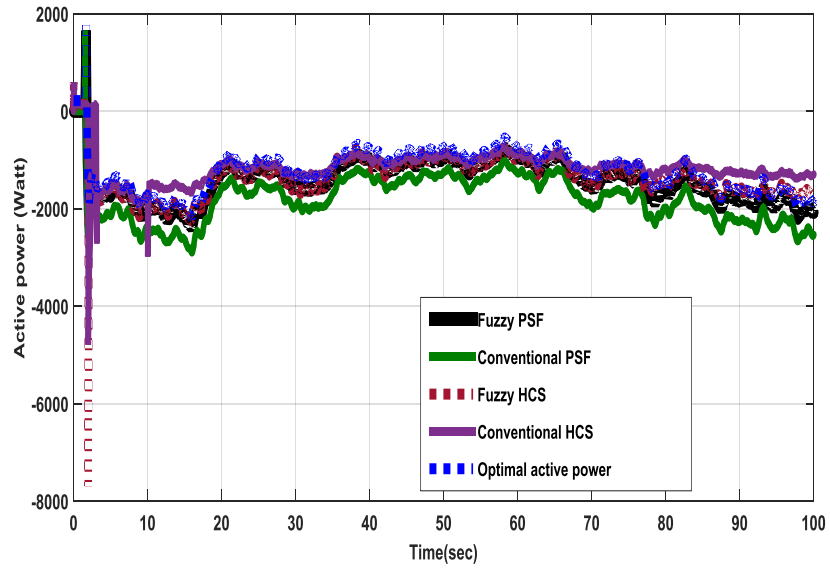


Figure13: The trajectory of active power

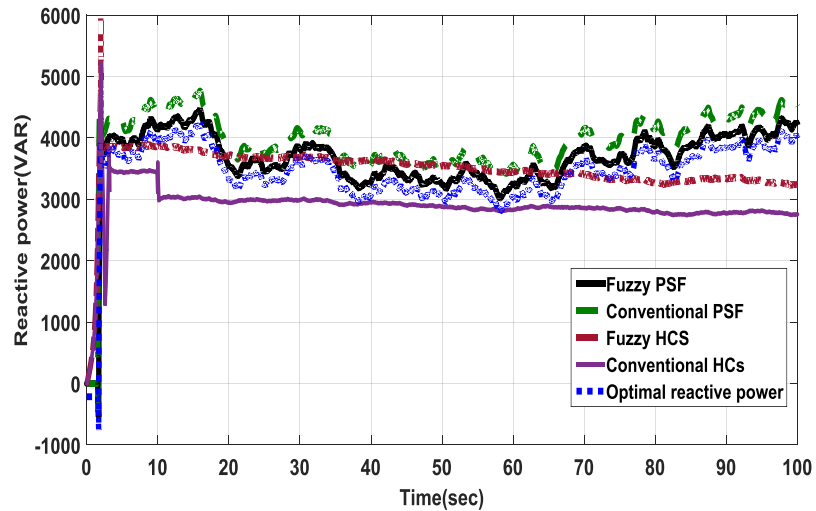


Fig.14 The trajectory of reactive power

The results explain the performance of proposed PSF fuzzy control technique. This control can secure the stability of the system and can maximize the power coefficient at 0.48 as in Figure 10. The integral term in PI fuzzy controller guarantees a system at zero steady-state tracking

error for the reference inputs. Achieving maximum active power. With variation of wind speed system can keep stability that make system more robust.

6. CONCLUSIONS

We have presented fuzzy controller for the maximum power point tracking of a wind energy conversion system. It is an effective optimal control for improvement of the performance of a variable-speed wind energy conversion system, for a squirrel-cage induction generator-based wind energy conversion system, the controller has successfully maximized the extraction of the wind energy. This was verified by the high power coefficients achieved at all the time.

Wind energy conversion system has been studied to illustrate the stabilization and robustness properties of the proposed fuzzy controller. The resulting PSF fuzzy controller is more efficient of tackling variable wind speed systems compared with the hill climb search technique. In addition, larger stability regions can be guaranteed

References

- [1] R. Spée and S. Bhowmik, "Novel control strategies for variable speed doubly fed power generation systems," *Renew. Energy*, vol. 6, no. 8, pp.907–915, 1993.
- [2] M. Ermis, H. Ertan, M. Demirekler, B. Saribatir, Y. Üçtug, M. Sezer, and I. Çardici, "Various induction generator schemes for wind-electricity generation," *Elect. Power Syst. Res.*, vol. 23, pp. 71–83, 1992.
- [3] P. Carlin, A. Laxson, and E. Muljadi, "The history and state of the art of variable-speed wind turbine technology," National Renewable Energy Lab., Golden, CO, Tech. Rep. NREL/TP-500-28 607, 2001.
- [4] A. Miller, E. Muljadi, and D. Zinger, "A variable speed wind turbine power control," *IEEE Trans. Energy Conversion*, vol. 12, pp. 181–186, June 1997.
- [5] G. Simões, B. Bose, and R. Spiegel, "Fuzzy logic based intelligent control of a variable speed cage machine wind generator system," *IEEE Trans. Power Electron.*, vol. 12, pp. 87–95, Jan. 1997.

- [6] H. Battista and R. J. Mantz, "Dynamical Variable Structure Controller for Power Regulation of Wind Energy Conversion Systems", *IEEE Trans. on Energy Conversion*, vol. 19, no. 4, pp 756-763, 2004.
- [7] X. Yang and X. Liu Qiang Wu, "Integral Fuzzy Sliding Mode Control for Variable Speed Wind Power System", *Proceedings of the IEEE International Conference on Automation and Logistics August 18 - 21, Jinan, China*, pp.1289-1294, 2007.
- [8] G.C. Venkatesh, S.V. Kulkarni, "Energy yield of passive stall regulated fixed speed wind turbine with optimal rotor speed", *Electric Power Systems Research* vol.76 ,pp 1019-1026, 2006.
- [9] E. Muljadi , C.P. Butterfield, "Pitch-controlled variable-speed wind turbine generation", *IEEE Transactions on industry application*, vol. 37, no. 1, pp 240-246, 2001.
- [10] N. A. Schinas, N. A. Vovos, and G. B. Giannakopoulos, "An Autonomous System Supplied Only by a Pitch-Controlled Variable-Speed Wind Turbine" *IEEE Transactions on Energy Conversion*, vol. 22, no. 2, pp 325-331, 2007.
- [11] B. Boukhezzara, L. Lupua, H. Siguerdidjanea, M. Handb, "Multivariable control strategy for variable speed,variable pitch wind turbines", *Renewable Energy* vol. 32, pp.1273-1287, 2007.
- [12] E. Adžić, Z. Ivanović, M. Adžić, V. Katić, „Optimum Fuzzy Control of Induction Generator in Wind Turbine Application“, 6th International Symposium on Intelligent Systems and Informatics - SISY 2008, Subotica,Serbia, Sept. 2008.
- [13] S. Heier, "Grid integration of wind energy conversion systems", *Chicester: Wiley; 1998.*
- [14] L. L. Freris, "Wind energy conversion systems", *UK: Prentice Hall; 1990.*
- [15] Lei Yazhou, Mullane Alan, Lightbody Gordon, Yacamini Robert. Modeling of the wind turbine with a doubly fed induction generator for grid integration studies. *IEEE Trans Energy Convers* 2006;21(1):257–64..
- [16] M. A. Chowdhury, N. Hosseinzadeh, M. M. Billah and S. A. Haque, "Dynamic DFIG Wind Farm Model With An Aggregation Technique", 6th International Conference on Electrical and Computer Engineering, Dhaka, Bangladesh, 18-20 December 2010, pp. 330-333.
- [17] W. P. Cameron, N. Michael, "Very short-term wind forecasting for Tasmanian power generation", *IEEE Transactions on Power Systems*, 21(2), pp.1-8. 2006.
- [18] P. Kundur, "Power system stability and control", *California: McGraw-Hill; 1994.*
- [19] M. G. Simoes, B. K. Bose, and R. J. Spiegel, "Fuzzy logic-based intelligent control of a variable speed cage machine wind generation system," *IEEE Trans. Power Electron.*,vol. 12, no.1, pp. 87–95, Jan. 1997.

- [20] A. G. Abo-Khalil, D. C. Lee, and J. K. Seok, "Variable speed wind power generation system based on fuzzy logic control for maximum power output tracking", in Proc. 35th Annual IEEE-PESC'04, vol. 3, pp. 2039-2043, 2004.
- [21] F. D. Bianchi, H. De Battista, and R. J. Mantz, "Robust Multivariable Gain-Scheduled Control of Wind Turbines for Variable Power Production," International Journal of Systems Control, vol.1, no.3, 2010, pp.103-112.
- [22] J. C. Geromel and R. H. Korogui, "Analysis and synthesis of robust control systems using linear parameter dependent Lyapunov functions," IEEE Trans. Autom. Control, vol.51, no.12, pp. 1984-1989, 2006.
- [23] Simoes, M. G., Bose, B. K., Spiegel, R. J., Fuzzy Logic-based Intelligent Control of a Variable Speed Cage Machine Wind Generation System, IEEE Transactions on Power Electronics, Vol. 12, pp. 87-95, Jan. 1997
- [24] M. Vekić, Z. Ivanović, S. Grabić, V. Katić: "Control of Variable Speed Wind Turbine Under Grid Disturbances", 13th International Symposium on Power Electronics – Ee 2005, Novi Sad (S&M), Nov. 2005, Paper No. T7- 1.1, ISBN 868521155-7.

الحصول علي أقصى قدرة من طاقة الرياح باستخدام طرق متعددة

يتلخص البحث في مقارنة بين طريقتين طريقة صعود التل وطريقة استخدام القدرة المتاحة كمرجع للنظام وهذين النظامين للحصول علي أقصى قدرة مستخرجة من طاقة الرياح وبتطبيق هذين التطبيقين علي نوعين من انواع المتحكم وهما طريقة المتحكم التقليدي وطريقة المتحكم الغيمي

PI conventional control and PI fuzzy control

وبتطبيق المتحكمان علي نظام طاقة الرياح المتجددة باستخدام برنامج ماتلاب اتضح ان طريقة استخدام القدرة المتاحة كمرجع للنظام باستخدام المتحكم الغيمي يعطي أفضل نتائج من حيث أعلى قيمة للقدرة المستخرجة وأيضا اتزان النظام مع تغير في سرعة الرياح.

Maximum Power Point Tracker of PV using Fuzzy Controller

Walaa Mohammed and Galal.Atlam

Dept. of Control and Industrial Electronics Eng., Faculty of Electronic Eng.,
Menoufia University, Menouf, EGYPT

(Received: 11-June-2015 – Accepted: 30-November-2015)

Abstract

This paper introduces two techniques to control systems. We introduce two methods for achieving maximum power. Appropriate conditions for the stability of system are drawn depend on perturb & observer (P&O) and Mamdani fuzzy logic. We present which of these techniques can extract maximum power under high disturbance. The proposed controllers design methodology are finally proved through a photovoltaic to maximize the Photovoltaic (PV) system.

1. Introduction

Our world suffers from reducing of energy in a high degree. Solving this problem is being by renewable energy. Photovoltaic energy (PV) takes part a pivotal grade; cause why its use has been high spread [1]. However of this, a PV generator has two difficult problem:

- 1) The load must equal PV conductance of the PV generator to ensure the maximum power transfer [1, 2].
- 2) The PV system faces external disturbances like temperature and solar irradiation [3].

Tracking the maximum power point (MPP) of a photovoltaic module/array is an important task in a PV control system, to maximize the PV module's efficiency [4]. However, the MPP locus varies over a wide range, depending on varying temperature and radiation intensity. Many techniques have been proposed Three Point Weight Comparison [5, 6],

Constant Voltage (CV) [7], Incremental Conductance (IC); it is an alternative to the P&O method and based on differentiating the PV power with respect to voltage and setting the result to zero [8], Short Current Pulse [9], Open Circuit Voltage [10]; this method is based on the voltage of PV generator at MPP which is approximately linearly proportional to its open circuit voltage, the Temperature Method [11] which uses the temperature to determine the MPP voltage, and methods derived from it [11]. These techniques are easily implemented and have been widely adopted for low-cost applications.

Thus, an MPPT can reduce the overall system cost. Perturb-and-Observe (P&O) is the most commonly used. However, P&O has some restriction like it fails under high changing environment conditions [12, 13].

On the other hand, speed and accuracy are considered as the principle parameters depend on some other methods like fuzzy logic (FLC) and classical stability analysis methods for fuzzy systems have been presented [14-17], but FLC methods need stability and performance analysis. To achieve the MPPT under strict theoretical analysis, the TS fuzzy model-based control is applied.

In this paper, we explain the work that presented in [12-17] for showing the difference between two methods and which of them can overcome the disturbances.

This paper is organized as follows. In section 2, we introduce the solar power generation system model. In section 3 shows the MPPT strategy and we present MPPT using traditional methods; (P&O), Mamdani fuzzy logic Simulation is concluded in section 4. Finally, section 5 states the conclusions.

2. PV SYSTEM CHARACTERISTICS

2.1 Photovoltaic array:

The solar power system considered depends on a photovoltaic array and a DC/DC buck converter. A schematic overview of the PV energy system is shown in Figure 1 [18].

The PV panel array consists of n_s - series cells and n_p parallel solar cells. I and V are the current and the voltage from PV array. If internal shunt and

series resistances are neglected according to their small values, the characteristic equation of current-voltage of a PV array can be described by a diode and a light-generated current source.

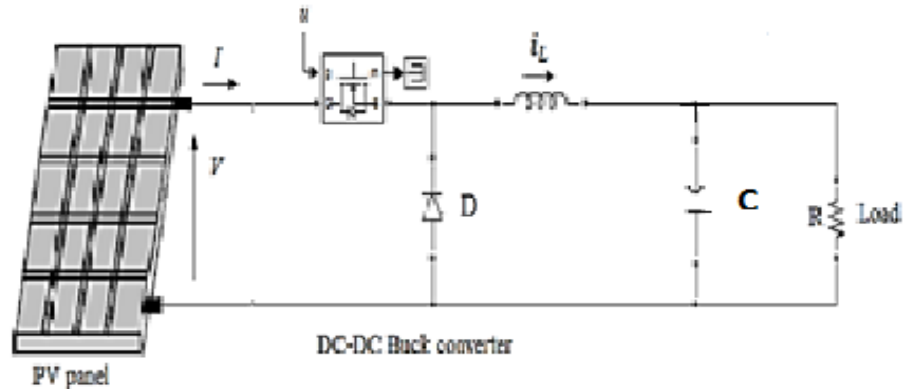


Figure 1: The PV configuration energy system

The PV array output current is written as the next equation [19]:

$$I = n_p I_{pt} - n_p I_{rv} \left(e^{\frac{K_{pv} V_{pv}}{n_s}} - 1 \right) \quad (1)$$

n_p and n_s are the number of the parallel and series cells $K_{pv} = q/(pKT)$, with $q = 1.6 \cdot 10^{-19}$ C is the electronic charge, $K = 1.38 \cdot 10^{-23}$ JK⁻¹ is the Boltzmann's constant, T is the cell temperature, p is an ideality factor, I_{pt} and I_{rv} are respectively the photocurrent and reverse saturation current which are presented by

$$I_{pt} = (I_{st} + K_I(T - T_f)) \frac{\beta}{100} \quad (2)$$

$$I_{rv} = I_{ra} \left(\frac{T}{T_f} \right)^3 \exp(qE_{bg} (1/T_f - 1/T) / gK) \quad (3)$$

Where, I_{st} is the short-circuit cell current at reference temperature and radiation and I_{ra} is the reverse saturation current at the reference temperature T_f , K_I is the short circuit current temperature coefficient and β is the solar radiation in Watt/m², E_{bg} is the band-gap energy of the semiconductor used in the cell. The power generation of the PV array [19]:

$$P = I_{pv} \cdot V_{pv}$$

$$P = n_p I_{pt} V_{pv} - n_p I_{ra} V_{pv} \left(\exp \left(K_{pv} V_{pv} / n_s \right) - 1 \right) \quad (4)$$

At the maximum power point and by taking the partial derivate of the power array with respect to the PV voltage we have:

$$\frac{dP}{dV_{pv}} = 0 \rightarrow I + V_{pv} \frac{dI}{dV_{pv}} = 0 \quad (5)$$

$$\frac{dP}{dV_{pv}} = I - \frac{n_p k_{pv}}{n_s} I_{rs} \exp \left(\frac{k_{pv} V_{pv}}{n_s} \right) \quad (6)$$

Because of the high nonlinearity, the maximum power point is hard to be solved from (6). For this reason it is difficult to get MPPT by ordinary methods.

2.2 DC/DC buck converter:

When a direct connection is made between the pv array and the load, the PV output module is rarely maximum and the operating point is not optimal [20] .To solve this problem, it is necessary to insert an adaptive device, an MPPT controller with a DC–DC converter, between the source and the load [21]. The Buck DC-DC converter is used so in order to adjust the array photovoltaic to the voltage range.

In a Buck Converter:

During ‘OFF’ Mode:-

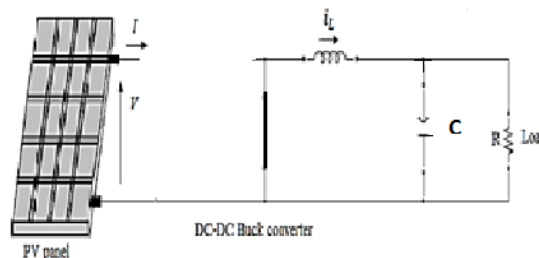


Figure 2: buck converter at off mode

From KVL

$$v_c + L \frac{di_L}{dt} = 0$$

From KCL

$$i_L - \frac{v_c}{R} - \frac{cdv_c}{dt} = 0$$

$$\begin{bmatrix} \frac{di_L}{dt} \\ \frac{dv_c}{dt} \end{bmatrix} = \begin{bmatrix} 0 & -1 \\ \frac{1}{L} & -1 \\ \frac{1}{C} & RC \end{bmatrix} \begin{bmatrix} i_L \\ v_c \end{bmatrix}, v_R = \begin{bmatrix} 0 & 1 \end{bmatrix} \begin{bmatrix} i_L \\ v_c \end{bmatrix} \quad (7)$$

During 'ON' Mode:-

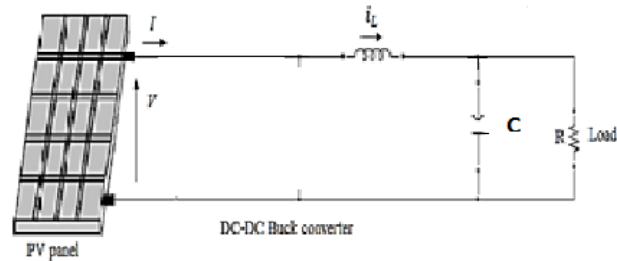


Figure 3: buck converter at on mode

From KVL
$$v - v_c - L \frac{di_L}{dt} = 0$$

From KCL
$$\frac{v_c}{R} + \frac{cdv_c}{dt} i_L = 0$$

$$\begin{bmatrix} \frac{di_L}{dt} \\ \frac{dv_c}{dt} \end{bmatrix} = \begin{bmatrix} 0 & -1 \\ \frac{1}{L} & -1 \\ \frac{1}{C} & RC \end{bmatrix} \begin{bmatrix} i_L \\ v_c \end{bmatrix} + \begin{bmatrix} i_L \\ v_c \end{bmatrix} v, v_R = \begin{bmatrix} 0 & 1 \end{bmatrix} \begin{bmatrix} i_L \\ v_c \end{bmatrix} \quad (8)$$

At discontinuous conduction mode

From KVL
$$\frac{di_L}{dt} = 0$$

From KCL
$$\frac{v_c}{R} + \frac{cdv_c}{dt} = 0$$

$$\begin{bmatrix} \frac{di_L}{dt} \\ \frac{dv_c}{dt} \end{bmatrix} = \begin{bmatrix} 0 & 0 \\ 0 & -1 \\ 0 & RC \end{bmatrix} \begin{bmatrix} i_L \\ v_c \end{bmatrix} + \begin{bmatrix} 0 \\ 0 \end{bmatrix} v, v_R = \begin{bmatrix} 0 & 0 \end{bmatrix} \begin{bmatrix} i_L \\ v_c \end{bmatrix} \quad (9)$$

Where, v is the voltage of PV array and i_L is the current on the inductance L. R is the resistances of the load and the battery,

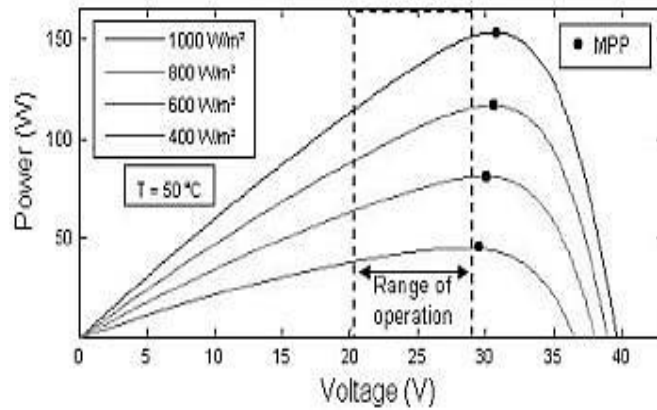


Figure 4: Relation between voltage and PV power

From (6) the maximum power is achieved at point when slope $dP_{pv}/dv_{pv}=0$ so Figure 4 shows the maximum power point at constant temperature with changes in irradiating amount.

3. MAXIMUM POWER POINT TRACKING (MPPT) CONTROLS

3.1 MPPT algorithm:

The power from PV arrays as in (4) the photocurrent and reverse saturation current, respectively are given by (2), (3) and the power slope by (6) [22].

When the power slope $dP_{pv}/dv_{pv}=0$, the system operates at the maximum power generation. The incremental conductance algorithm is depend on the differentiation of PV power to its voltage and on condition of zero slope of P-V curve in maximum power point (MPP) [23]. Based on the P-V characteristic curve, the MPPT algorithm can be given [22]: The basic relation between the input (V_{in}) and output (V_{out}) voltage of this converter is given by:

$$V_{out} = dV_{in} \quad (10)$$

By using duty cycle d , there is a linear relationship between the two voltages. Therefore, in the algorithm implementation, it is essential to control and change only d . The reference voltage is determined from the

incremental conductance method [16, 23]. The fuzzy logic controller is constructed which is robust against the parameter uncertainties.

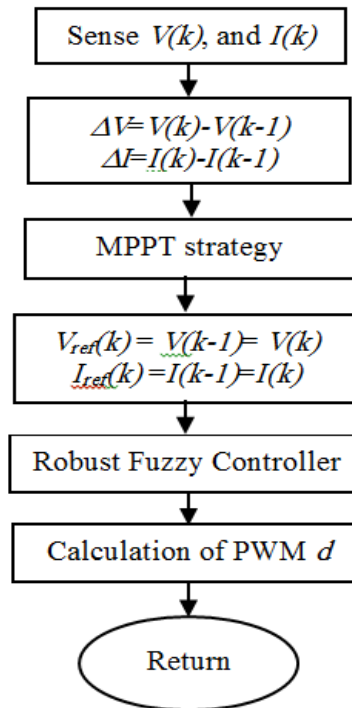


Figure 5: Flow chart of the proposed strategy

Figure 3 shows a flowchart of the proposed maximum power point tracking. First, we measure the values of voltage and current of PV arrays then calculate difference between the current and the last value and apply the strategy of MPPT technique to calculate reference values of voltage and current. Finally, the controller apply the suitable duty cycle.

3.2 Perturb & observe (P&O) MPPT technique:

The Perturb and Observe method is the most algorithms used in practice by almost authors to track the maximum power point [24-29] among others. Its principle is depending on the perturbation of the system by the increase/decrease of the duty-cycle of the converter and the observation of the effect on the output power [30-32]. If a given perturbation leads to an increase (decrease) in the output power of the PV, then the subsequent perturbation is generated in the same (reverse) direction, otherwise the

perturbation is inverted. The duty cycle is varied and the process is repeated even the maximum power point has been achieved, that drives the system to oscillate about the MPP. A common problem in P&O algorithms is that the array terminal voltage is oscillated every MPPT cycle; therefore, when the MPP is reached, the output power perturbs around the maximum, minimizing the generable power by the PV system. This is mainly true in constant or slowly-varying atmospheric conditions but also under highly changing atmospheric conditions [33].

3.3 Mamdani’s fuzzy inference method:

Fuzzy logic controllers (FLC) are presented in the tracking of the MPP [34-37]. The fuzzy controller has four components. (i) the “rule-base” needs the knowledge, collection of rules, of how best to control the system. Table 1 shows the different fuzzy rules used in Mamdani fuzzy controller to track the maximum power point. (ii) The inference mechanism modifies which control rules are much related at the present time and then makes decision which input to the plant must be. (iii) The fuzzification interface simply adjusts the inputs for interpreting and comparing to the rules in the rule-base, inputs are expressed as linguistic variables denoted NB (Negative Big), NS(Negative Small), Z(Zero), PS(Positive Small), PB(Positive Big). The fuzzification of the input variables by triangular MFs. (iv) the defuzzification interface converts the conclusions reached by the inference mechanism into the inputs to the plant (crisp value) [34]. defuzzication of the rules in order to obtain the crisp values of the duty cycle perturbations. The input variables and the control action for tracking of the maximum power point are five triangle membership function illustrated in Figure 4 to Figure 6.

Table 1: FLC Rules Base

DP \ DV	NB	NS	Z	PS	PB
NB	NS	NB	NB	PB	PS
NS	Z	NS	NS	PS	Z
Z	Z	Z	Z	Z	Z
PS	Z	PS	PS	NS	Z
PB	PS	PB	PB	NB	NS

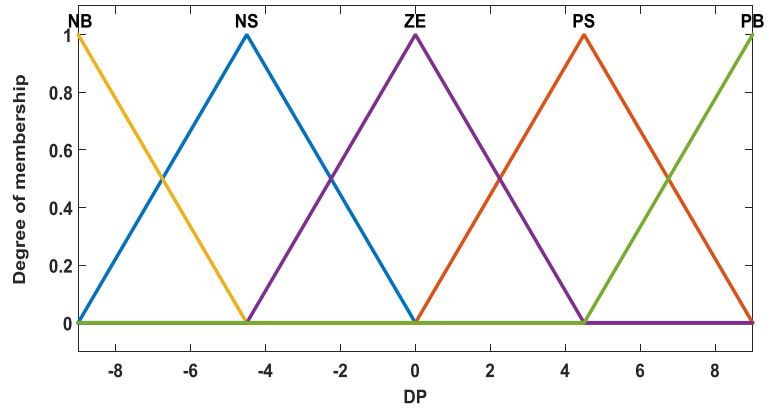


Figure 6: Membership functions for the Power change

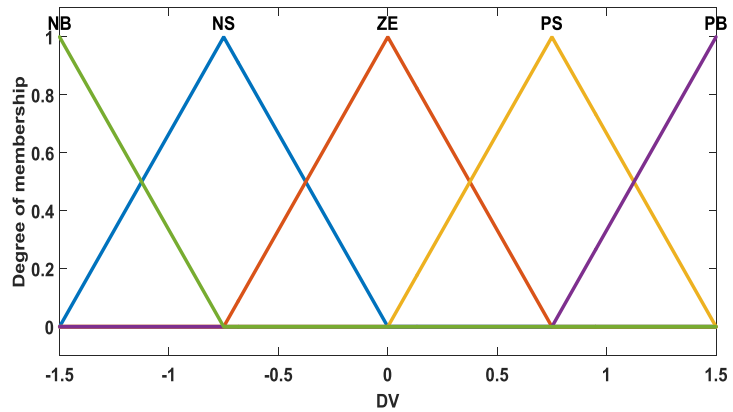


Figure 7: Membership functions for the change of PV voltage

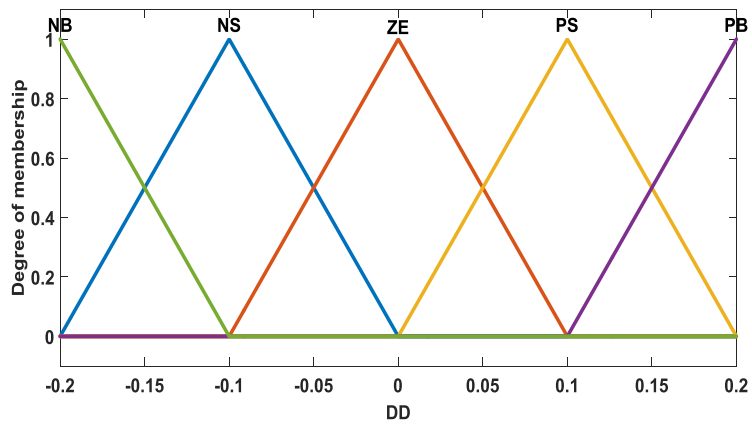


Figure 8: Membership functions for the duty cycle u

4. SIMULATION AND RESULTS

In this section, simulations are performed the PV power control system stated in (9). We consider constant temperature $T=298^{\circ}\text{K}$ with varying insolation shown in Figure 9. The parametric uncertainties RL and RM are considered within 35% of their nominal values. Fig.10 present comparison between three control signals. The difference between O/P voltages in Figure 11. The desired O/P power for three techniques show in Figure 12. It can be seen that the PV power quickly achieves to the maximum value, while the controller provides high robustness to uncertainty.

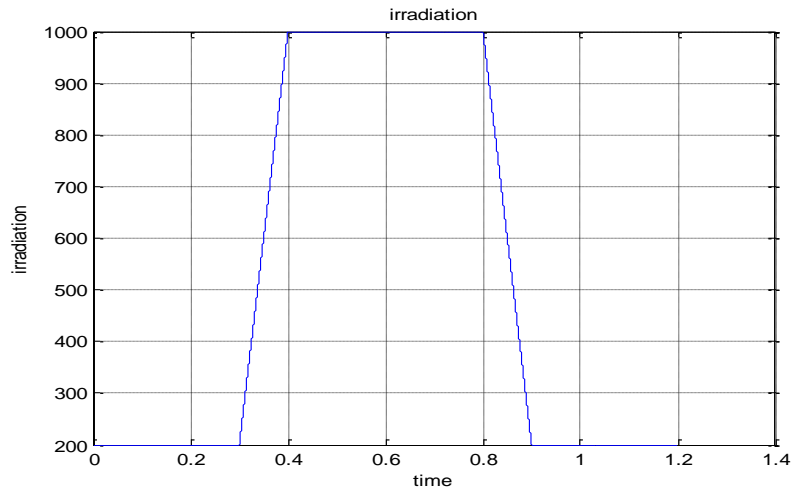


Figure 9: Varying insolation

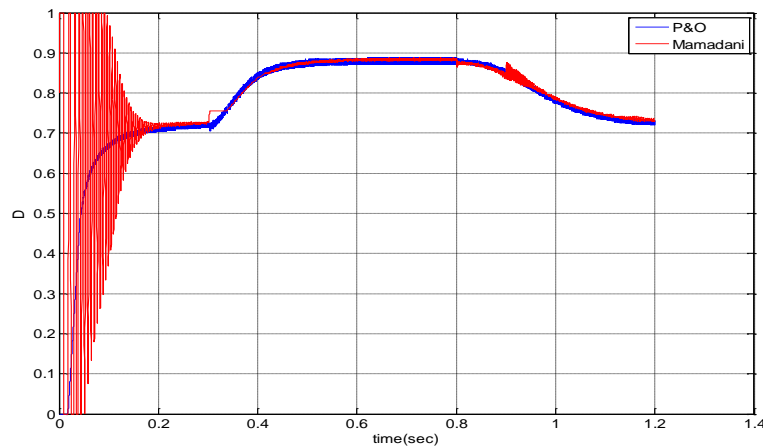


Figure10: Control signal for three strategy

We can observe in Figure 10 there is high oscillation at first to detect the suitable duty cycle of buck converter the control signal of Mamadani fuzzy is the most stable after transient time, least oscillation and high response for sudden change.

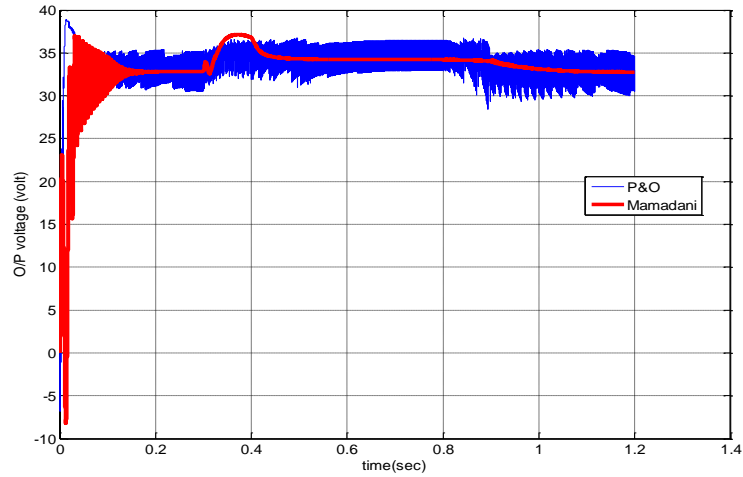


Fig.11 Three O/P voltage of three methods

Figure 11 shows two O/P voltage from two strategy and P&O method is the most method has oscillation in his O/P.

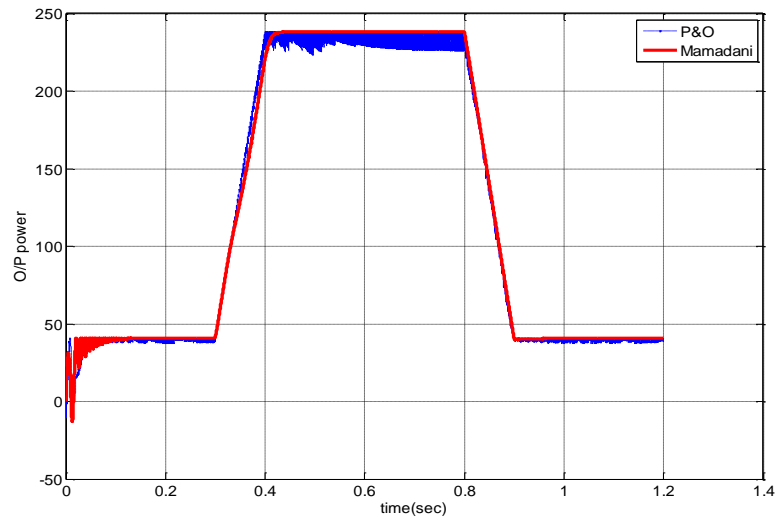


Fig.12 maximum power of three techniques

It can be seen that the performance of the system under the control of the fuzzy controller provides a good tracking for maximum power with more stability and it is clear in Figure12.

5. CONCLUSION

The resulting Mamadani fuzzy controller is capable of trackling multivariable systems subject to large parameter uncertainties. Larger stability regions can be guaranteed. Photovoltaic (PV) has been given to illustrate the stabilizability property of the proposed fuzzy controllers. In order to verify the performance of the proposed controller, we have compared it with P&O method and Mamdani fuzzy logic controller and we can deduce that Mamadani fuzzy controller can track the maximum power point with simple rule base and member ship functions. In prospective the strategy MPPT of fuzzy logic controller (FLC) is well be implemented on a dsPIC.

References

- [1] B. Yafaoui, and R. C. Wu, “*Photovoltaic energy system part 2: System control technology,*” IEEE Canadian Review, vol.61, pp.14–17, 2009.
- [2] D. Hohm, and M. Ropp, “*Comparative study of maximum power point tracking algorithms using an experimental, programmable, maximum power point tracking test bed,*” IEEE Conference Record of the Photovoltaic Specialists, pp. 16991-702, 2000.
- [3] O. C. Noureddine, M. Abdelkader, B. Mohamed-Seghir, B. Linda, “*Robust Controller to Extract the Maximum Power of a Photovoltaic System ,*” Journal of Electrical and Electronics Engineering, vol. 1, pp.117–122, 2014.
- [4] P. A. Lehman, C. E. Chamberlin, G. Pauletto, and M. A. Rocheleau, “*Operating experience with a photovoltaic-hydrogen energy system,*” presented at the Hydrogen 1994: 10th World Hydrogen Energy Conf., Cocoa Beach, FL, Jun.
- [5] V. Salas, E. Olias, A. Barrado, and A. Lazaro, Review of the maximum power point tracking algorithms for stand-alone photovoltaic systems, Solar Energy Mater, Solar Cells, vol. 90, pp. 1555– 1578, 2006.
- [6] K. H. Hussein, I. Muta, T. Hoshino, and M. Osakada, Maximum photovoltaic power tracking: An algorithm for rapidly changing

- atmospheric condition, Proc. Inst. Electr. Eng., Gen. Transmiss. Distrib., vol. 142, no. 1, pp. 59–64, 1995.
- [7] G.J.Yu, Y.S.Jung, J.Y.Choi, I.Choy, J.H.Song and G.S.Kim, A Novel Two-Mode MPPT Control Algorithm Based on Comparative Study of Existing Algorithms, Proc. Photovoltaic Specialists Conference, pp. 1531-1534, 2002.
- [8] A. Mellit and Kalogirou, Soteris A, MPPT-based artificial intelligence techniques for photovoltaic systems and its implementation into field programmable gate array chips, Energy, 2014 .
- [9] T. Noguchi, S. Togashi and R. Nakamoto, ShortCurrent Pulse-Based Maximum-Power-Point Tracking Method for Multiple Photovoltaic-andConverter Module System, IEEE Trans. Ind. Electron., vol. 49, no.1, pp. 217-223, 2002.
- [10] D.Y. Lee, H.J. Noh, D.S. Hyun and I.Choy, An Improved MPPT Converter Using Current Compensation Method for Small Scaled PVApplications, Proc. APEC, pp. 540-545, 2003,.
- [11] M. Park and I.K. Yu, A Study on Optimal Voltage for MPPT Obtained by Surface Temperature of Solar Cell, Proc. IECON, pp. 2040-2045, 2004.
- [12] J. K. Hedrick and A. Girard, Control of Nonlinear Dynamic Systems: Theory and Applications, 2005.
- [13] E.Kamal A. Aitouche, Robust Scheduler fuzzy Controller of DFIG Wind Energy Systems, IEEE Trans. Sustainable Energy, vol. 4, no. 3, pp.706-715, 2013.
- [14] Mei Shan Ngan ,Chee Wei Tan, A study of maximum power point tracking algorithms for stand-alone Photovoltaic Systems, Applied Power Electronics Colloquium (IAPEC), 2011 IEEE, vol. 22 - 27, pp. 978-1-4577-0007-1
- [15] Sera.D, Kerekes, T. , Teodorescu, R. ;and Blaabjerg, F. , Improved MPPT Algorithms for Rapidly Changing Environmental Conditions, Power Electronics and Motion Control Conference, EPE-PEMC 2006, vol. 1-4244-0121-6, pp. 1614 - 1619, 2006.
- [16] Faranda, R. Leva, S. , Maugeri, V., MPPT techniques for PV Systems: Energetic and cost comparison, Power and Energy Society General Meeting - Conversion and Delivery of Electrical Energy in the 21st Century,IEEE, pp. 1-6, 2008.
- [17] T. Tafticht, K. Agbossou, , M.L. Doumbia, A. Chériti, An improved maximum power point tracking method for photovoltaic systems, ELSEVIER. Renewable EnergyVolume 33, Issue 7, July 2008, Pages 1508–1516
- [18] N. HARRABI, M. SOUISSI, A. AITOUCHE, “*Maximum Power Control for Photovoltaic Power based on Fuzzy Takagi-Sugeno Model* ,” papier journal JEE.2014.

- [19] C.S. Chiu, *TS fuzzy maximum power point tracking control of solar power generation systems*, IEEE Trans. Energy Convers, vol. 25, no 4, pp. 1123-1132, 2010.
- [20] C. Larbes , A. Cheikh, S.M Obeidi, T. and Zerguerras, *Genetic algorithms optimized fuzzy logic control for the maximum power point tracking in photovoltaic system*, Renewable Energy, vol.34, no. 10 ,pp. 2093-2100, 2009.
- [21] A.F. Boehinger, *Self adaptive DC converter for solar spacecraft power supply*, IEEE Trans. Aerospace and Electronic Sys., AES-4, (1), pp. 102–111, 1968.
- [22] J.-A. Jiang, T.-L.Huang; Y.-T. Hsiao, and C.-H. Chen, “*Maximum Power Tracking for Photovoltaic Power Systems*,” Journal of Science and Engineering, vol. 8, no 2, pp. 147-153, 2005.
- [23] C. Yin YangQuan, C.S.-M. Zhong , “*Robust stability and stabilization of uncertain fractional-order descriptor nonlinear system*,” Preprints of the 19th World Congress The International Federation of Automatic Control Cape Town, South Africa. August 24-29, 2014.
- [24] Z. Salameh, D. Taylor, *Step-up maximum power point tracker for photovoltaic arrays*, Solar Energy, vol. 44, no. 1 ,pp. 57–61,1990.
- [25] W. Denzinger, *Electrical power subsystem of globlastar*, Proceedings of the European Space Conference, pp. 171–174, 1995.
- [26] W.J.A. Teulings, J.C. Marpinard, A. Capel, *A maximum power point tracker for a regulated power bus*, Proceedings of the European Space Conference, 1993.
- [27] Y. Kim, H. Jo, D. Kim , *A new peak power tracker for cost-effective photovoltaic power systems*, IEEE Proc. Energy Conversion Eng. Conf. IECEC 96, vol.3, pp. 1673–1678, 1996.
- [28] Ch. Hua, J. Lin, Ch. Shen , *Implementation of a DSP-controlled PV system with peak power tracking*, IEEE Trans. Ind. Electron., vol. 45, no.1, pp. 99–107,1998.
- [29] H. Al-Atrash, I. Batarseh, K. Rustom, *Statistical modeling of DSP-based hill-climbing MPPT algorithms in noisy environments*, Applied Power Electronics Conference and Exposition, APEC 2005, Twentieth Annual IEEE, vol. 3, 2005, pp. 1773–1777 , 2005.
- [30] A. Chouder, F. Guijoan and S. Silvestre , *Simulation of fuzzy-based MPP tracker and performance comparison with perturb & observe method*, Revue des Energies Renouvelables, vol. 11, no.4, pp.577 –586, 2008.
- [31] J.L. Santos, F. Antunes, A. Chehab, C. Cruz , *A maximum power point tracker for PV systems using a high performance boost converter* , Solar Energy, vol. 80, no.7, pp. 772–778, 2006.
- [32] X. Liu, L.A.C. Lopes, *An improved perturbation and observation maximum power point tracking algorithm for PV arrays*, IEEE 35th

- Annual Power Electronics Specialists Conference, PESC 04, vol. 3, pp. 2005–2010, 2004.
- [33] T. ESRAM and P. L. Chapman, “Comparison of photo-voltaic array maximum power point tracking techniques,” IEEE Trans. Energy Conv., Vol. 22, pp. 439–449, 2007.
- [34] K.M. Passino, S. Yurkovich, Fuzzy control, Reading MA : Addison Wesley, vol. 42 , 1998.
- [35] R Kadri, JP Gaubert, “An Improved Maximum Power Point Tracking for Photovoltaic Grid-Connected Inverter Based on Voltage-Oriented Control,” IEEE Trans. Ind. Electron., vol.58, no. 1, pp.66-75, 2011.
- [36] Wilamowski BM, Li X., *Fuzzy system based maximum power point tracking for PV system*, 28th Annual Conf. of the IEEE Ind. Electron. Society, vol.4, pp. 3280–84, 2002.
- [37] H. Boumaaraf, A. Talha and O. Bouhali , *Modeling and control of grid-connected photovoltaic systems*, Journal of Electrical Engineering vol. 14 , no. 3,2014.

إستخدام المتحكم الغيمي في الحصول علي أقصى قدرة من الطاقة الشمسية

يتلخص البحث في الحصول علي اقصى قدرة من الخلايا الشمسية بالمقارنة بين طريقة معتادة وهي طريقة الاضطراب والملاحظة والطريقة الاخرى هي طريقة استخدام المتحكم الغيمي والنظام المطبق باستخدام برنامج ماتلاب يتكون من مصفوفة من الخلايا الشمسية و محول للطاقة المستخرجة وعن طريقه يمكن التحكم في قيمة الجهد للحصول علي أقصى طاقة وبقارنة النتائج اتضح ان النظام الغيمي قادر علي الحصول علي أقصى قدرة مستخرجة من النظام وأيضا تحقيق اتزان النظام مع التغير في درجة الحرارة وكمية الاشعة الساقطة عي الخلايا الشمسية.

بيان بأسماء السادة المحكمين للبحوث المنشورة بعدد يناير 2016 م
من [مجلة المنوفية لبحوث الهندسة الإلكترونية النصف سنوية]
حسب الترتيب الأبجدي

م	إسم المحكم	جهة العمل
1	أ.د./ السيد محمود الربيعي	كلية الهندسة الإلكترونية بمنوف
2	أ.د./ سعيد أمين الحلفاوى	كلية الهندسة الإلكترونية بمنوف
3	أ.د./ شعبان مبروك عشيبه	كلية الهندسة بشبين الكوم
4	أ.د./ صلاح صبري عبيه	الرئيس العام للمعامل البحثية بجامعة زويل
5	أ.د./ عبد الحلیم عبدالنبي ذكرى	كلية الهندسة- جامعة عين شمس
6	أ.د./ فايز ونيس ذكى	كلية الهندسة- جامعة المنصورة
7	أ.د./ مجدى عبدالستار قطب	كلية الهندسة الإلكترونية بمنوف
8	أ.د./ محمد مبروك شرف	كلية الهندسة الإلكترونية بمنوف
9	أ.د./ معوض إبراهيم معوض	كلية الهندسة الإلكترونية بمنوف
10	أ.د./ هشام فتحي على	كلية الهندسة - جامعة المنيا

مجلة المنوفية لبحوث الهندسة الإلكترونية

① يرسل الباحث بحثه باسم الأستاذ الدكتور / عميد الكلية ورئيس لجنة النشر العلمي من ثلاث نسخ .

② الصفحة الأولى تحتوي على :-

- أ. عنوان البحث .
- ب. المؤلفين ووظائفهم وأماكن عملهم .
- ج. الكلمات الرئيسية **keywords** بما لا يزيد على خمسة .
- د. ملخص البحث لا يزيد على (300) كلمة بدون معادلات أو أرقام مراجع .
- هـ. في أسفل الصفحة يكتب العنوان الكامل للمؤلفين وكذلك العنوان الإلكتروني أو الفاكس والتليفون إن وجد .
- و. يقدم البحث أثناء التحكيم بخط كبير ومناسب ويترك مسافة بين السطور .
- ي. يقدم البحث طبقاً للنماذج المعلنة (إرشادات للمؤلف) على موقع المجلة على شبكة الإنترنت .

③ يكتب البحث على عمود واحد بنفس أسلوب كتاب دوريات عائلة المجالات الدولية (INT.J) ونفس نماذج الحروف المتبعة ويكون الحجم النهائي لكل إصدار هو (21سم * 28سم) .

④ تكتب بعد الملخص مقدمة البحث (INTRODUCTION) التي تحتوي على الهدف من البحث وكذلك إسهامات الباحثين الآخرين التي تم البناء عليه وكذا الإسهام الحقيقي للبحث .

⑤ في الخلاصة (CONCLUSION) يجب ذكر المميزات إن وجدت وكذلك القيود والتطبيقات .

⑥ المراجع تكتب في قسم منفصل في نهاية البحث بالأسلوب المتبع في (IEEE) ويشار في البحث بأرقامها داخل أقواس مثلاً [1] .

⑦ الأشكال والصور يجب أن تكون عند حد الضرورة ويجب أن تكون أصلية وليست منسوخة وأن تكون واضحة ومعبرة وتكون دائماً بالأبيض والأسود والكتابة على الرسم يجب أن تكون ذات حجم يناسب حجم الرسم .

⑧ يتم ترقيم الصفحات أسفلها بالقلم الرصاص .

⑨ يصاحب البحث قرص مدمج مكتوب على (WORD) .

مجلة المنوفية لبحوث الهندسة الإلكترونية

- ① بالنسبة لأعضاء هيئة التدريس والهيئة المعاونة بالكلية يكون رسم الاشتراك بالكلية (25 جنيهاً) سنوياً ويتم السداد شخصياً لمن يرغب في أن تصله نسخة من كل إصدار ويدفع رسوم نشر عن كل بحث عدد صفحاته (ثمانية صفحات) فأقل مبلغ (275 جنيهاً) ولكل صفحة زائدة عن ذلك رسم قدره (10 جنيهاً).
- ② يتم النشر للزملاء أعضاء هيئة التدريس من داخل الجامعة نظير رسم قدرة (325 جنيهاً) للبحث الذي لا يتعدى (ثمانية صفحات) ولكل صفحة زائدة عن ذلك رسم قدره (15 جنيهاً).
- ③ للباحثين من خارج جامعة المنوفية تنشر بحوثهم نظير رسم قدرة (350 جنيهاً) للبحث الذي لا يتعدى (ثمانية صفحات) ولكل صفحة زائدة عن ذلك رسم قدره (20 جنيهاً).
- ④ للباحثين من خارج جمهورية مصر العربية تنشر بحوثهم نظير رسم قدرة (100 دولار أو ما يعادلها) للبحث الذي لا يتعدى (ثمانية صفحات) ولكل صفحة زائدة عن ذلك رسم قدره (5 دولار أو ما يعادلها).
- ⑤ رسم الاشتراك السنوي للأفراد داخل البلاد (50 جنيهاً) سنوياً.
- ⑥ رسم الاشتراك السنوي للهيئات داخل البلاد (300 جنيهاً) سنوياً.
- ⑦ رسم الاشتراك للأفراد خارج البلاد (50 دولار) سنوياً أو ما يعادلها.
- ⑧ رسم الاشتراك للهيئات خارج البلاد (300 دولار) سنوياً أو ما يعادلها.

وذلك عن العددين سنوياً ويعامل العدد الواحد بواقع النصف من القيمة

INFORMATION FOR AUTHORS

The Minufiya Journal of Electronic Engineering Research (MJEER) publishes only research papers. The journal does not publish essay or technical reporting types of paper. Prospective authors are encouraged to examine the journal itself for details of layout. Detailed instructions, which should be fully adhered at time of publication, are available upon request from the editor office. However submitted papers shall not be sent to referees before full adherence to the following requirements:

1. The submitted paper should not have been submitted earlier or at the same time to any other journal in Egypt or abroad.
2. Papers should be submitted in English in both of the following two form:
 - an original and three copies in A4 size
 - stored on a (CD) using WINWORD, Times New Roman, size 13
3. The margins in all pages except the first page are 3.5 cm from the top and the bottom, and 2.5 cm from the left and right. The first page should have margins 5 cm from the top. Text should be justified to the left and the right margins.
4. Only the abstract, the acknowledgments, the list of references, and the list of symbols are to be single line spaced. Other sections are to be 1.5 line spaced.
5. Paper title is to be typed centered in bold capital letters. Author(s) Name(s) should be typed in plain capital letters, centered, and placed 3 single spaces under the paper title. Footnote, size 10, giving the author(s) title(s) and affiliation(s) should be provided.
6. English abstract, maximum 200 words, should be provided immediately before the "Introduction" with the word ABSTRACT as heading flush left.
7. Figures and tables are to be totally integrated within the text. Captions should be located under the figure and on top of the table and clearly spaced within the main text. Lettering should be large enough to be readable after 80% reduction.
8. Reference should be cited in the text between square brackets and listed at the end of the paper with the word REFERENCES as heading flush left.
9. Headings are to be bold, flush left, with Arabic numerals. Major headings are all capital, subheading are initial capital, and only the first letter of each third level headings is capital.
10. Arabic summary within 10 lines is to be provided at the end of the paper preceded by Arabic translation of the paper title and abstract . For non-Arabic speaking authors a free of charge translation of the paper title and abstract can be provided by the editors.
11. For prospective authors a nonrefundable down payment of:
 - a) 275.0 LE for the regular paper of 8 pages and 10.0 LE for each extra page if they are faculty staff members,
 - b) 3250.0 LE for the regular paper of 8 pages and 15.0 LE for each extra page if they are staff members in the university of Minufiya
 - c) 350.0 LE for the regular paper of 8 pages, and 20.0 LE for each extra page if they are members of other institution.
 - d) 100.0 USD for the regular paper of 8 pages, and 5.0 USD for each extra page if they are members of foreign institutions.

This amount is to be paid upon submission of the paper. In case of acceptance, the remaining fees should be settled with the treasurer before enrollment of the paper in the next possible issue. Publication fees cover cost of one copy of the journal, and 5 reprint.

Annual subscriptions : personal, 50.0 LE in Egypt and 50.0 USD abroad, institutional : 300.0 LE in Egypt and 300.0 USD abroad.

N.B. the ideas expressed in the papers are strictly those of the authors. The editors do not hold themselves responsible for the views expressed by the author.

Prof. Dr. Mohamed F. El-Kordy

مجلة المنوفية لبحوث الهندسة الإلكترونية

عنوان المراسلة:

جمهورية مصر العربية

محافظة المنوفية

منوف – رمز بريدي 32952

كلية الهندسة الإلكترونية

تليفون: 048 -3661334

فاكس: 048 -3660716

البريد الإلكتروني: Srabie1@yahoo.com

الحساب المصرفي:

البنك المركزي المصري – حساب الخزانة الموحدة – جامعة

المنوفية – كلية الهندسة الإلكترونية بمنوف – المجلة العلمية

للكلية – حساب رقم [9/450/80836/1]

INFORMATION FOR AUTHORS

The Minufiya Journal of Electronic Engineering Research (MJEER) publishes only research papers. The journal does not publish essay or technical reporting types of paper. Prospective authors are encouraged to examine the journal itself for details of layout. Detailed instructions, which should be fully adhered at time of publication, are available upon request from the editor office. However submitted papers shall not be sent to referees before full adherence to the following requirements:

1. The submitted paper should not have been submitted earlier or at the same time to any other journal in Egypt or abroad.
2. Papers should be submitted in English in both of the following two form:
 - an original and three copies in A4 size
 - stored on a (CD) using WINWORD, Times New Roman, size 13
3. The margins in all pages except the first page are 3.5 cm from the top and the bottom, and 2.5 cm from the left and right. The first page should have margins 5 cm from the top. Text should be justified to the left and the right margins.
4. Only the abstract, the acknowledgments, the list of references, and the list of symbols are to be single line spaced. Other sections are to be 1.5 line spaced.
5. Paper title is to be typed centered in bold capital letters. Author(s) Name(s) should be typed in plain capital letters, centered, and placed 3 single spaces under the paper title. Footnote, size 10, giving the author(s) title(s) and affiliation(s) should be provided.
6. English abstract, maximum 200 words, should be provided immediately before the "Introduction" with the word ABSTRACT as heading flush left.
7. Figures and tables are to be totally integrated within the text. Captions should be located under the figure and on top of the table and clearly spaced within the main text. Lettering should be large enough to be readable after 80% reduction.
8. Reference should be cited in the text between square brackets and listed at the end of the paper with the word REFERENCES as heading flush left.
9. Headings are to be bold, flush left, with Arabic numerals. Major headings are all capital, subheading are initial capital, and only the first letter of each third level headings is capital.
10. Arabic summary within 10 lines is to be provided at the end of the paper preceded by Arabic translation of the paper title and abstract. For non-Arabic speaking authors a free of charge translation of the paper title and abstract can be provided by the editors.
11. For prospective authors a nonrefundable down payment of:
 - a) 275.0 LE for the regular paper of 8 pages and 10.0 LE for each extra page if they are faculty staff members,
 - b) 325.0 LE for the regular paper of 8 pages and 15.0 LE for each extra page if they are staff members in the university of Minufiya
 - c) 350.0 LE for the regular paper of 8 pages, and 20.0 LE for each extra page if they are members of other institution.
 - d) 100.0 USD for the regular paper of 8 pages, and 5.0 USD for each extra page if they are members of foreign institutions.

This amount is to be paid upon submission of the paper. In case of acceptance, the remaining fees should be settled with the treasurer before enrollment of the paper in the next possible issue. Publication fees cover cost of one copy of the journal, and 5 reprint.

Annual subscriptions : personal, 50.0 LE in Egypt and 50.0 USD abroad, institutional : 300.0 LE in Egypt and 300.0 USD abroad.

N.B. the ideas expressed in the papers are strictly those of the authors. The editors do not hold themselves responsible for the views expressed by the author

مجلة المنوفية لبحوث الهندسة الإلكترونية

كلية الهندسة الإلكترونية - جامعة المنوفية



1-25

كلية الهندسة الإلكترونية - جامعة المنوفية
Faculty of Electronic Engineering - Minufiya University

يناير 2016

المجلد الخامس والعشرون - العدد الأول